UNIVERSITY OF CALIFORNIA
SANTA CRUZ

THE WHEN, HOW AND WHY OF BIVALVE SHELL GROWTH: SCLEROCHRONOLOGY AS A TOOL TO UNDERSTAND PHYSIOLOGY IN JURASSIC AND FUTURE OCEANS

A dissertation submitted in partial satisfaction
of the requirements for the degree of

DOCTOR OF PHILOSOPHY

in

EARTH SCIENCES

by

Daniel E. Killam

December 2018

The Dissertation of Daniel Killam is approved:

_____
Professor Matthew Clapham, chair

_____
Professor James Zachos

_____
Professor Kristy Kroeker

_____
Dean Paul Koch

_____
Lori Kletzer
Vice Provost and Dean of Graduate Studies

Table of Contents

ACKNOWLEDGMENTS

This work was supported by funding from the Casey Moore Fund, Myers Oceanographic Trust, AMNH Lerner Gray Fund for Marine Research, Paleontological Society and Conchologists of America. I am thankful for their support, which enabled me to collect a lot of clams in unusual places. I thank my advisor Matthew Clapham for taking a chance on that USC grad who cold emailed him six years ago. Thanks to committee members Paul Koch, Jim Zachos and Kristy Kroeker for being a constant source of advice and answers. Thank you to Adina Paytan for the opportunity she provided me to travel to Israel in 2016 and again for connecting me with a collaborator who will become my postdoc advisor.

Thank you to research technicians Colin Carney, Rob Franks, Dyke Andreasen, Brandon Cheney and Moty Ohevia for their technical support. This work would not have happened without their expertise. Sincere thanks to curators Henk Mienis, Mariagabriella Fornasiero, and Anna Vaccari, who provided me with access to collections and their insight. Thank you to collaborators Renato Posenato, Marco Franceschi, and Tariq Al-Najjar.

Thank you to my mentees Ryan Thomas, Ismari Najera, Diana Reyna, Edgar Palominos, Evelin Diaz, Sarah Sullivan and Morgan Carothers, who taught me so much during our time together. I'm indebted to my friends Marko Manojlovic, Sarah Neuhaus, Carolyn and Darby Begeman, Kim Bitterwolf, Bethany Nagid, Joey Valizan, Rachel Maxwell, Mikey Nayak, Anand Keseravaju, Kenske Fukumori, Sean

Eckley, Terry Wells, the Borlands, and many more, who were there for me through thick and thin.

Thank you to the love of my life Dana Shultz for always charging my batteries. Thank you to my mama Jennifer Killam for the 28 years and counting of unconditional love, support and guidance. Thanks to my sister Emily for rescuing me many a time, and my aunts and uncles Susie, Anne, Debbie, Sue and Dean for being my secondary parents on demand.

Finally, thank you Dudley Bradstreet Killam Jr., for being my role model and the main advisor in the thesis of my life since always and forever. This is for you, Dad.

ABSTRACT:

THE WHEN, HOW AND WHY OF BIVALVE SHELL GROWTH: SCLEROCHRONOLOGY AS A TOOL TO UNDERSTAND PHYSIOLOGY IN JURASSIC AND FUTURE OCEANS

Daniel Killam

Bivalve shells contain growth lines which are formed as a result of periodic environmental or physiological stress, analogous to tree rings. The study of these regular growth increments in the hard parts of bivalves and other calcifying organisms is called sclerochronology. In this thesis, I have examined the ways that sclerochronology can be useful in fields where it is underutilized. The first chapter involves aggregating hundreds of past bivalve seasons of growth worldwide to help answer the question: why do bivalves stop growing in certain seasons and where does it happen? We discuss the primacy of temperature over seasonal food supply as the major determinant of seasonal growth in bivalves, and the latitudinal gradients of likelihood of shutdown that result from this. The second chapter is an investigation of bivalve growth in deep time, looking at the rate of growth of an enigmatic Early Jurassic group called the Lithiotids. For the first time, we have isotopically calibrated their growth, determining that it is quite fast in comparison to other giant bivalves through time but does not corroborate prior hypotheses that they harbored photosymbiotic algae in their tissue. Finally, in chapters three and four we report on investigations of carbon, oxygen and nitrogen stable isotopes of giant clam shells in the Red Sea and relate their growth rate to those environmental proxies. In chapter three, we report interspecific and intrashell differences in carbon and oxygen isotopes

for different *Tridacna* species, corroborating the proposed shallow life habit of the rare endemic T. squamosina, and discuss how the outer shell layer of the giant clams records higher formation temperatures than the interior. Chapter four reports on the unexpected acceleration of growth of modern giant clams in the Northern Red Sea, and we propose that fertilization by anthropogenic nitrate aerosols is recorded in the nitrogen isotopes of their shell organic material. Together, these chapters represent applications of sclerochronology to understand bivalve physiology in the deep and near past, the present and potentially the future.

INTRODUCTION

Bivalves are influential members of many aquatic ecosystems. They bridge the water column and the benthos through their prodigious water filtration, substrate engineering and their status as a food source to higher trophic levels (Vaughn and Hoellein 2018). Their carbonate shells accrete with regular growth lines, serving as a high-resolution skeletal diary of their lives analogous to tree rings (Jones and Quitmyer 1996). The study of these periodically accreted hard parts in bivalves and other calcifying taxa is known as sclerochronology and is the marine/limnological equivalent to dendrochronology on land. In contexts where stratigraphy is limited by time averaging, which prevents the investigation of inter- and subannual phenomena in the fossil record, sclerochronology has enabled the investigation of Miocene climate oscillations (Batenburg et al. 2011), Triassic annual temperature ranges (Nützel et al. 2010), Cretaceous tidal growth increments (Walliser et al. 2018), and other research questions that require high resolution proxies to investigate.

As in the sedimentological record, any investigation of bivalve growth increments first requires the calibration of an age model. Bivalve shells feature periodic growth cessation or slowdown lines, typically dark, semi-translucent organic-rich regions separating thicker, opaque white bands which represent times of faster growth (Jones and Quitmyer 1996). These bands can be daily, tidal, monthly or annual in periodicity (Schöne 2008). The first chapter in this thesis is an investigation of the environmental triggers leading to the formation of these annual growth cessations. We aggregated nearly 300 direct modern observations of bivalve season of

growth in relation to various environmental data sources, and concluded that temperature is the dominant control on bivalve growth at most latitudes. The relationship between temperature and the occurrence of winter cessation is stronger than that of latitude alone, while food supply displayed no significant relationship. The season of cessation of bivalves could have broader application to understand thresholds of temperature stress in the fossil record.

Chapter Two is an applied deep-time sclerochonological investigation of the growth of an enigmatic group of bivalves known as the "Lithiotis" fauna. These aberrant hyper-elongated bivalves produced large biostromes in shallow tropical lagoons during the Pliensbachian and Toarcian stages of the Early Jurassic (Posenato and Masetti, 2012). Their flattened morphology, unusual size and restriction to shallow tropical-subtropical latitudes has led some researchers to propose their status as a putatively photosymbiotic taxon analogous to the modern giant clams, using symbiotic algae to accelerate their growth (Fraser et al. 2004, Vermeij 2013). We were able to determine from an isotopic calibration that growth bands in their shells are fortnightly in periodicity, and then extrapolated to find that the largest species, *Cochlearites loppianus*, can grow up to 5 cm/year, while the other species grow 1-2 cm/year. This corresponds to over 200 g of carbonate precipitation per year, which would imply that the lithiotids were indeed fast growers. However, in a review of other modern and fossil "hypercalcifier" bivalves, we determined that the lithiotids and rudists are within the range of shell growth energy expenditure experienced by fossil and modern nonsymbiotic taxa. We review recent developments in the literature

which suggest that the unusual elongated morphology of the lithiotids and rudists are more indicative of a "mudsticking" oyster-like lifestyle than that of modern photosymbiotic aggregating corals (Chinzei 2013).

But while the lithiotids may have been an example of a big bivalve that did not need algae to achieve accelerated growth, the giant clams (*Tridacna*) are the most iconic representatives of bivalve photosymbiosis in the modern day. Their brilliantly colored mantles are rich in symbiotic zooxanthellae of the same *Symbiodinium* clades found in reef-building corals (Klumpp et al. 1992; Norton et al. 1992). However, while understanding of the environmental limitations behind coral symbiosis is intensively studied, comparatively little is known of the impact that photosymbiosis has on geochemical proxy records within giant clam carbonate, and how those proxies can be applied to better understand the physiology and environmental vulnerability of giant clams in the past and future.

My third chapter considers the comparative ecology of the three species of giant clams known from the Gulf of Aqaba in the Northern Red Sea: *Tridacna maxima*, *T. squamosa* and *T. squamosina*. The three species exhibit differing rates of photosymbiotic activity, with *T. maxima* and *T. squamosina* having higher levels of chlorophyll activity than the more heterotrophic *T. squamosa* (Jantzen et al. 2008, Richter et al. 2008). We wanted to determine in this system whether we could discern systematic differences between the carbon and oxygen isotopes ($\delta^{13}C$ and $\delta^{18}O$ values, respectively) of their shells in relation to their levels of photosymbiosis and comparative life habit, and whether that difference would manifest also within the

shell, as an offset between the interior and exterior shell layers of the clam. Previous workers have had mixed results in discerning a photosynthetic offset in shell carbonate of mollusks (Jones et al. 1986, Romanek et al. 1987, Jones and Jacobs 1992), but no workers have ever tested three tridacnids from the same environment. Because photosymbiosis preferentially fixes lighter ^{12}C into photosynthate products, we hypothesized that the $\delta^{13}C$ ratio of the outer shell layer would be higher as it is closer to the site of greatest photosynthetic activity (the outer mantle), where drawdown of ^{12}C might lead to calcifying fluid with a higher isotopic ratio (Gannon et al. 2017). Instead, we found no systematic offsets in $\delta^{13}C$ values between species or shell layers, but did find statistically significant differences between the $\delta^{18}O$ values of *Tridacna squamosina* and the other species, as well as between the shell layers of all species. Because oxygen isotope values correspond directly to the temperature of formation for bivalve carbonate, we were able to track back that *T. squamosina* has a higher temperature of shell formation than its congeners in the Red Sea, which relates to its proposed shallower life habit. This work confirms that the extremely rare *T. squamosina*, only known from a few dozen life specimens, is indeed an obligate shallow dweller as proposed by prior workers (Richter et al. 2008). The outer shell layers of all clams measure 1.5 °C higher temperatures than the interior of the shell, which has relevance for any future work utilizing the outer shell layer for paleoclimatic study.

My final chapter investigates the comparative growth of fossil and modern assemblages of giant clams from sites surrounding the Gulf of Aqaba in the Northern

Red Sea. As with other reefs worldwide, coral reefs are under increasing stress from climate change, ocean acidification and nutrient stress due to pollution. Contrary to expectations, we observe an acceleration of growth in modern *Tridacna* compared to fossil specimens, consistent across all three species. This opposes trends observed in corals of the Red Sea, which have experienced slower growth (Cantin et al. 2010). We find that growth is significantly related to temperature, though mean recorded temperatures do not differ between modern and fossil specimens. We also investigated the nitrogen isotope composition (measured by $\delta^{15}N$ values) of shell organic material in fossil and modern specimens. Aquaculture studies of giant clams have determined that giant clams grow more quickly when nitrogen sources such as nitrate and ammonia are added, as these compounds directly fertilize the increased activity of photosymbionts within the clams (Belda et al. 1993). Using nitrogen isotopes to trace changing nutrient supply available to giant clams, we found a consistent decrease of mean $\delta^{15}N$ values in modern specimens consistent with an increased influx of ^{14}N-rich anthropogenic nitrate aerosols, a nitrogen flux not present in preindustrial times to the degree it is now (Wankel et al. 2010, Chen et al. 2007). We propose that the influx of nitrate has fertilized the growth of modern giant clams in the Red Sea, in addition to possible temperature changes.

This thesis represents several attempts to use bivalve sclerochronology as a proxy for the physiology of animals in the past and present. There is a demand for better baselines of organismal health that can be used to unite paleontological and neontological records, to understand the rise and fall of taxa in the face of

environmental change (Dietl and Flessa 2011). The shell diaries of bivalves are a flexible and high-resolution record that can be applied to answer such cross-disciplinary questions, whether we are trying to understand the reactions of marine organism to seasonal variability, to pollution, or to the current climate crisis placing organisms under unprecedented environmental stress.

References:

Batenburg SJ, Reichart G-J, Jilbert T, Janse M, Wesselingh FP, Renema W (2011) Interannual climate variability in the Miocene: High resolution trace element and stable isotope ratios in giant clams. Palaeogeography, Palaeoclimatology, Palaeoecology 306:75–81

Belda CA, Cuff C, Yellowlees D (1993) Modification of shell formation in the giant clam *Tridacna gigas* at elevated nutrient levels in sea water. Marine Biology 117:251–257

Chinzei K (2013) Adaptation of oysters to life on soft substrates. Historical Biology 25:223–231

Dietl GP, Flessa KW (2011) Conservation paleobiology: putting the dead to work. Trends in Ecology & Evolution 26:30–37

Fraser NM, Bottjer DJ, Fischer AG (2004) Dissecting "Lithiotis" bivalves: implications for the Early Jurassic reef eclipse. Palaios 19:51–67

Gannon ME, Pérez-Huerta A, Aharon P, Street SC (2017) A biomineralization study of the Indo-Pacific giant clam *Tridacna gigas*. Coral Reefs 36:503–517

Jantzen C, Wild C, El-Zibdah M, Roa-Quiaoit HA, Haacke C, Richter C (2008) Photosynthetic performance of giant clams, *Tridacna maxima* and *T. squamosa*, Red Sea. Marine Biology 155:211–221

Jones DS, Jacobs DK (1992) Photosymbiosis in *Clinocardium nuttalli*: Implications for tests of photosymbiosis in fossil molluscs. PALAIOS 7:86–95

Jones DS, Quitmyer IR (1996) Marking Time with Bivalve Shells: Oxygen Isotopes and Season of Annual Increment Formation. PALAIOS 11:340–346

Klumpp DW, Bayne BL, Hawkins AJS (1992) Nutrition of the giant clam *Tridacna gigas* (L.) I. Contribution of filter feeding and photosynthates to respiration and growth. Journal of Experimental Marine Biology and Ecology 155:105–122

Norton JH, Shepherd MA, Long HM, Fitt WK (1992) The zooxanthellal tubular system in the giant clam. The Biological Bulletin 183:503–506

Nützel A, Joachimski M, Correa ML (2010) Seasonal climatic fluctuations in the Late Triassic tropics—High-resolution oxygen isotope records from aragonitic bivalve shells (Cassian Formation, Northern Italy). Palaeogeography, Palaeoclimatology, Palaeoecology 285:194–204

Posenato R, Masetti D (2012) Environmental control and dynamics of Lower Jurassic bivalve build-ups in the Trento Platform (Southern Alps, Italy). Palaeogeography, Palaeoclimatology, Palaeoecology 361–362:1–13

Richter C, Roa-Quiaoit H, Jantzen C, Al-Zibdah M, Kochzius M (2008) Collapse of a new living species of giant clam in the Red Sea. Current Biology 18:1349–1354

Vaughn CC, Hoellein TJ (2018) Bivalve Impacts in Freshwater and Marine Ecosystems. Annual Review of Ecology, Evolution, and Systematics 49:183–208

Vermeij GJ (2013) The evolution of molluscan photosymbioses: a critical appraisal. Biological Journal of the Linnean Society 109:497–511

Walliser EO, Mertz-Kraus R, Schöne BR (2018) The giant inoceramid *Platyceramus platinus* as a high-resolution paleoclimate archive for the Late Cretaceous of the Western Interior Seaway. Cretaceous Research 86:73–90

Wankel SD, Chen Y, Kendall C, Post AF, Paytan A (2010) Sources of aerosol nitrate to the Gulf of Aqaba: Evidence from $\delta^{15}N$ and $\delta^{18}O$ of nitrate and trace metal chemistry. Marine Chemistry 120:90–99

CHAPTER 1

Identifying the Ticks of Bivalve Shell Clocks:

Seasonal Growth in Relation to Temperature and Food Supply

Abstract

Sclerochronology uses shell growth lines or bands for the construction of environmental time-series and the measurement of organism growth, but more study is needed to constrain the triggers of the dark cessation bands observed in many bivalve groups. We constructed a database of direct observations of modern growth seasonality across the class Bivalvia and compared the occurrence of seasonal growth bands to environmental data including latitude, temperature, and chlorophyll-a concentration. Bivalves with cold-season (winter) cessations are more common towards the poles, with logistic regression showing that temperature, followed by latitude of occurrence, displays the strongest relationship with occurrence of winter cessation. Remotely sensed and directly measured chlorophyll-a concentration show no significant relationship. Summer cessations are sparse and only weakly associated with environmental controls but are concentrated at the subtropical latitudes among temperate bivalves at their equatorial extremes. The rarity of summer cessations can be explained by the limited annual ranges of temperature in the tropics, combined with the exponential relationship of metabolic rate to temperature leading to a narrow window between normal functioning and mortality at high temperatures. This data suggests that, unless annual temperatures have low variability like in equatorial or polar regions, the season of growth cessation across bivalves is primarily a function

of temperature tolerance through restriction of scope for growth. At most latitudes, growth bands can be interpreted as being primarily triggered by temperature stress, rather than seasonal starvation.

Introduction

Bivalves secrete their shells at varying rates throughout the year, often forming white opaque increments correlating to optimal growth conditions and dark translucent growth lines or bands during adverse conditions when viewed under transmitted light (Schöne, 2008). These bands are useful for the identification of growth seasonality of extinct organisms (Stevenson and Dickie 1954; Richardson 1993; Jones and Quitmyer 1996; Veinott and Cornett 1996), and by extension their environmental preferences and thresholds of stress. The seasonal allocation of energy to shell growth within and between species has been proposed to be controlled primarily by temperature (Beukema et al. 1985, Jones and Quitmyer 1996), food supply (Incze et al. 1980; Pilditch et al. 1999), or spawning (Sato 1995), and is moderated by ontogeny (Ivany et al. 2003). While there is broad agreement that water temperature is an important determinant of seasonal skeletal growth in bivalves (Wefer and Berger 1991), it is less certain whether dark growth bands can be ascribed primarily to temperature stress rather than being a function integrating food supply, seasonal spawning, or other factors across species.

Previous attempts to relate overall annual shell growth to latitude usually focused on total growth or growth rate rather than the seasonal distribution of growth band formation (Weymouth et al. 1931; Ansell 1968; Bachelet 1980; Watson et al.

2012). Bivalves live longer and grow more slowly at higher latitudes (Moss et al. 2016), and specimens at lower latitudes within their range reach greater maximum sizes and shell thicknesses than high latitude counterparts (Watson et al. 2012). Past work often modeled growth of bivalves using a Von Bertalanffy growth curve fitted with a seasonally varying coefficient (Cloern and Nichols 1978), or used principal component analysis to quantify the influence of different environmental variables on growth within a species (Witbaard et al. 1999). However, a cross-species attempt to relate growth to latitude was inconclusive, largely because of the confounding effects of relative shell shape (Vakily 1992). Other studies uncovered a strong seasonal relationship between metabolic rate and soft tissue growth with both temperature and food supply, but seasonal variability in growth of hard parts, while investigated intensively from the standpoint of individual species, has not been aggregated across taxa (Brockington and Clarke 2001). However, there is some evidence that the seasonal timing of growth band formation may also switch across the latitudinal range of a species. Pleistocene and modern oysters experience warm-season (summer) cessations in shell extension at the equatorial end of their range and cold-season (winter) cessations at the polar end (Kirby et al. 1998), as do quahogs (Ansell 1968; Surge and Walker 2006) and other mollusks such as limpets (Surge et al. 2013), but it is not clear whether these patterns can be generalized across bivalves.

Bivalves have a limited energy budget and experience constricted aerobic scope for growth when adverse stresses such as extreme temperatures, low food availability, or excess turbidity increase the energy expenditure required for survival

(Schöne 2008). Metabolic oxygen supply and demand become increasingly mismatched at temperature extremes because of the temperature-dependence of metabolic rate and the increasing need for cellular protection and damage repair (Pörtner 2012; Sokolova 2013). Likewise, limited food supplies reduce total energy production such that less is available for growth, reproduction, or other activities once basal metabolic and maintenance needs are met (Sokolova 2013). In addition, gametogenesis represents a significant energy investment for bivalves and occurs on seasonal scales (Newell and Bayne 1980; Sato 1995; Gaspar et al. 1999).

These dynamics affect bivalve populations in response to climate change (Pörtner et al. 2005), while acute stresses may cause mortality during extreme conditions such El Niño warming events (Urban 1994), but the influence on seasonal scales is still poorly understood. Seasonally moderated sources of physiological stress are distinct from acute environmental stresses because they are periodic and gradual. Many organisms are more susceptible to temperature changes, and therefore suffer proportionally larger restriction of scope for growth, when such stresses occur over a long period, a concept known as "thermal inertia" (Peck et al. 2009; Lah et al. 2017). These chronic sources of stress and their impacts on scope for growth represent a gap in knowledge, largely due to the difficulty in simulating realistic environmental variation at population scale in an experimental setting. Because metabolic rate and temperature follow an exponential relationship (Martin and Huey 2008; Payne and Smith 2017), it can be difficult to conduct cross-species comparisons of physiological tolerance at the narrow interval between normal seasonal stress and mortality.

Bivalves inhabit environments with widely differing degrees of environmental variation, from the relatively stable deep subtidal to the extreme intertidal, exacerbating the difficulty of simulating cross-species responses with experimental designs capturing the true diversity of habitats. Shell formation has been found to represent a relatively small proportion of bivalve energy budgets and could be precisely the type of minor energy allocation that would be mediated by sublethal seasonal stress (Watson et al. 2017). Annual band formation could therefore be a marker of this inertial response across species and environments, because the bands indicate a slowdown in growth potentially leading up to complete seasonal cessation in response to sustained environmental stress.

We focused on formation of shell bands potentially visible in fossil specimens to ground-truth paleobiological studies where we inherently lack direct observations of growth in extinct organisms. We coded seasonal growth as a binary variable, which can be related to continuous variables such as latitude, temperature, productivity, and depth using logistic regression. This cross-species analysis will assist in determining the most likely environmental constraints on the triggers of growth band formation and the physiology of extinct bivalve species.

Methods

We surveyed the existing literature of bivalve growth, gathering 294 direct observations of marine or brackish estuarine bivalve growth for 115 species from 183 publications in ecology, earth science and aquaculture journals (Fig. 1) (see Online Supplemental File, data set 1). These observations included absolute latitude and

season of growth cessation if one was present. We focused on direct observations of cessation through mark-recapture, internal growth band or population length-frequency studies because other techniques, such as post-hoc observations of external growth bands, are believed to be confounded by tidal, reproductive and other intermittent growth cessations (Schöne, 2008). We coded cessation as 1 and continuous growth as 0 by season; for example, a species growing year-round at a location at winter and summer would have values of [0, 0]. Because fall and spring are less certain in their comparative definition in differing climate zones, we use 'winter' and 'summer' to refer to cold-season and warm-season cessations, respectively. We recorded a shutdown when the researchers made mention of 'cessation,' 'shutdown,' 'negligible growth' or other similar keywords in reference to specific months or seasons (climatological season rather than calendar season). We avoided observations of juvenile or senescent individuals, which are more likely to experience year-round growth or constricted growth seasons, respectively (Ivany et al. 2003). If juvenile or senescent status were unclear (keywords such as "spat", "juvenile", "post-reproductive," etc.), we only integrated observations with an explicit age falling in the mid-range of its species' respective growth curve, avoiding those at the indeterminate rapid juvenile stage or flattened senescent state. Authors varied in their terminology, sometimes noting 'slowdowns' with unclear criteria behind their meaning, as opposed to clearer terminology such as 'shutdown' or 'cessation.' Where these occurred, we noted that they were slowdowns, rather than complete cessations and ran analyses to confirm that trends were consistent with and

without these slowdown cases. Among our collected data, too few sources noted the occurrence of a cessation specifically corresponding to gametogenesis or reproduction to conduct a global analysis of their occurrence.

Some publications also recorded local temperature range based on high and low temperatures, which we recorded when provided. To control for possible methodological differences in temperature measurement between studies (depth and temporal resolution), we also downloaded daily remotely sensed sea surface temperature for the years 2004–2014 from the NOAA OI SST V2 Dataset (see Online Supplemental File, data set 4). This 0.25-degree gridded data allowed us to determine the influence of true daily high and low temperature on the occurrence among the bivalves in our dataset.

We also recorded chlorophyll-a (chl-a) concentration when reported in the study, which can be used as a proxy for productivity. While bivalves have flexibility in their food supply, we settled on chl-a and therefore phytoplankton abundance as the best measure of food availability because phytoplankton, as primary producers, represent the greatest proportional amount of biomass and are the most seasonally variable in abundance, often blooming at the end of the winter months and outmassing higher trophic levels of plankton by several orders of magnitude (Harris 1986). Grazing zooplankton, by contrast, often lag phytoplankton in their appearance and thus display weaker seasonality. Because chl-a was not reported in all papers, we also downloaded monthly average 4.6 km grid chl-a concentration data output from the VGPM global productivity model as a proxy for food supply (growth data with

appended satellite productivity data in Online Supplemental File, data set 2). This model aggregates remote spectrometry data from the MODIS satellite observatory and uses a model-based approach to control for environmental confounding variables such as coastal turbidity and cloud cover (Behrenfeld and Falkowski 1997). We correlated each of our observation sites to the nearest pixel in the dataset using BEAM remote sensing visualization software and found average monthly chl-a results for the period 2003–2014. While satellite ocean color data has been used to study temporal variability in coastal productivity, we sought to corroborate these results with an independent set of *in situ* direct observations of productivity from our sites, as coastal productivity can sometimes be subject to localized trends (D'Ortenzio et al. 2002; Lavender et al. 2004; Yamada et al. 2005; Hyde et al. 2007). To this end, we also aggregated direct chl-a-based measurements of productivity from various data sources collected within the same satellite grid cell and at similar depths to the observed bivalves (these independent chl-a sources are included in the Online Supplemental File, data set 3). These data were then averaged to monthly resolution for easier comparison to the remote sensing output.

We compiled and analyzed the relative contribution of environmental factors including absolute latitude, low/high seasonal temperature (lowest and highest daily values reported), low/high seasonal monthly mean productivity and local temperature range via principal components analysis (PCA) on a correlation matrix. Visual analysis of these four environmental variables on paired PCA plots allowed us to

identify patterns in occurrence of cessation types in bivalves in relation to their local environmental conditions.

Results

Cessation Related to Latitude and Temperature

Winter cessations are prevalent in bivalves above 25 degrees latitude, becoming increasingly common at higher latitudes, whereas summer cessations are concentrated in the subtropical zone between 15–30 degrees (Fig. 2). A small subset of populations, many of which are constricted at the polar end of their range including the Gulf of California, Gulf of Mexico, and Adriatic (Quitmyer et al. 1985; Arneri et al. 1998; Schöne et al. 2002) (Fig. 1), have both winter and summer cessations. In our data, populations with no recorded seasonal cessation (growing year-round) are common at the equatorial latitudes (Fig. 2).

We first separated cessation type by season and related each binary variable to absolute latitude. There is a significant positive relationship between latitude and the occurrence of winter cessation (Fig. 3A) (log-odds ratio 0.055, $p < 0.0001$), with the odds of winter cessation increasing by 5.6% per degree latitude (95% CI: 3.4–8.2%). This association, as well as all others following (for winter cessation events), hold regardless of whether "slowdown" events are excluded (log-odds ratio 0.059, $p < 0.0001$).

Summer cessation also has a significant relationship with latitude, with a one degree increase in latitude leading to 3% decrease in probability of shutting down in the summer months (log-odds ratio -0.029, $p = 0.0114$). However, the relationship is

a much weaker fit to the data (Fig. 3B) compared to the winter cessation model (Fig. 3A), with a predicted summer cessation probability of only 50% at equatorial latitudes. The predicted summer cessation probabilities fail to converge towards 1 at the lower, high-temperature latitudes largely because the occurrences of summer cessation are concentrated at the lower temperate latitudes rather than in the equatorial zone where bivalves tend to grow year-round.

Winter cessation is significantly associated with minimum local seasonal temperature, with a stronger relationship than that of latitude alone. The odds of winter cessation increased by 14.7% for each degree Celsius decrease in temperature (log-odds ratio = -0.13, $p < 0.0001$, 95% CI: 8.1–21.4%) (Fig. 3C). Populations with winter cessations also experience a significantly wider temperature range (mean 15.27°C) than species without such a cessation (mean 11.25°C) (Welch's t-test: $t = 3.82$, $df = 87.64$, $p < 0.0001$). A multiple logistic regression (Table 1) showed that this relationship is significant, independent of the influence of latitude (temperature range is known to increase with latitude within the range of our data). There is no significant difference in mean temperature range between species with a summer cessation and those without. Summer cessation displays no significant relationship with summer maximum locally recorded temperature (log-odds ratio 0.009, $p = 0.7$). However, summer cessation does relate significantly to highest mean remotely sensed daily sea-surface temperature (log-odds ratio 0.106, $p = 0.0015$). Among the recorded temperatures in our database, there was great variability in methodology of temperature data collection and reporting, in terms of frequency, depth, and method

of collection, which necessitated using a more standardized remote sensing data source to see whether true annual maxima were being excluded. This relationship is slightly stronger when only temperate bivalves occurring above 20 degrees latitude are included, which experience more annual variability in temperature (log-odds ratio 0.153, p-value < 0.001).

Effects of Food Supply

There is no significant relationship between the occurrence of winter cessation and remote-sensed winter minimum chl-a concentration, which we set as the lowest monthly mean chl-a from October to March in the Northern hemisphere, and April to September in the Southern hemisphere (log-odds ratio: -0.005, p = 0.27). The majority of observation sites instead experience a productivity maximum in the late winter or early spring months according to the chl-a data. While phytoplankton productivity is dependent on insolation that is seasonally modulated, it is also limited by nutrient scarcity during times of thermal stratification. Shelf phytoplankton in the temperate zone typically thrive during the period when insolation is increasing but upwelling from deeper-nutrient rich waters has not been disrupted by the formation of a thermocline (Legendre 1981). Direct observations of monthly chl-a concentration were available for 34 stations, and corroborate the results observed from the remote-sensing sourced data (Online Supplemental File, data set 3). A logistic regression showed no significant relationship between occurrence of a winter cessation and the directly measured low winter productivity of the study sites (lowest monthly mean

from winter months), even when normalized by the sites' annual average to remove significant inter-site variability (log-odds ratio: 0.101, $p = 0.52$).

Combined Effects of Multiple Stressors

We can also interpret the relationship of winter cessation to multiple environmental variables using principal component analysis (Fig. 4A). PC1 explains 52% of the variance and reflects the effects of minimum temperature and latitude. PC2 explains 26% of the variance, associated with winter minimum chl-a and annual temperature range. Bivalves with winter cessations tend to occur at low values on PC1, indicating higher latitude and colder annual minimum temperatures, whereas bivalves that grow throughout the winter tend to cluster at higher values of PC1 with warmer annual minimum temperatures. In contrast, observations of winter cessations are distributed along the PC2 axis, indicating a weaker relationship with minimum chl-a or annual temperature range. A similar PCA plot showing the distribution of summer cessations relating to summer maximum temperature, latitude, temperature range, and summer minimum chl-a shows little grouping or correspondence of cessation in relation to the environmental variables (Fig. 4B).

For a quantitative test of the relative significance of the different variables, we used a multiple logistic regression. When integrating latitude, winter minimum chl-a concentration, temperature range, and minimum local temperature into the equation predicting winter cessation, minimum local temperature and temperature range are the only coefficients with p-values indicating significance (Table 1). Quantitatively

and qualitatively, food supply has little correspondence to the data, and temperature has the strongest influence on cessation occurrence, followed by latitude.

Discussion

Latitude and Temperature

The most powerful predictor of growth seasonality in bivalves, and thus the formation

of a dark growth line in the shells, is temperature. Winter cessation is the most prevalent growth pattern among our recorded observations, especially above 25° latitude, where seasonality is more extreme. Among these individuals, the most important variable explaining cessation is low annual temperature, followed by the observed range of temperature. Latitude also explains a significant amount of the variance, because it is a proxy for temperature that approximately decreases from equator to pole. This result is consistent with laboratory studies of single bivalve species, which also find temperature to be a hard constraint on bivalve scope for growth, independent of food supply (Laing 2000). Despite the presence of strong winter productivity at some of our study locations, winter cessations may dominate because very low temperature can prevent bivalves from filter feeding and/or metabolizing ingested material to fuel shell growth.

Although cold temperatures are a reliable trigger of winter cessation among bivalves, summer cessations are not as closely linked to high temperature and are not as widespread. Logistic regression plots of summer cessation do not converge near 1 for the highest temperatures experienced by bivalves in our dataset, unlike winter

cessations in response to low temperature. This is largely because summer cessations are rare near the equator; growth cessations display a stronger relationship with daily remote sensed temperature data when equatorial observations are excluded. The spatial patterns of summer cessations, concentrated in the subtropical latitudes around 15–30 degrees, likely arises from a combination of unusually stable temperatures in equatorial regions, as well as from physiological limitations and adaptations in bivalves.

Subtropical latitudes are distinguished by large seasonal temperature ranges and warm fsummer maximum temperatures. Bivalves experiencing summer cessation in this band of latitudes may experience true high temperature-triggered shell growth cessation, as they may be under temperature stress at both extremes and cannot merely adapt to the warmest temperatures. Equatorial habitats have low annual temperature variability, so summer temperatures are typically not high enough in comparison to the annual average to place most bivalves under regular metabolic stress (Conover 1992). Though some equatorial species experience interruptions in shell formation during times of acute heat stress, such as on the coast of South America during El Niño warming events (Lazareth et al. 2006), these interruptions are a sign of near-mortality due to low-frequency extremes, rather than an encoded response of the organism to annual temperature fluctuations.

High-temperature cessations may be rare in general due to the effects of temperature on ectotherm physiology. The exponential relationship between temperature and metabolic rate leads to an asymmetrical thermal performance curve

in many species, with a sharp transition between warm-water optimum and declining performance (Martin and Huey 2008; Payne and Smith 2017). As a result, some mollusks show a sigmoidal relationship between shell formation rate and temperature, with a similarly sharp transition from temperature-accelerated growth to mortality (Irie and Morimoto 2016). The abrupt decline in fitness and shell formation rate near the high-temperature extreme leads to a narrow window for inducing a heat stress-related growth band, while still remaining below the threshold temperature that would trigger mortality Furthermore, equatorial bivalves can adapt their entire metabolic regime to ensure survival at these extremes, prioritizing growth at higher temperatures at the expense of efficiency at lower normal seasonal temperatures (Riascos et al. 2012), and can also reschedule their growth to prioritize growth during cooler summer nights (Schöne et al. 2006). Bivalves therefore may maintain a greater safety margin in their thermal physiology (Martin and Huey 2008), minimizing the likelihood of high-temperature growth band formation to avoid the risk of mortality, potentially explaining the comparative rarity of summer cessations in our dataset.

With temperature exerting a strong control on the overall metabolic rate of bivalves, the allocation of energy to shell extension may be one of the first expenditures to be curtailed during times of extreme temperature. This aligns with the results of a lab culture study, which confirmed that temperatures outside of a normative range experienced by the pearl oyster *Pinctada margaritifera* influences the expression of genes related to biomineralization (Joubert et al. 2014). Bivalve shell growth is consistent with an energy balance between metabolic costs and

available energy supply dictating scope for growth in invertebrate organisms (Sokolova 2013). Bivalves grow their shells during times of favorable temperature, but not when temperatures fall outside certain seasonal thresholds (Schöne 2008). This suggests that the constricted scope for growth resulting from low, or less commonly high, ambient temperature results in the bivalve reducing energy allocated for shell extension.

Food Supply

Although food availability can influence growth rate, especially of soft tissue mass (Thompson and Nichols 1988), chl-a has a limited relationship with the occurrence of winter cessations at a global scale in our dataset. While some previous observations of winter cessation have been proposed to be due to starvation resulting from low seasonal productivity (Incze et al. 1980), in our collected observations we observed no significant relationship between seasonal chl-a availability and the occurrence of a cessation. A majority of stations have winter minimum chl-a concentration between the months of February and April, yet most of our recorded cessations begin at the start of winter. While we anticipated phytoplankton to exhibit high seasonal variability due to the impact of seasonal insolation and temperature on photosynthetic output, our dataset shows no such clear patterns in seasonal phytoplankton abundance across latitudes, confirming other prior attempts to find such trends (Winder and Cloern 2010). In many regions of the world, phytoplankton experience complex seasonal variability deviating from the 12-month period that would be expected if seasonal insolation and temperatures were the major controlling

variables, and many experienced no seasonal regularity at all (Winder and Cloern 2010). Other experimental attempts to determine timing of bivalve shell growth in relation to peak food availability have had varying levels of success across species, with some finding a poor or mixed relationship (Schöne et al. 2006) but others arguing for a stronger link (Joubert et al. 2014). In general, we assert that while productivity may influence bivalve growth, at most latitudes it does not experience the seasonality needed to explain the occurrences of annual growth cessation observed in our dataset.

It is possible that limitations in the coverage or resolution of remotely sensed chl-a productivity may have obscured a relationship between food supply and growth cessations. Remote-sensing sourced chl-a models are calibrated from observational data (D'Ortenzio et al. 2002; Lavender et al. 2004; Yamada et al. 2005; Hyde et al. 2007) and have been widely used to assess productivity (Halfar et al. 2004), but the models may be less accurate in oceanographically complex coastal regions. Nevertheless, to rule out the possibility of inaccuracies in the coastal productivity proxy, we also compared the occurrence of growth cessations to direct measurements made at the same locations (see Online Supplemental File, data set 3). The use of direct chl-a measurements did not strengthen the relationship with growth cessation, suggesting an overall limited effect of food supplies on growth band formation.

Many bivalve species also exhibit great flexibility in their food sources outside of phytoplankton, consuming particulate organic matter, detritus, and bacteria (Stephenson and Lyon 1982; Langdon and Newell 1989; Kang et al. 1999), but these

other food sources are less likely to exhibit annual seasonality relating to insolation or temperature in a manner that is consistent between sites. Zooplankton, for example, usually lag behind in abundance following spring phytoplankton blooms due to their longer generation time, and also have been found to exhibit great interannual plasticity in their phenology (Mackas et al. 2012). The other food sources, due to a comparative lack of seasonality, could represent another potential explanation for the lack of a seasonal relationship between chl-a and growth. A significant proportion of the species in our dataset may be calling upon alternate food sources during times of seasonal food stress.

Polar and high-latitude bivalves may represent an exception to the trends seen in our dataset. *Arctica islandica* and other high-latitude bivalves can experience winter cessations at times of low non-phytoplankton food availability in locations with almost no annual variability in temperature (Witbaard 1996; Sejr et al. 2002, Schöne et al. 2005; Butler et al. 2013). For example, the northernmost populations of *A. islandica* open their valves more widely when chl-a is high, with the gaping in turn correlating to faster shell growth (Ballesta-Artero et al. 2017). Our dataset lacks the coverage in polar regions necessary to identify significant predictive relationships between the occurrence of winter cessations and food supply in these localities. These extreme environments, where food supply displays stronger seasonal signatures than temperature, could be an exception to the temperature-growth relationship we observed across bivalves at subtropical to subpolar latitudes. Polar environments, with low temperature variability but extreme seasonal variations in food quantity,

could represent an energetic regime that requires true annual starvation-related cessations in growth for bivalves.

Other Cessation Triggers

Although temperature is a key overarching control on bivalve growth, and food supply may be important where temperature is extremely stable, other factors can locally be significant. For example, salinity stresses often affect species in intertidal zones exposed to monsoonal influxes of freshwater, such as the coasts of India. Bivalves in these regions are exposed to frequent reductions of salinity during the rainy season which trigger them to close their shells to maintain homeostatic osmotic pressure (Nayar and Rao 1985). Many bivalves also experience short cessations during spawning times when energy is dedicated to gonadal development rather than shell growth (Sato 1995). These interruptions are usually distinguished by thin, well-defined dark growth lines of uneven periodicity rather than the thick, periodic bands which match up to seasonal temperature trends, or may not result in the formation of a growth line at all, particularly for the bivalves whose gametogenic period coincides with improving condition indices (Newell and Bayne 1980; Gaspar et al. 1999). Such growth bands can nevertheless make it difficult to discern the start or end of growth seasons, particularly when trying to identify growth from external rather than internal growth bands (Clark 1974). In general, across the bivalves recorded in our dataset, reproductive events are not a consistently recorded trigger of growth bands useful for diagnosing periodicity of samples along the growth axis in a shell, though additional study of the latitudinal and environmental factors determining

bivalve spawning time may help shed more light on the interactive effects of spawning time and annual shell growth cessation. Further work could identify whether there are phylogenetic or spatial associations influencing the occurrence of reproductive interruptions and the biases they introduce to estimates of life history based on annual bands.

Implications for Sclerochronology

Sclerochronology, the study of sequential growth bands in calcifying organisms, has been broadly applied to help answer paleoclimatological and paleophysiological questions. Because shell-growth patterns provide unique utility to reconstruct seasonality due to their higher resolution in comparison to sedimentological records, it is important to understand the seasonal controls on shell deposition. Bivalves with a winter cessation will record warmer average annual temperatures but, as the climate warms, that cessation might disappear or even switch seasons, necessitating a correction between paleoclimate proxy records from populations at different times, and also corrections between taxa (Schöne et al. 2006). If that cessation was due more to food supply than temperature, its seasonality could be altered through time if the nutrient regime at that location changed, also influencing the fidelity and comparability of proxy records. These questions can only be addressed if the dominant cause of bivalve growth cessation is known, and we propose that these annual bands are primarily a function of temperature related stress, rather than starvation.

A study of the cessation temperatures of bivalves during a past climate change would help shed light on whether bivalves are able to evolve their thermal tolerance in response to changing temperatures. Shifts in the seasonality of growth cessations (from winter to summer, or the reverse) in response to changing temperature may imply limited adaptability in thermal tolerance. Bivalves may instead be forced to migrate or may suffer stunted growth or local extinction. In contrast, shifts in the onset temperature of growth cessation would indicate that the species can, at least partially if not totally, adapt to changing temperatures by adjusting its thermal tolerance window.

Conclusion

The formation of dark growth lines or bands in bivalves from subtropical to subpolar latitudes is primarily triggered by low temperature exposure rather than seasonal food deprivation. This suggests that temperature-linked metabolic constraints, manifesting as reduced scope for growth, are the primary control on bivalve shell growth across most latitudes. Conversely, high-temperature restrictions across bivalve species are less widespread. Summer cessations may be infrequent because warm equatorial oceans have limited temperature variability. In addition, thermal performance curves are asymmetrical, with a narrow window between optimum and mortality at high temperatures, so the range of temperatures over which growth bands can form is limited. Bivalves may also need to maintain a greater safety margin at high temperatures because of the risk of mortality with small temperature increases. At equatorial latitudes, cessations are likely caused by non-temperature

related local factors, but the majority of bivalves grow almost year-round. Bivalves with summer cessations may be constricted outside of their ideal temperature regime by geographic or other factors.

Food supply is not a primary control on the seasonal timing of growth cessation but may become locally important in regions of low temperature variability and high productivity variability, such as in polar areas. Although nutrition may be important in certain situations, such as in polar environments where temperature is stable, food supply does not vary systematically or predictably with time or space, as bivalves have flexibility to use different food sources, and temperature may have a stronger influence on aerobic scope for growth. Other environmental stresses, such as reduced salinity, can also trigger growth band formation, but only in unusual local circumstances.

The primary importance of temperature in the formation of growth bands provides opportunities for assessing the impacts of climate changes on marine organisms. Studies of growth band timing in fossil populations across ancient climate change events can constrain whether bivalves are able to adapt their physiological thermal tolerances to temperature change by shifting the onset temperature of growth cessation. More investigation is needed into whether seasonal cessation is a deeply conserved or more adaptable response to changing environmental conditions.

Acknowledgements

We wish to thank Sarah Sullivan for assisting with gathering publications and entering data, Robert O'Malley and Oregon State for hosting the VGPM data

products, NOAA for its online database of daily SSTs, as well as the SeaWIFS project which provided the ocean color basis for the productivity model. We wish to thank David Rodland and an anonymous reviewer for their helpful peer reviews, as well as Bernd Schöne for additional editorial comments.

Supplemental Material

Data are available from the PALAIOS Data Archive:

http://www.sepm.org/pages.aspx?pageid=332.

References

Ansell AD (1968) The Rate of Growth of the Hard Clam *Mercenaria mercenaria* (L) throughout the Geographical Range. ICES J Mar Sci 31:364–409

Aru V, Balling Engelsen S, Savorani F, Culurgioni J, Sarais G, Atzori G, Cabiddu S, Cesare Marincola F (2017) The Effect of Season on the Metabolic Profile of the European Clam *Ruditapes decussatus* as Studied by ^{1}H-NMR Spectroscopy. Metabolites 7:36

Bachelet G (1980) Growth and recruitment of the tellinid bivalve *Macoma balthica* at the southern limit of its geographical distribution, the Gironde estuary (SW France). Mar Biol 59:105–117

Ballesta-Artero I, Witbaard R, Carroll ML, Meer J van der (2017) Environmental factors regulating gaping activity of the bivalve *Arctica islandica* in Northern Norway. Mar Biol 164:116

Behrenfeld MJ, Falkowski PG (1997) Photosynthetic rates derived from satellite-based chlorophyll concentration. Limnol Oceanogr 42:1–20

Beukema JJ, Knol E, Cadée GC (1985) Effects of temperature on the length of the annual growing season in the tellinid bivalve *Macoma balthica* (L.) living on tidal flats in the Dutch Wadden Sea. Journal of Experimental Marine Biology and Ecology 90:129–144

Brockington S, Clarke A (2001) The relative influence of temperature and food on the metabolism of a marine invertebrate. Journal of Experimental Marine Biology and Ecology 258:87–99

Cardoso JFMF (2007) Growth and reproduction in bivalves: An energy budget approach. University of Groningen

Clark G (1974) Growth Lines in Invertebrate Skeletons. Annual Review of Earth and Planetary Sciences 2:77–99

Cloern JE, Nichols FH (1978) A von Bertalanffy growth model with a seasonally varying coefficient. Journal of the Fisheries Research Board of Canada 35:14791482

Conover DO (1992) Seasonality and the scheduling of life history at different latitudes. Journal of Fish Biology 41:161–178

D'Ortenzio F, Marullo S, Ragni M, Ribera d'Alcalà M, Santoleri R (2002) Validation of empirical SeaWiFS algorithms for chlorophyll-a retrieval in the Mediterranean Sea. Remote Sensing of Environment 82:79–94

Gaspar MB, Ferreira R, Monteiro CC (1999) Growth and reproductive cycle of *Donax trunculus* L.,(Mollusca: Bivalvia) off Faro, southern Portugal. Fisheries Research 41:309–316

Halfar J, Godinez-Orta L, Mutti M, Valdez-Holguín JE, Borges JM (2004) Nutrient and temperature controls on modern carbonate production: An example from the Gulf of California, Mexico. Geology 32:213–216

Harris G (1986) Phytoplankton Ecology: Structure, Function and Fluctuation. Chapman and Hall, New York

Hyde KJW, O'Reilly JE, Oviatt CA (2007) Validation of SeaWiFS chlorophyll a in Massachusetts Bay. Continental Shelf Research 27:1677–1691

Incze LS, Lutz RA, Watling L (1980) Relationships between effects of environmental temperature and seston on growth and mortality of *Mytilus edulis* in a temperate northern estuary. Mar Biol 57:147–156

Irie T, Morimoto N (2016) Intraspecific variations in shell calcification across thermal window and within constant temperatures: Experimental study on an intertidal gastropod *Monetaria annulus*. Journal of Experimental Marine Biology and Ecology 483:130–138

Ivany LC, Wilkinson BH, Jones DS (2003) Using Stable Isotopic Data to Resolve Rate and Duration of Growth throughout Ontogeny: An Example from the Surf Clam, *Spisula solidissima*. PALAIOS 18:126–137

Jones DS, Quitmyer IR (1996) Marking Time with Bivalve Shells: Oxygen Isotopes and Season of Annual Increment Formation. PALAIOS 11:340–346

Joubert C, Linard C, Moullac GL, Soyez C, Saulnier D, Teaniniuraitemoana V, Ky CL, Gueguen Y (2014) Temperature and Food Influence Shell Growth and Mantle Gene Expression of Shell Matrix Proteins in the Pearl Oyster *Pinctada margaritifera*. PLOS ONE 9:e103944

Kang CK, Sauriau PG, Richard P, Blanchard GF (1999) Food sources of the infaunal suspension-feeding bivalve *Cerastoderma edule* in a muddy sandflat of Marennes-Oléron Bay, as determined by analyses of carbon and nitrogen stable isotopes. Mar Ecol Prog Ser 187:147–158

Kirby MX, Soniat TM, Spero HJ (1998) Stable isotope sclerochronology of Pleistocene and Recent oyster shells (*Crassostrea virginica*). PALAIOS 13:560

Lah RA, Benkendorff K, Bucher D (2017) Thermal tolerance and preference of exploited turbinid snails near their range limit in a global warming hotspot. Journal of Thermal Biology 64:100–108

Laing I (2000) Effect of temperature and ration on growth and condition of king scallop (*Pecten maximus*) spat. Aquaculture 183:325–334

Langdon C, Newell R (1989) Utilization of detritus and bacteria as food sources by two bivalve suspension-feeders, the oyster *Crassostrea virginica* and the mussel *Geukensia demissa*. Marine Ecology Progress Series 58:299–310

Lavender SJ, Pinkerton MH, Froidefond J-M, Morales J, Aiken J, Moore GF (2004) SeaWiFS validation in European coastal waters using optical and bio-geochemical measurements. International Journal of Remote Sensing 25:1481–1488

Lazareth CE, Lasne G, Ortlieb L (2006) Growth anomalies in *Protothaca thaca* (Mollusca, Veneridae) shells as markers of ENSO conditions. Clim Res 30:263–269

von Leesen G, Beierlein L, Scarponi D, Schöne BR, Brey T (2017) A low seasonality scenario in the Mediterranean Sea during the Calabrian (Early Pleistocene) inferred from fossil *Arctica islandica* shells. Palaeogeography, Palaeoclimatology, Palaeoecology

Legendre L (1981) Hydrodynamic Control of Marine Phytoplankton Production: The Paradox of Stability++Contribution to the programme of GIROQ (Groupe interuniversitaire de recherches océanographiques du Québec). In: Nihoul J.C.J. (eds) Elsevier Oceanography Series. Elsevier, pp 191–207

Mackas DL, Greve W, Edwards M, Chiba S, Tadokoro K, Eloire D, Mazzocchi MG, Batten S, Richardson AJ, Johnson C, Head E, Conversi A, Peluso T (2012) Changing zooplankton seasonality in a changing ocean: Comparing time series of zooplankton phenology. Progress in Oceanography 97–100:31–62

Martin TL, Huey RB (2008) Why "Suboptimal" Is Optimal: Jensen's Inequality and Ectotherm Thermal Preferences. The American Naturalist 171:E102–E118

Miller C (2012) Biological Oceanography. Wiley-Blackwell,

Moore TS, Campbell JW, Dowell MD (2009) A class-based approach to characterizing and mapping the uncertainty of the MODIS ocean chlorophyll product. Remote Sensing of Environment 113:2424–2430

Moss DK, Ivany LC, Judd EJ, Cummings PW, Bearden CE, Kim W-J, Artruc EG, Driscoll JR (2016) Lifespan, growth rate, and body size across latitude in marine Bivalvia, with implications for Phanerozoic evolution. Proc R Soc B 283:20161364

Nayar KN, Rao KS (1985) Molluscan Fisheries of India. Marine Fisheries Information Service, Technical and Extension Series 61:1–7

Newell RIE, Bayne BL (1980) Seasonal changes in the physiology, reproductive condition and carbohydrate content of the cockle *Cardium* (=*Cerastoderma*) *edule* (Bivalvia: Cardiidae). Mar Biol 56:11–19

Payne NL, Smith JA (2017) An alternative explanation for global trends in thermal tolerance. Ecol Lett 20:70–77

Peck LS, Clark MS, Morley SA, Massey A, Rossetti H (2009) Animal temperature limits and ecological relevance: effects of size, activity and rates of change. Functional Ecology 23:248–256

Pilditch CA, Grant J (1999) Effect of temperature fluctuations and food supply on the growth and metabolism of juvenile sea scallops (*Placopecten magellanicus*). Marine Biology 134:235–248

Pörtner HO, Langenbuch M, Michaelidis B (2005) Synergistic effects of temperature extremes, hypoxia, and increases in CO_2 on marine animals: From Earth history to global change. J Geophys Res 110:C09S10

Rao GS (1988) Biology of *Meretrix casta* (Chemnitz) and *Paphia malabarica* (Chemnitz) from Mulky estuary, Dakshina Kannada. CMFRI Bulletin 42:148–153

Riascos JM, Avalos CM, Pacheco AS, Heilmayer O (2012) Testing stress responses of the bivalve *Protothaca thaca* to El Niño–La Niña thermal conditions. Marine Biology Research 8:654–661

Richardson CA (1993) Bivalve shells: chronometers of environmental change. 419–434

Rysgaard S, Nielsen TG, Hansen BW (1999) Seasonal variation in nutrients, pelagic primary production and grazing in a high-Arctic coastal marine ecosystem, Young Sound, Northeast Greenland. Mar Ecol Prog Ser 179:13–25

Sato S (1995) Spawning Periodicity and Shell Microgrowth Patterns of the Venerid Bivalve *Phacosoma japonicum*. Veliger 38:

Schöne BR (2008) The curse of physiology—challenges and opportunities in the interpretation of geochemical data from mollusk shells. Geo-Mar Lett 28:269–285

Schöne BR, Lega J, W. Flessa K, Goodwin DH, Dettman DL (2002) Reconstructing daily temperatures from growth rates of the intertidal bivalve mollusk *Chione cortezi* (northern Gulf of California, Mexico). Palaeogeography, Palaeoclimatology, Palaeoecology 184:131–146

Schöne BR, Rodland DL, Fiebig J, Oschmann W, Goodwin D, Flessa KW, Dettman D (2006) Reliability of Multitaxon, Multiproxy Reconstructions of Environmental Conditions from Accretionary Biogenic Skeletons. The Journal of Geology 114:267–285

Sejr MK, Jensen TK, Rysgaard S (2002) Annual growth bands in the bivalve *Hiatella arctica* validated by a mark-recapture study in NE Greenland. Polar Biol 25:794–796

Sison CP, Glaz J (1995) Simultaneous Confidence Intervals and Sample Size Determination for Multinomial Proportions. Journal of the American Statistical Association 90:366–369

Sokolova IM, Frederich M, Bagwe R, Lannig G, Sukhotin AA (2012) Energy homeostasis as an integrative tool for assessing limits of environmental stress tolerance in aquatic invertebrates. Marine Environmental Research 79:1–15

Stephenson RL, Lyon GL (1982) Carbon-13 depletion in an estuarine bivalve: Detection of marine and terrestrial food sources. Oecologia 55:110–113

Stevenson JA, Dickie LM (1954) Annual Growth Rings and Rate of Growth of the Giant Scallop, *Placopecten magellanicus* (Gmelin) in the Digby Area of the Bay of Fundy. J Fish Res Bd Can 11:660–671

Surge D, Walker KJ (2006) Geochemical variation in microstructural shell layers of the southern quahog (*Mercenaria campechiensis*): Implications for reconstructing seasonality. Palaeogeography, Palaeoclimatology, Palaeoecology 237:182–190

Surge D, Wang T, Gutiérrez-Zugasti I, Kelley PH (2013) Isotope sclerochronology and season of annual growth line formation in limpet shells (patella vulgata) from warm- and cold-temperate zones in the eastern north atlantic. PALAIOS 28:386–393

Thompson JK, Nichols FH (1988) Food availability controls seasonal cycle of growth in Macoma balthica (L.) in San Francisco Bay, California. Journal of Experimental Marine Biology and Ecology 116:43–61

Urban H-J (1994) Upper temperature tolerance of ten bivalve species off Peru and Chile related to El Niño. Marine Ecology Progress Series 139–145

Vakily JM (1992) Determination and comparison of bivalve growth, with emphasis on Thailand and other tropical areas. WorldFish,

Veinott GI, Cornett RJ (1996) Identification of annually produced opaque bands in the shell of the freshwater mussel Elliptio complanata using the seasonal cycle of $\delta^{18}O$. Canadian Journal of Fisheries and Aquatic Sciences 53:372–379

Watson S-A, Morley SA, Peck LS (2017) Latitudinal trends in shell production cost from the tropics to the poles. Science Advances 3:e1701362

Watson S-A, Peck LS, Tyler PA, Southgate PC, Tan KS, Day RW, Morley SA (2012) Marine invertebrate skeleton size varies with latitude, temperature and carbonate saturation: implications for global change and ocean acidification. Global Change Biology 18:3026–3038

Wefer G, Berger WH (1991) Isotope paleontology: growth and composition of extant calcareous species. Marine geology 100:207–248

Weymouth FW, McMILLIN HC, Rich WH (1931) Latitude and Relative Growth in the Razor Clam, *Siliqua patula*. Journal of Experimental Biology 8:228–249

Widdows J, Johnson D (1988) Physiological energetics of *Mytilus edulis*: Scope for Growth. Marine Ecology Progress Series 46:113–121

Wilson JG, Elkaim B (1991) Tolerances to high temperature of infaunal bivalves and the effect of geographical distribution, position on the shore and season. Journal of the Marine Biological Association of the United Kingdom 71:169–177

Winder M, Cloern JE (2010) The annual cycles of phytoplankton biomass. Philos Trans R Soc Lond B Biol Sci 365:3215–3226

Witbaard R, Duineveld GCA, Wilde PAWJ de (1999) Geographical differences in growth rates of *Arctica islandica* (Mollusca: Bivalvia) from the North Sea and adjacent waters. Journal of the Marine Biological Association of the United Kingdom 79:907–915

Yamada K, Ishizaka J, Nagata H (2005) Spatial and Temporal Variability of Satellite Primary Production in the Japan Sea from 1998 to 2002. J Oceanogr 61:857–869

Figures

Figure 1: Map of occurrences, with blue representing winter cessations and red representing no winter cessation. Points are semi-transparent, so purple indicates summer and winter cessation observations at the same locality.

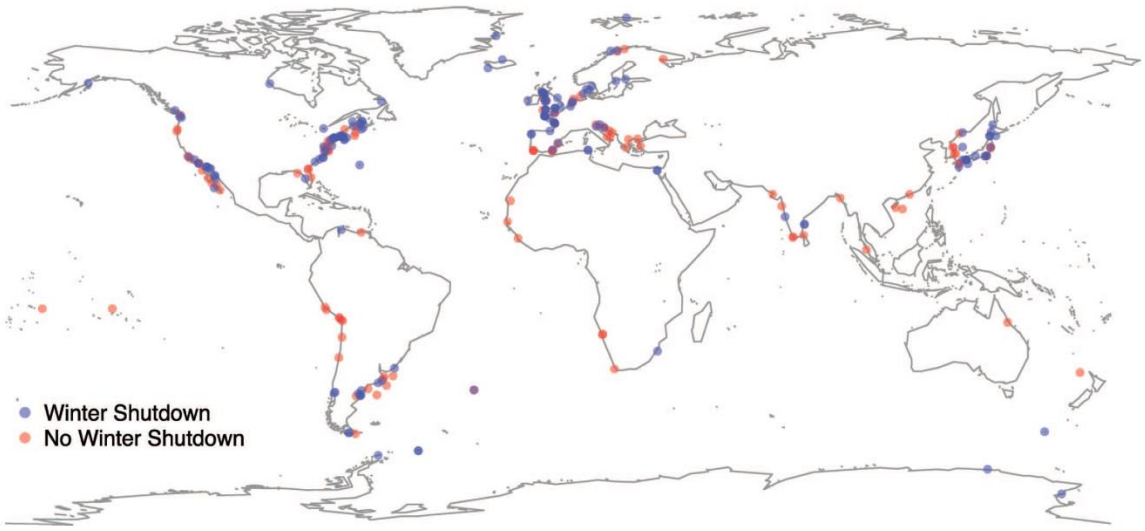

Figure 2: Proportion of occurrences of cessation types within 5° latitude bins, showing the comparative distributions of growth seasonalities for bivalves displaying respective cessations. **Top left:** Winter cessation. **Top right:** Summer cessation. **Bottom left:** Those that grow year-round. **Bottom right:** Those with both winter and summer cessations. Error bars represent multinomial confidence intervals with $\alpha = 0.05$ (Sison and Glaz 1995).

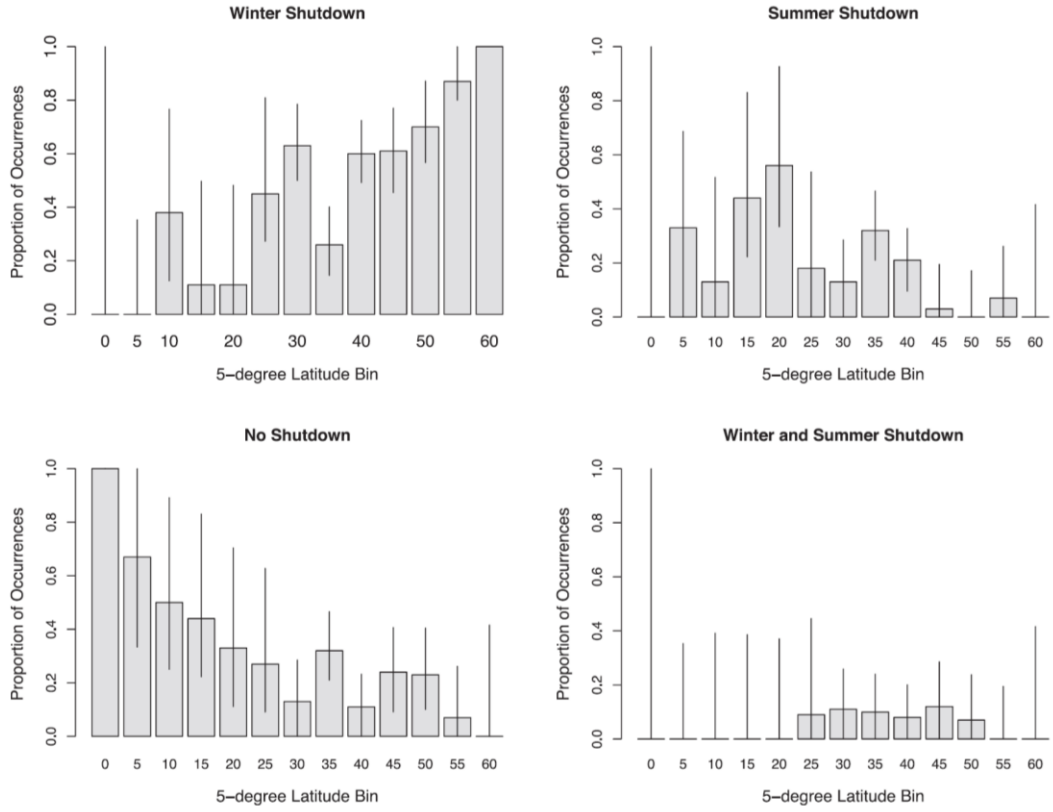

Figure 3: Logistic regression analyses comparing growth cessation to environmental variables. **Top:** Relationship between absolute latitude and the probability of winter cessation. **Second from top:** Relationship between absolute latitude and the probability of summer cessation. **Third from top:** Relationship between winter minimum recorded temperature and the probability of winter cessation. **Bottom:** Relationship between winter low monthly mean chlorophyll-a (mg/m^3) concentration and the probability of winter cessation.

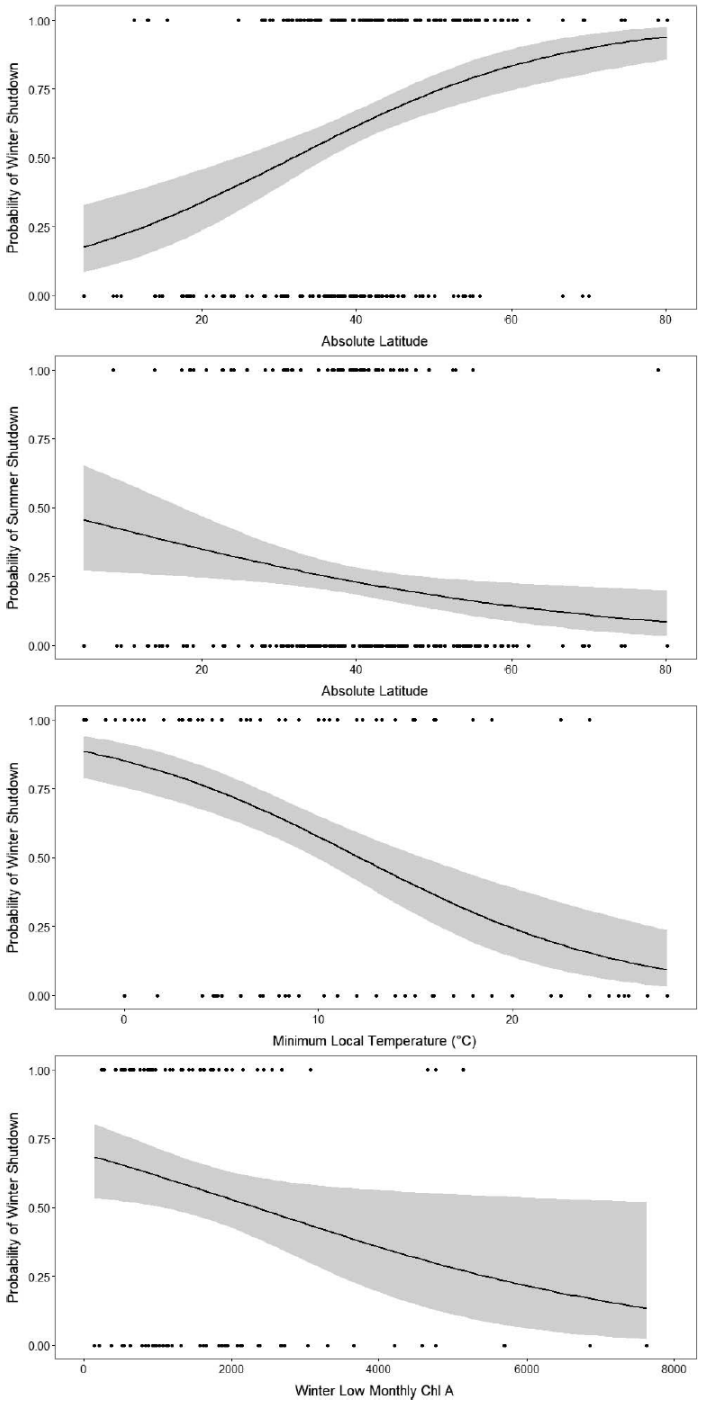

Figure 4: Principal component analysis plots of bivalve occurrences. **A**) Occurrence of winter cessation (blue) with lack of winter cessation (red) as related to absolute latitude, temperature range, minimum winter chlorophyll-a and minimum temperature. The blue winter cessations are largely grouped to the left of the plot, defined by high latitude and low minimum temperature, which follow the dominant principal component, PC1. Bivalves lacking a winter cessation primarily occur in conditions of high minimum temperature and low latitude. Minimum winter chlorophyll-a is orthogonal to this dominant axis, explaining less of the resulting grouping. **B**) PCA results for summer growth cessations, substituting maximum temperature and minimum summer chlorophyll-a. The occurrences of summer cessations appear well intermixed throughout the plot with little correspondence to any particular environmental variable.

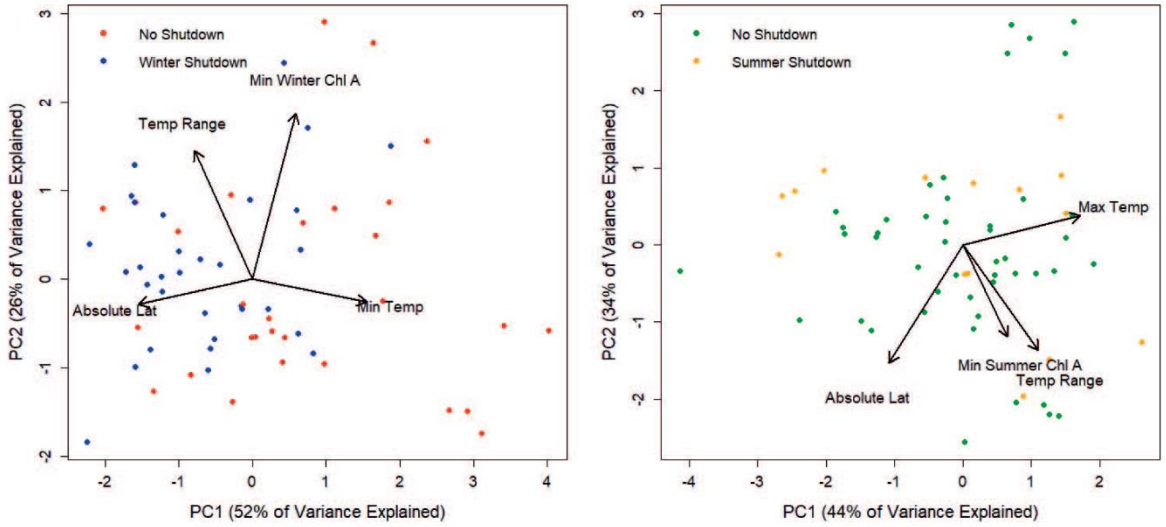

Table 1: Results for multiple logistic regression of environmental variables with winter cessation.

	Estimate	Std. error	z value	Pr(>|z|)	Significant?
Intercept	0.706	1.74	0.406	0.685	
Absolute latitude	-0.0083	0.0274	-0.303	0.7617	
Minimum local temp	-0.145	0.0573	-2.53	0.0114	*
Temp. range	0.102	0.0338	3.02	0.00256	**
Chlorophyll A minimum	0.00053	0.0003	1.77	0.0767	

CHAPTER 2

Sclerochronology and comparative growth of the Early Jurassic "Lithiotis" bivalves

Abstract

The Lithiotid bivalves were a fauna of gregarious tropical shallow-dwelling biostrome builders which thrived during the Pliensbachian and Toarcian stages of the Early Jurassic, when corals were largely eradicated following the End-Triassic extinction event. The Lithiotids reached extreme sizes of up to 70 cm, but little is known of their growth rate in comparison to other large bivalves through time. Other giant bivalves such as the modern giant clams make use of excess photosymbiotic nutrition to accelerate the growth of their hypercalcified shells. Using oxygen isotope paleothermometry in the shells of a Cochlearites specimen from the Trento carbonate platform of Northern Italy, we have calibrated thin growth increments in its shell as fortnightly in periodicity. Extrapolating this growth period across a collection of additional shells, we find *Cochlearites* grew at around 4 cm/year (equating to around 200 g of carbonate per year), while Lithiotis and Lithioperna grew at only 1.5-2 cm per year. While Cochlearites did indeed grow at rates classifying as hypercalcification, it was not the most likely of the three genera to be photosymbiotic. This is likely evidence of the poor correspondence between accelerated growth rate and photosymbiosis in bivalves. Comparing past calibrations of the growth of other historical and modern giant bivalves, we propose that multiple groups through time including the Lithiotids and Cretaceous rudists have used an alternate "mudsticking"

life habit to enable accelerated growth. While we cannot definitively prove that the Lithiotids lacked symbionts, we can say that they were not necessary to explain their unusual morphology.

Introduction

The "Lithiotis" bivalves were a fauna of aberrant, elongated and flattened biostrome builders distributed around the tropics during the Pliensbachian and Toarcian stages of the Early Jurassic. Three monospecific genera are generally included as members of the fauna: *Lithiotis*, *Cochlearites* and *Lithioperna*, and were largely restricted to shallow coastal lagoon environments (Posenato and Masetti 2012). The members of the fauna are inferred to have been highly gregarious due to their often monospecific mound assemblages, with the thin valves forming large imbricated masses of shells sometimes tens of meters thick (Lee 1983, Nauss and Smith 1988). *Lithiotis* arose in the Early Pliensbachian and became important reef-builders in the Late Pliensbachian, when coral reefs had not yet recovered from the end-Triassic extinction (Nauss and Smith 1988; Fraser et al. 2004; Franceschi et al. 2014). Their origination during the supposed early Jurassic "reef gap" was posited to be an example of a failed succession, with the lithiotid bivalves being successors which filled the carbonate builder niche of corals during a time of their near-eradication from shelf environments (Fraser et al. 2004), but cohabiting corals and lithiotids have since been found in close association (Brame et al. 2018).

Cochlearites loppianus and *Lithiotis problematica* reached over 70 and 50 centimeters in shell height, respectively (Chinzei 1982, Posenato and Masetti 2012), even larger than the largest modern mound-building aggregating oyster, *Crassostrea gigas*, which reaches 40 cm in exceptional circumstances (Chinzei 2013). Past researchers have explained the gigantism of *Lithiotis problematica* and *Cochlearites loppianus* as being a consequence of a partnership with algal photosymbionts (Fraser et al. 2004; Vermeij 2013). Modern corals, giant clams (*Tridacna*) and other bivalves harbor photosynthetic endosymbionts in their mantle tissue, which provide additional energy to enable growth accleration (Klumpp and Griffiths 1994; Li et al. 2018). Because there is no direct fossil evidence for the photosymbiont cells themselves, their presence in fossil specimens is usually inferred from a few key morphological characters believed to be characteristic of photosymbiotic bivalves (Vermeij 2013). These factors include restriction to low-latitude oligotrophic environments, accelerated shell growth ("hypercalcification"), epifaunal, gregarious life histories, the presence of transparent shell "windows" to bring in light, and elongation of shell regions believed to harbor the symbionts in order to maximize surface area for insolation (Lipps and Stanley 2016). A growing compendium of such aberrant bivalve taxa have been proposed as putatively photosymbiotic based on these criteria (Vermeij 2013).

Lithiotis has been proposed as photosymbiotic based on a radial, "banana bunch" orientation inferred to maximize light exposure for individuals in their aggregates, analogous to the growth of coral heads (Fraser et al. 2004). The thin left

valve covering the body cavity may have been transparent and window-like (Savazzi 1996), and their extreme elongation could have oriented the shell vertically to maximize exposure to light (Vermeij 2013). However, exceptions to this model, which may suggest an alternate mode of life for lithiotids, have been identified. These workers identify *Lithiotis* and *Cochlearites* as oyster-like "mudsticker" bivalves that used their elongated forms to baffle sediment and enable the development of monospecific mud mounds (Chinzei 2013). The elongated shape and abandonment of the ligamental area in adult life by *Lithiotis* in this model is an adaptation to the accelerated sedimentation around the valves of the animal in its mesotrophic environment (Chinzei 1986).

Accurate assessments of lithiotid growth rates would assist in better constraining their comparative physiology relative to other hypercalcifying bivalves through time. However, only limited investigation of lithiotid sclerochronology has been undertaken. Accorsi Benini (1985) calculated a slow growth rate of only 2.5-3 mm per year for *Lithiotis*, while Chinzei (1982) proposed a faster but still meager growth rate of 6.25 mm/yr. Both studies estimated growth from widths between neighboring dark and light growth bands uncovered via acetate peels or transmitted light through thin sections of shell. But because bivalves are known to create annual, subannual, fortnightly and even daily increments depending on surrounding environmental characteristics (Schöne et al. 2006), these workers could only assign an assumed period for the growth bands and extrapolate from there to more broadly estimate overall lithiotid growth. A more definitive estimation of the shell growth of

these organisms could be constructed if shell oxygen isotopes were used to identify a true year of growth through the ontogeny of the organism.

The relative concenterations of ^{18}O and ^{16}O in skeletal carbonate are known to vary directly in relationship to ambient seawater temperature (Grossman and Ku 1986). This ratio, usually reported relative to a known standard with the metric $\delta^{18}O$, has been used in numerous paleoclimatic reconstructions based on fossil bivalve shells (Schöne and Gillikin 2013). The equation provides a measure in units of per mille, given by the equation:

$$\delta^{18}O\ ‰ = \left[\frac{^{18}O/^{16}O_{(sample)}}{^{18}O/^{16}O_{(standard)}} - 1\right] \times 1000$$

Lithiotids are challenging to analyze due to their primarily aragonitic mineralogy (with a proposed thin calcitic outer layer) (Broglio Loria and Posenato 1996). Aragonite is more susceptible to diagenetic alteration than calcite (Cubillas et al. 2005), particularly in samples of this age, but previous paleoclimatic proxy reconstructions have used aragonitic shells as old as Jurassic and Triassic in age, when adequate preservation can be found (Malchus and Steuber 2002; Hendry et al. 2001). Because growth increments are preserved in many lithiotid shells even in the absence of original mineralogy (Chinzei 1982; Accorsi Benini 1985), we can extrapolate the estimated periodicity of successfully calibrated shells to a broader sample of more poorly preserved individuals. We can then build from those growth estimates to calculate approximate energy expenditure on shell deposition in lithiotids in order to compare to the modern and fossil hypercalcifying taxa, particularly

focusing on known symbiotic taxa and aggregating oysters, to determine which model of calcification better explains lithiotid growth.

Methods

We obtained samples of *Lithiotis problematica, Cochlearites loppianus* and *Lithioperna scutata* from the collections of the University of Padova Museum of Geology and Paleontology, the Civic Museum of Natural History in Verona, and the University of Ferrara Museum (Table 1). These specimens were mostly collected in the late 19th century from quarries, roadcuts and other localities that are no longer accessible (Figure 1). We sectioned shells with a lapidary saw blade and mounted them on glass slides, and we then cut them again to 2 mm thickness for observation with cathodoluminescence microscopy (CL). In the vacuum-sealed CITL Mk5 CL stage attached to a binocular microscope, the sample is bombarded by a cold-cathode electron beam, which causes geological samples to luminesce with visible light when diagenetically altered by manganese-rich meteoric fluids (Marshall and Mariano 1988). After screening our samples to eliminate areas that visually appeared original in mineralogy (microcrystalline, chalky opaque white) but glowed bright orange, we then collected 2 mg samples from candidate shell areas using a Dremel tool with carbide cutting bit, smeared the powder on glass slides using acetone and observed the resulting spectra generated via X-Ray Diffraction powder analysis (XRD). The spectra generated were then analyzed with X'pert software to find the best spectral peak matches (Figure 2). Aragonite and calcite can be discerned by distinct peaks which appear due to the differing bond geometry of the two carbonate polymorphs

(Kontoyannis and Vagenas 2000). After the comparative analysis of several potential sites, we selected several representative diagenetic stages for imaging with FEI Quanta 3D field emission microscope at the UCSC W.M. Keck Center for Nanoscale Optofluidics. We searched for samples that display the same prismatic aragonitic microstructure observed in prior investigations of well-preserved lithiotids, with minimal bridging of neighboring tablets and no growth of blocky secondary calcitic grains (Figure 2).

After surveying sample quality with the previous techniques, transects of sequentially milled powder (50-70 micrograms) were collected across several shells (Table 1). The isotope samples were then weighed into steel cups and roasted at 60°C under vacuum to remove water and volatile organics. After roasting, the samples were placed into glass vials with 1-2 cm of silver wire (to react with sulfur compounds) and acidified at 75°C with orthophosphoric acid in a ThermoScientific Kiel IV Carbonate Device coupled to a ThermoScientific MAT-253 dual-inlet Isotope Ratio Mass Spectrometer (IRMS). The resulting CO_2 is cryogenically separated from water and introduced to the IRMS. During an analytical run, samples are standardized relative to Vienna Pee Dee Belemnite (VPDB) versus four NBS-18 limestone standards and an in-house granular Carrera Marble standard (CM12), and two NBS-19 limestone standards are run "as-a-sample" for quality control. Long-term precision for 50-70 microgram samples is 0.08‰ for $\delta^{18}O$ and 0.05‰ $\delta^{13}C$.

Oxygen isotope values for lithiotid aragonite specimens reflect the temperature of formation (Grossman and Ku, 1986). However, because of

uncertainties regarding ambient salinity, and therefore $\delta^{18}O$ of seawater in lithiotid lagoons, we only estimated growth directly from annual oscillations in $\delta^{18}O$ values, not temperature. We used $\delta^{18}O$ transects to calibrate the periodicity of growth bands for University of Padova Natural History Museum 4628z (*Cochlearites loppianus*), the shell that displays the best seasonal sinusoid (Figure 3). Growth bands were observed and photographed in relation to the transect with a binocular microscope, stitched with Microsoft Image Composite Editor and then measured to scale in ImageJ. Once the periodicity of the bands was confirmed we then returned to shells which did not present original mineralogy. We cross-sectioned these recrystallized shells and and again used stitched, scaled microscope images to manually measure the width of narrow increments following the contours of the body cavity (example of such increments shown in Figure 4). As is the case with other bivalves, these internal increments are not correlated to the exterior ornamentation of the lithiotid shells with any known periodicity. These widths were then averaged and multiplied by 25 to obtain annual average extension rates for each specimen (shell height). These growth periodicities were combined with observations of lithiotid maximum height and observed height of several specimens from literature to determine a von Bertalannfy growth constant k using the following Von Bertalanffy growth equation:

$$L_t = L_\infty(1 - e^{-k(t-t_o)})$$

where L_t is the shell height at a chosen time t, L_∞ is the asymptotic shell height (the maximum theoretical size estimated from known maximum shell size), t is the time taken to reach L_t, and t_0 is the time at length 0 (the intercept). The k value for the

lithiotids can then be compared to known k values from historical and modern bivalve hypercalcifiers (Table 2).

As noted by prior workers, k values can vary through the life of the organism and based on the window of lengths used to calculate the growth constant (Yamaguchi 1975). While k is often called a growth constant, it is possibly more appropriate to think of it as an age constant. The unusual shell geometry of lithiotids and their seeming lack of a senescent deceleration in growth as noted by Chinzei (1982) and Accorsi Benini (1985) implies that k values should not be used alone to understand their comparative growth rate, so we also compared their energy investment in shell formation according to the methods of Watson et al. (2017), who used preset parameters to estimate the proportional amount of energy required for bivalve calcification at multiple latitudes. These parameters include an energy of carbonate formation of 1.5 J/mg for carbonate and 29 J/mg for shell organic material (Palmer 1992).

This technique can be used to estimate the relative amount of energy used by lithiotids to create shell carbonate per unit time, for comparison to other large bivalves with isotopically confirmed growth rates and size data from the literature, including *Tridacna gigas* (Elliot et al. 2009), *Pinna nobilis* (Richardson et al. 1999), *Crassostrea gigantissima* and *C. virginica* (Kirby 2000), a selection of rudists (Steuber 1996, 1998, 2000), megalodontids (Nützel et al. 2010), the giant inoceramid *Platyceramus platinus* (Walliser et al. 2018), and other bivalves (Table 2). We estimated total and incremental volume and mass of shell precipitated using standard

geometric equations for volume corresponding approximately to each bivalve's shell shape. For example, lithiotids are approximated as a rectangular prism, rudists as a cone, and megalodontids as a wedge. Some groups such as Tridacnidae have known equations calibrating shell volume and mass by length and where applicable we have noted these in the references and Supplemental Data. We used standard densities of aragonite and calcite for different bivalve mineralogies, and gathered estimates of bivalve weight percent organic content where available.

Results

Screening for Diagenesis

Upon initial surveys using CL microscopy, we observed large areas of luminescent carbonate in shells of *Lithiotis*, *Cochlearites* and *Lithioperna*, consistent with Mn-rich secondary calcite, particularly in the sparry interior of the shells which was likely originally infilled by "chalky aragonite" (Savazzi 1996). The orange luminescent regions also concentrated around cracks in the exterior surface of the shells, suggesting significant levels of substitution with manganese. Patchy regions of less luminescent materials were observed, which correspond to white, opaque microcrystalline regions with visible growth bands. These patchy regions display XRD spectra consistent with a mixture of aragonite and secondary calcite (Figure 2). The characteristic double spike of aragonite at 26-28° is present alongside the characteristic single peak of calcite at 29-30° (Kontoyannis and Vagenas 2000). Alternatively, samples from the interior sparry regions of all lithiotid shells appear to

be exclusively calcite, having no trace of characteristic aragonite spectral peaks (Figure 2).

SEM imagery of regions judged to be both well and poorly preserved based on CL and XRD were compared to SEM images of well-preserved lithiotid carbonate from figured specimens (Chinzei 1982, Savazzi 1996). In *Cochlearites* shell 4628z, samples from the outer edge retain sharp needles of prismatic aragonite similar to the observations of Chinzei (1982) in his well-preserved specimens, as well as original nacreous structures (Figure 2). In poorly preserved regions, particularly from the interior of shells, we see large angular blocks of secondary calcite with almost no traces of original microstructure preserved (Figure 2). While lithiotids may have been bimineralic by some assessments (Broglio Loria and Posenato 1996), with a thin external calcitic layer, the thin outer layers of calcite are luminescent and present microstructurally as blocks of neomorphic calcite in the lithiotid specimens we examined, corroborating the observations of Chinzei (1982).

Interspecimen isotope comparison

Extensively recrystallized shell regions display extreme negative $\delta^{18}O$ values, with shell 61 displaying mean $\delta^{18}O$ values of -14.2‰, and shell 4595 averaging -6.3‰ (all isotopic data available in Supplemental Materials), implying that their oxygen isotopic composition has been reset by exchange with ^{18}O-depleted meteoric fluids (Marshall 1992). Specimens 4628z, 4630z and 7319, which contain significant proportions of aragonite and original microstructures, have $\delta^{18}O$ values similar to

expected values from Pliensbachian seawater, but 4630z and 7319 have a positive correlation between $\delta^{13}C$ and $\delta^{18}O$ (Spearman's rho = 0.41, $p < 0.005$; Figure 5), potentially suggesting alteration by pore fluids after burial (Allan and Matthews 1982). *Cochlearites* shell 4628z does not have a significant correlation between $\delta^{13}C$ and $\delta^{18}O$ values (Spearman's rho = -0.256, $p = 0.39$), similar to well-preserved Trento platform limestones (Franceschi et al. 2014). While specimens 4630z and 7319 retain much of their original microstructure, they record higher average $\delta^{18}O$ values than 4628z with less variance. Higher oxygen isotope values can result from exchange with evaporative water bodies that have higher $\delta^{18}O$ values (Marshall 1992; Moore 2013), and 4630z and 7319z came from sites in the Lessini Mountains where many lithiotid beds have been noted to exhibit evidence of an emersion phase, covered by shallow marshes and evaporative ponds during periods of regression (Posenato and Masetti 2012). Shell 7319 and 4630z may have been isotopically reset by early postmortem isotope exchange with the waters of their evaporation-prone lagoonal environments as indicated by their relatively constrained positive oxygen isotope values, while shell 4628z represents the true range of temperatures experienced during the life of the organism, possibly due to rapid burial. We suspect post-mortem resetting of these higher values as there is no seasonal sinusoid in the oxygen isotopic values and they are constrained to a narrow range of values.

Annual Growth Rates

Cochlearites shell 4628z exhibits a sinusoidal $\delta^{18}O$ pattern between -1.7 and -4.2‰ through two transects on the dorsal and ventral sides of the valve (Figure 3).

These paleotemperatures would roughly correspond to annual range of temperatures between 24 and 34 °C, using the paleotemperature equation of Grossman & Ku (1986) with seawater $\delta^{18}O$ of -1‰, although the upper temperature extreme could have been lower if there was a seasonal influx of low-salinity monsoonal water (Arias 2008). Section 1 shows two summers and a winter, coinciding with 24-25 growth increments. Section 2 appears to show three summers and two winters, with 24 bands separating the neighboring low $\delta^{18}O$ values (high summer temperatures) and also 24 between the neighboring high $\delta^{18}O$ peaks (low winter temperatures). However, the higher $\delta^{18}O$ value which we interpret as a winter value does not appear to record the amplitude of an entire seasonal oscillation as indicated by the lack of a similar seasonal extreme as that recorded in the prior winter season, instead likely recording a seasonal winter cessation of growth combined with under-sampling. The increments constrict in width coinciding with that potential winter temperature "dip," further suggesting a seasonal cessation at that location in the shell. The flattening of recorded temperature oscillations due to a growth slowdown coupled with a cessation at the seasonal winter low temperature is a phenomenon common in bivalve sclerochronology (Schöne et al. 2006). As these two sections are collected from opposing sides of the valve, they do not represent contemporaneous periods, but instead may be separated by multiple years of growth.

Prior investigations of Jurassic belemnite rostra (Dunca et al. 2006), Cretaceous inoceramid shells (Walliser et al. 2018) and modern bivalves (Richardson 1990) showed tidal periodicity corresponding to the 15-day period between spring

and neap tides (24-25 increments per year), and the *Cochlearites* shell appears to follow this rhythm of calcification. Each annual $\delta^{18}O$ cycle contains 24-25 finer growth lines of less than 1 mm in width, implying fortnightly growth periodicity for the smallest increments. Modern members of the Pteriidae have been demonstrated to consistently present high-resolution microgrowth increments of daily periodicity (Caceres-Puig et al. 2011, Loria and Huato-Soberanis 2014), and such cycles of calcification are thought to be conserved traits present in many bivalve groups (Wada 1961). These cycles of daily growth have been shown in other bivalves to condense into fortnightly bundles (Richardson et al. 1990). As *Cochlearites, Lithiotis* and *Lithioperna* have been assigned in the most recent phylogenetic analysis to be a clade closely related to modern isognomonid bivalves (Fraser 2002) and inhabited differing nutritional niches of the same lagoonal basin environment (Posenato and Masetti 2012), it is highly likely that this fortnightly growth rhythm was the dominant control of growth across the three species, at least on the Trento carbonate platform. Our calibration of fortnightly bands is for a horizontal transect of growth, but this calibration can be applied in the longitudinal direction as well because the extension of *Cochlearites* and *Lithiotis* shells was driven by continuous ventral migration of a small spoon-shaped body cavity (Chinzei 1982). Both horizontal and vertical growth lines were the manifestation of the migration of this round, spoon-like body cavity. Measurements of longitudinal shell extension, using these calibrated fortnightly growth bands, indicates a growth rate of 20-50 mm per year in *Cochlearites* (mean

40.1 mm/yr). *Lithiotis* and *Lithioperna* both grew more slowly, at means of 17.6 mm/yr and 21.8 mm/yr respectively.

Shell Growth Rate and Energy Investment

The k values of *Lithiotis*, *Cochlearites* and *Lithioperna* are 0.08, 0.1 and 0.04 respectively (Table 2). These values are smaller than those known from present-day tridacnids (Munro and Heslinga 1982) and smaller than that of the giant mussel *Pinna nobilis* (k=0.2) as well as the modern oyster *Crassostrea virginica* (k=0.27) (Richardson et al. 1999, Kirby et al. 2000). Combining the implied longevity data from known growth rate values with the known density of aragonite, we obtain peak values of 221-406 g carbonate precipitated per year for *Cochlearites*, 191 g/yr for Lithioperna and 50-60 g/yr for *Lithiotis*. *Cochlearites*' precipitation rate is similar to the 200 g/yr rate postulated for the giant rudist bivalve *Vaccinites ultimus* (Steuber 2000) (Table 2). While little to none of the original matrix in Lithiotids is still preserved, it has been proposed that the lithiotid bivalves exhibited a high organic content in their shells, with a brown carbon-rich waxy sheen on many especially well-preserved specimens and an abundance of organic-rich nacre (Savazzi 1996). Assuming a 5% organic content by weight, at the upper end of organic content known for present-day oysters (Taylor and Martin 1972), and calcification costs of 1.5 J/mg for carbonate and 29 J/mg for shell organic material (Palmer 1992, Watson et al. 2017), we obtain maximum energy investment values for all lithiotid species between 175 J/year for the very thin-valved, slow-growing *Lithiotis* and up 1228 J/yr for the larger, faster growing *Cochlearites*, lower than the implied energy investment for the

rudist and megalodontid bivalves but higher than that estimated from *Pinna nobilis*, one of fastest growing bivalves of the present day (Table 2).

Discussion

Comparison of growth among the lithiotids

Cochlearites had the fastest rate of shell extension with a mean across all specimens of 40.1 mm/year, whereas *Lithioperna* grew at 21.8 mm/year, and *Lithiotis* only 17.6 mm/year (Figure 4). Due to its thin, transparent opercular valve and seeming orientation radially to maximize orientation to light, *Lithiotis* was previously proposed to be the most likely candidate of the three genera for coral-like photosymbiotic hypercalcifying biology (Fraser et al. 2004), but on the Trento platform, *Cochlearites* and *Lithioperna* grew faster despite being considered less morphologically or ecologically indicative of symbiosis (Fraser et. al 2004). *Cochlearites* has a much thicker, non-transparent opercular valve and lived in the deeper portion of the lagoon with less sunlight (Chinzei 1982, Posenato and Masetti 2012), while *Lithioperna* lacks the highly derived *Lithiotis* morphology altogether and is thought to have inhabited lower-energy, terrigenously influenced localities (Fraser et al. 2004). While some modern photosymbiotic bivalves grow at relatively slow rates and reach small maximum sizes, such as the Fraginae (Li et al. 2018), the comparative slow growth of *Lithiotis* suggests its energetic investment in shell growth was quite low, which would not be indicative of an excess of photosymbiotic nutrition compared to the closely related *Cochlearites* and *Lithioperna*.

Comparison with other putative and confirmed photosymbiotic bivalves

Comparison of growth rate across bivalve taxa with differing shell thickness and shapes is difficult. One of the most common methods is the use of the growth constant k from the Von Bertalanffy equation, which was recently used to construct a global compendium of bivalve growth in relation to latitude (Moss et al. 2016). We can also use a similar approach to quantify the relative extension rates of different giant bivalve clades through time. The k values of the "Lithiotis" fauna range from of 0.03 to 0.1, with *Lithiotis* displaying the lowest values due to its smaller estimated annual growth and longer estimated longevity (Table 2). These values are lower than the k values found in modern *Tridacna*, which have been found to display k values of up to 0.187 depending on species (Munro and Heslinga 1982). Lithiotid k values are also lower than those known from many conventional heterotrophic bivalves, though this is more a function of the very short longevity and comparative extreme first year growth exhibited by most short-lived small bivalves. Large animals tend to exhibit lower k values due to the longer time it takes them to reach that size on average (Atkinson and Sibly 1997).

In terms of Von Bertalanffy growth constants, unsurprisingly the closest analogs of the lithiotids may be the rudist bivalves, with examples of the gregarious elevator-type *Vaccinites ultimus* displaying growth constants of 0.07 and 0.11 (Table 2). The rudists were similar to *Lithiotis* and *Cochlearites* in adopting one extremely elongated, asymmetric lower valve and a smaller opercular valve. In addition, the lithiotids and elevator rudists both have relatively small body volumes compared to

shell shape, with only the topmost part of the shell being occupied by tissue and the rest below filled with chalky carbonate deposits (Steuber 2000). Past workers have proposed that both taxa are “mudstickers”, utilizing a hyperextended shell valve to remain above the surface of the sediment in with access to food and away from the potentially dysoxic surface of the sediment (Chinzei 1982). In addition, as gregarious bivalves they would be able to work as an aggregate to baffle soft sediment and accelerate this process, excluding any potential competitors not adapted for life in the soft mud.

In the modern day, examples of this life strategy are rare. Modern oysters such as *Crassostrea virginica* do occasionally exhibit extreme growth rates of as much as 7.4 cm per year ($k > 0.6$) (Kirby 2000), but do not exhibit the sticklike morphology of the lithiotids. Juvenile *Pinna nobilis* grow at rates nearing 20 cm/yr ($k=0.2$) and live elevated above seagrass beds (Richardson et al. 1999), but their densities never approach that known to be common in lithiotid buildups (Coppa et al. 2010). The closest modern analog to the lithiotids may be the freshwater mussel *Etheria elliptica* var. *cailliaudi,* found in Lake Victoria (Yonge 1962, Chinzei 1982). The mussels in this locality display an unusual hyper-elongated lower valve and live in colonies embedded in soft sediment. No studies of the growth rate of that hyperelongated *cailliudi* morphotype have been conducted but *Etheria elliptica* from other regions of Africa have been found to exhibit k-values of 0.07 (Akele et al. 2017), very similar in magnitude to that of *Lithiotis*.

The lithiotids grew rapidly in the vertical direction, but their shells were flattened and primarily constructed of a single valve. We can quantify their level of calcification in terms of energy investment by calculating their shell volume, multiplying by density of shell aragonite and then, after estimating the relative fraction of organic material and carbonate, using previously calibrated energies of formation for aragonite and shell organic material to determine lifetime and annual Joules of energy invested in carbonate formation (Palmer 1992). Setting a 5 weight percent organic content for the shells of *Lithiotis* and *Cochlearites*, we find that *Cochlearites*' rapid growth rate suggests an extremely high energy investment of 600-1200 J/year in calcification costs for some specimens (Table 2). *Lithiotis*, with its narrower shell and slower growth rate, invested less than 200 J/year.

The extremely high rate of energetic investment displayed by *Cochlearites* is matched by few modern organisms in the dataset (Figure 6, Table 2). *Pinna nobilis*, by this measure, exhibits a fairly small energy investment relative to its length due to its very thin mostly-calcitic shell. *Tridacna gigas*, while precipitating a very thick shell at a rapid rate, does so with an extremely low weight percent organic content (less than 0.1%), greatly reducing the cost of formation (Dreier et al. 2014). *Crassostrea virginica*, while not often considered a hypercalcifier, can in some cases grow over 7 cm per year, and with a relatively thick shell that implies investment of nearly 1000 J/year of energy into shell formation. Its Oligocene counterpart *Crassostrea gigantissima*, which extended its >3 cm thick shell in excess of 2 cm per year, would have invested 4 times more energy than that (Kirby 2000).

In the fossil record, the rudist bivalves again show similar growth coefficients to *Cochlearites*. With their conical thickened valves, *Vaccinites* grew over 4 cm/year according to some measurements (Steuber 1998). Both the lithiotids and elevator rudists may have had an inherent energy advantage due to slow growth of their comparatively small body cavity, because an increase in shell size did not mean more energy expended on tissue maintenance and homeostatic exertion, as is the case for other invertebrates (Gillooly et al. 2001). In addition, they monopolized their environments by engineering the substrate. Modern oysters inhabiting single-species mounds have been found to grow faster than those in less dense assemblages (Bartol et al. 1999). Lithiotids and rudists may have been enabled to reach their unusual length by the protection their self-baffled mud mounds limiting interspecies competition. Modern oysters are "foundational species" which engineer their environment to reduce disturbance, enabling them to monopolize space and exclude potential competitors within their niche (Kimbro and Grosholz 2006). The microenvironment of individual lithiotids would also be more regulated within the crannies of their dense shell aggregations than in the wider shallow, tidally-mediated chaotic environment experienced on the Trento carbonate platform (Nauss and Smith 1982), leaving them with an excess of energy to expend on their overengineered shells.

There is also the possibility that calcification was energetically cheaper during the Pliensbachian epoch when the lithiotids thrived. Our calculations assume an energy of formation of 1.5 J/g for carbonate based on modern calibrations (Palmer

1992), but if the Trento carbonate platform was of abnormally high aragonite saturation state compared to present conditions, the energy required to precipitate shell material would be lower, as has been found for modern coral reefs (Silverman et al. 2007) and in bivalves (Thomsen et al. 2015). Also, while the calibration of Palmer (1992) has been used in interspecific comparisons of calcification energy for a variety of mollusk groups (Watson et al. 2017), little investigation has been taken to ground-truth the specific number of 1.5 J/g is truly representative of all mollusks, which exhibit a variety of calcification physiologies. We do not know if the lithiotids exhibited uniquely efficient calcification processes, which would reduce the energy demands associated with building their large shells. Nevertheless, the rise and fall of differing calcifying taxa has been linked to environmental triggers experienced by mollusks in the modern oceans. The expansion and contraction of rudist reef-building during the Cretaceous has also been suggested to be closely associated with volcanic CO_2-linked dips in carbonate oversaturation (Wissler et al. 2003; Weissert and Erba 2004). Carbonate platforms of Pliensbachian Italy have been proposed to be supersaturated refugia for lithiotids and hypercalcifying algae, and the extirpation of hypercalcifying taxa from the region in the early Toarcian has been attributed to an acidification-related crisis (Trecalli et al. 2012). Our results confirm that the lithiotids did have uniquely high energetic demands introduced by calcification. Their hypermorphic shell development may have been aided by a favorable environment, which may also explain why we find no organisms resembling them in the present day.

Were the lithiotids photosymbiotic?

The evidence remains equivocal, but additional energy sources likely weren't necessary to explain the unusual growth rate and morphology of the lithiotids. They possessed aberrant shells which extended at a rapid rate, but that is a characteristic shared with the nonsymbiotic *Pinna nobilis*. They appear to have invested an unusual quantity of their energy budget into calcification, but Cenozoic and modern non-symbiotic oysters also are champion calcifiers in this regard (Kirby 2000). Past suggestions that lithiotids inhabited oligotrophic reef-like habitats and grew towards sunlight (Fraser et al. 2004) have been overshadowed by more recent models assigning them to a mesotrophic environment (Posenato and Masetti 2012; Franceschi et al. 2014). However, the modern photosymbiotic heart cockles also inhabit mesotrophic environments, so living in a low-irradiance turbid environment does not rule out their symbiosis alone (Jones and Jacobs 1992).

Perhaps the most convincing repudiation of lithiotids as photosymbiotic calcifiers has come through improvement in understanding of rudist bivalves. Our analyses confirm that lithiotid calcification most closely resembles that of the rudists in the record of modern and ancient calcifiers. Rudists were classically thought to be photosymbiotic coral imitators due to their presence in tropical shelf environments which excluded reef-building corals (Scott 1995). However, other workers have since demonstrated that corals and rudists frequently cohabitated, with rudists inhabiting the inshore reef environment (Skelton et al. 1997; Steuber 2000). Rudist "reefs" were argued to have had no original relief in life position, instead being primarily

sediment-supported in nature (Gili et al. 1995). Unusual tubular microstructures in their upper shell were proposed to enable the exposure of the mantle to light (Vogel 1975), and *Lithiotis* and *Cochlearites* share similar tubular structures (Chinzei 1982). Later workers noted the extensive similarities in microstructure between rudists and modern oysters, which use low-density chalky aragonite and hollow vesicles to enable them to "float" on loose siliciclastic substrate (Chinzei 1982; Al-Aasm and Veizer, 1986; Vermeij 2014). Large deepwater rudist taxa that lived outside the photic zone but exhibited similar gregarious life histories were found, suggesting that photosymbiosis was not needed to explain their unusual physiology (Lewy 1995). While we cannot prove the absence of photosymbionts within lithiotid tissue, we suggest that hypercalcification is not a consistent marker of photosymbiosis in lithiotids or other bivalves. Efforts to explain unusual physiology as a function of symbionts may discount the ability of bivalves to engineer environments which favor accelerated growth.

Lithiotids have been noted to form "banana-bunch" or "bouquet"-like aggregations, suggesting an orientation radially to maximize exposure to light (Fraser et al. 2004). But such formations have since been described for modern *Crassostrea* and other mudstickers, due to growth of several individuals originating from a shared dead oyster valve which acted as the original recruitment platform (Chinzei 2013). Another unresolved question is the potential symbiont that would have been available to photosymbiotic bivalves at this time. Recent molecular clock investigations have proposed that the Symbiodiniacae evolved in the Middle to Late Jurassic, which post-

dates the radiation and extinction of the lithiotids (LaJeunesse et al. 2018). Symbiosis is a prerequisite to explain many cases of hypercalcification in modern taxa, but these present-day models may never have been a good fit to improve our understanding of the lithiotids.

Conclusion

While proving the absence of photosymbiosis is challenging, we can assert that symbionts were not necessary to enable the unusual physiology and ecology of the lithiotids. *Lithiotis* and *Cochlearites* may instead have been able to proliferate due to their unique sediment-baffling ability, aided by the specialization of an elongated, sticklike lower valve, and their fanlike aggregations enhanced this sediment trapping ability. These soft-bottom, sediment-supported buildups excluded competitors and created favorable microenvironments which enhanced their calcifying ability in regions which competitors could not inhabit. During a time when calcification may have been aided by supersaturated water, their hypermorphic valves were not harmful to their fitness, and instead reinforced the resilience of their niche and led to their extreme valve morphology. Even assuming modern-day costs of calcification, the lithiotids exhibited rates of shell growth and energy investment seen in non-symbiotic bivalves. This supports the proposal that symbionts were not necessary to explain lithiotid growth, and that fast growth poorly correlates with photosymbiosis in the fossil record. However, the demise of the lithiotids in the acidification crisis of the early Toarcian mirrors the physiological stresses being experienced of modern oysters. While the lithiotids may not have fallen due to a bleaching crisis like that

currently befalling modern zooxanthellate corals, their rise and fall still may present lessons relevant to understanding the shell-building physiology of present-day taxa.

References

Accorsi Benini C (1985) The large Liassic bivalves: symbiosis or longevity. Palaeogeography, Palaeoclimatology, Palaeoecology 52:21–33

Akélé GD, Montcho SA, Lalèyè PA (2017) Growth of freshwater *Etheria elliptica* oyster (Lamarck, 1807) reared in cages in the Pendjari River (Benin, West Africa). Aquat Living Resour 30:17

Al-Aasm IS, Veizer J (1986) Diagenetic stabilization of aragonite and low-Mg calcite; II, Stable isotopes in rudists. Journal of Sedimentary Research 56:763–770

Allan JR, Matthews RK (1982) Isotope signatures associated with early meteoric diagenesis. Sedimentology 29:797–817

Ansell AD (1968) The Rate of Growth of the Hard Clam *Mercenaria mercenaria* (L) throughout the Geographical Range. ICES Journal of Marine Science 31:364–409

Arias C (2008) Palaeoceanography and biogeography in the Early Jurassic Panthalassa and Tethys Oceans. Gondwana Research 14:306–315

Atkinson D, Sibly RM (1997) Why are organisms usually bigger in colder environments? Making sense of a life history puzzle. Trends in Ecology & Evolution 12:235–239

Barry JP, Whaling PJ, Kochevar RK (2007) Growth, production, and mortality of the chemosynthetic vesicomyid bivalve, *Calyptogena kilmeri* from cold seeps off central California. Marine Ecology 28:169–182

Bartol IK, Mann R, Luckenbach M (1999) Growth and mortality of oysters (*Crassostrea virginica*) on constructed intertidal reefs: effects of tidal height and substrate level. Journal of Experimental Marine Biology and Ecology 237:157–184

Bayne BL, Worrall CM (1980) Growth and production of mussels *Mytilus edulis* from two populations. Mar Ecol Prog Ser 3:317–328

Beckvar N (1981) Cultivation, spawning, and growth of the giant clams *Tridacna gigas, T. derasa, and T. squamosa* in Palau, Caroline Islands. Aquaculture 24:21–30

Berg CJ, Alatalo P (1985) Biology of the tropical bivalve *Asaphis deflorata* (Linne, 1758). Bulletin of Marine Science 37:827–838

Berg Jr CJ, Alatalo P (1984) Potential of chemosynthesis in molluscan mariculture. Aquaculture 39:165–179

Brame H-MR, Martindale RC, Ettinger NP, Bodin S, Debeljak I, Vasseur R, Lathuilière B, Kabiri L (2018) Stratigraphic distribution and paleoecological significance of Early Jurassic (Pliensbachian-Toarcian) lithiotid-coral reefal deposits from the Central High Atlas of Morocco. Palaeogeography, Palaeoclimatology, Palaeoecology

Broglio Lorigo C, Posenato R (1996) Adaptive strategies of Lower Jurassic and Eocene multivincular bivalves. In: Cherchi A. (eds) Autecology of selected fossil organisms: achievements and problems. Bollettino della Società paleontologica italiana, pp 45–61

Brown JR (1988) Multivariate analyses of the role of environmental factors in seasonal and site-related growth variation in the Pacific oyster *Crassostrea gigas*. Marine ecology progress series Oldendorf 45:225–236

Brown JR, Hartwick EB (1988) Influences of temperature, salinity and available food upon suspended culture of the Pacific oyster, *Crassostrea gigas*: I. Absolute and allometric growth. Aquaculture 70:231–251

Cáceres-Puig JI, Huato-Soberanis L, Melo-Barrera FN, Saucedo PE (2011) Use of calcein to estimate and validate age in juveniles of the winged pearl oyster *Pteria sterna*. Aquatic Living Resources 24:329–335

Cameron CJ, Cameron IF, Paterson CG (1979) Contribution of organic shell matter to biomass estimates of unionid bivalves. Can J Zool 57:1666–1669

Chinzei K (1982) Morphological and structural adaptations to soft substrates in the Early Jurassic monomyarians *Lithiotis* and *Cochlearites*. Lethaia 15:179–197

Chinzei K (2013) Adaptation of oysters to life on soft substrates. Historical Biology 25:223–231

Coppa S, Guala I, Lucia GA de, Massaro G, Bressan M (2010) Density and distribution patterns of the endangered species *Pinna nobilis* within a Posidonia oceanica meadow in the Gulf of Oristano (Italy). Journal of the Marine Biological Association of the United Kingdom 90:885–894

Cubillas P, Köhler S, Prieto M, Chaïrat C, Oelkers EH (2005) Experimental determination of the dissolution rates of calcite, aragonite, and bivalves. Chemical Geology 216:59–77

Dreier A, Loh W, Blumenberg M, Thiel V, Hause-Reitner D, Hoppert M (2014) The isotopic biosignatures of photo-vs. thiotrophic bivalves: are they preserved in fossil shells? Geobiology 12:406–423

Duncа E, Doguzhaeva L, Schöne BR, Van de Schootbrugge B (2006) Growth patterns in rostra of the Middle Jurassic belemnite *Megateuthis giganteus*: controlled by the moon. Acta Universitatis Carolinae–Geologi ca 49:107–117

Feng D, Peckmann J, Li N, Kiel S, Qiu J-W, Liang Q, Carney RS, Peng Y, Tao J, Chen D (2018) The stable isotope fingerprint of chemosymbiosis in the shell organic matrix of seep-dwelling bivalves. Chemical Geology 479:241–250

Fitt WK, Rees T a. V, Yellowlees D (1995) Relationship between pH and the availability of dissolved inorganic nitrogen in the zooxanthella-giant clam symbiosis. Limnology and Oceanography 40:976–982

Franceschi M, Dal Corso J, Posenato R, Roghi G, Masetti D, Jenkyns HC (2014) Early Pliensbachian (Early Jurassic) C-isotope perturbation and the diffusion of the Lithiotis Fauna: Insights from the western Tethys. Palaeogeography, Palaeoclimatology, Palaeoecology 410:255–263

Fraser NM (2002) Early Jurassic Reef Eclipse: Paleoecology and Sclerochronology of the "Lithiotis" Facies Bivalves. PhD, University of Southern California

Fraser NM, Bottjer DJ, Fischer AG (2004) Dissecting "Lithiotis" bivalves: implications for the Early Jurassic reef eclipse. Palaios 19:51–67

Gili E, Masse J-P, Skelton PW (1995) Rudists as gregarious sediment-dwellers, not reef-builders, on Cretaceous carbonate platforms. Palaeogeography, Palaeoclimatology, Palaeoecology 118:245–267

Gillooly JF, Brown JH, West GB, Savage VM, Charnov EL (2001) Effects of Size and Temperature on Metabolic Rate. Science 293:2248–2251

Glover CP, Kidwell SM (1993) Influence of organic matrix on the post-mortem destruction of molluscan shells. The Journal of Geology 101:729–747

Grossman EL, Ku T-L (1986) Oxygen and carbon isotope fractionation in biogenic aragonite: temperature effects. Chemical Geology: Isotope Geoscience Section 59:59–74

Hare PE (1963) Amino Acids in the Proteins from Aragonite and Calcite in the Shells of *Mytilus californianus*. Science 139:216–217

Hendry JP, Perkins WT, Bane T (2001) Short-term environmental change in a Jurassic lagoon deduced from geochemical trends in aragonite bivalve shells. Geological Society of America Bulletin 113:790–798

Howe HV (1937) Large oysters from the Gulf Coast Tertiary. Journal of Paleontology 355–366

Jones DS, Jacobs DK (1992) Photosymbiosis in *Clinocardium nuttalli*; implications for tests of photosymbiosis in fossil molluscs. PALAIOS 7:86–95

Jones DS, Quitmyer IR (1996) Marking time with bivalve shells: oxygen isotopes and season of annual increment formation. Palaios 340–346

Jones DS, Williams DF, Arthur MA (1983) Growth history and ecology of the Atlantic surf clam, *Spisula solidissima* (Dillwyn), as revealed by stable isotopes and annual shell increments. Journal of Experimental Marine Biology and Ecology 73:225–242

Kahle D, Wickham H (2013) ggmap: Spatial Visualization with ggplot2. The R Journal 5:144–161

Kauffman EG, Harries PJ, Meyer C, Villamil T, Arango C, Jaecks G (2007) Paleoecology of giant inoceramidae (*Platyceramus*) on a Santonian (Cretaceous) seafloor in Colorado. Journal of Paleontology 81:64–81

Kimbro DL, Grosholz ED (2006) Disturbance Influences Oyster Community Richness and Evenness, but Not Diversity. Ecology 87:2378–2388

Kirby MX (2000) Paleoecological Differences Between Tertiary and Quaternary *Crassostrea* Oysters, as Revealed by Stable Isotope Sclerochronology. PALAIOS 15:132–141

Klumpp DW, Griffiths CL (1994) Contributions of phototrophic and heterotrophic nutrition to the metabolic and growth requirements of four species of giant clam (Tridacnidae). Marine Ecology Progress Series 103–115

Kontoyannis CG, Vagenas NV (2000) Calcium carbonate phase analysis using XRD and FT-Raman spectroscopy. Analyst 125:251–255

Krantz DE, Jones DS, Williams DF (1984) Growth rates of the sea scallop, *Placopecten magellanicus*, determined from the $^{18}O/^{16}O$ record in shell calcite. The Biological Bulletin 167:186–199

LaJeunesse TC, Parkinson JE, Gabrielson PW, Jeong HJ, Reimer JD, Voolstra CR, Santos SR (2018) Systematic Revision of Symbiodiniaceae Highlights the Antiquity and Diversity of Coral Endosymbionts. Current Biology 28:2570-2580.e6

Lee CW (1983) Bivalve mounds and reefs of the central High Atlas, Morocco. Palaeogeography, Palaeoclimatology, Palaeoecology 43:153–168

Lewy Z (1995) Hypothetical endosymbiontic zooxanthellae in rudists are not needed to explain their ecological niches and thick shells in comparison with hermatypic corals. Cretaceous Research 16:25–37

Li J, Volsteadt M, Kirkendale L, Cavanaugh C (2018) Characterizing photosymbiosis between Fraginae bivalves and *Symbiodinium* using phylogenetics and stable isotopes. Frontiers in Ecology and Evolution 6:45

Lipps JH, Stanley GD (2016) Photosymbiosis in Past and Present Reefs. Coral Reefs at the Crossroads. Springer, Dordrecht, pp 47–68

Lombardi SA, Chon GD, Lee JJ-W, Lane HA, Paynter KT (2013) Shell Hardness and Compressive Strength of the Eastern Oyster, *Crassostrea virginica*, and the Asian Oyster, *Crassostrea ariakensis*. The Biological Bulletin 225:175–183

Loría PLM, Huato-Soberanis L (2014) Efficacy of calcein and Coomassie Blue dyeing of shell growing-edges and micro growth-bands: Ageing juvenile of *Pinctada mazatlanica* (Pterioida: Pteriidae). Revista de Biología Tropical 62:957–968

Loriga C, Posenato R (1996) Adaptive strategies of Lower Jurassic and Eocene multivincular bivalves. Bollettino della Società Paleontologica Italiana 45–61

MacDonald BA, Thompson RJ (1985) Influence of temperature and food availability on the ecological energetics of the giant scallop *Placopecten magellanicus*. I. Growth rates of shell and somatic tissue. Marine ecology progress series Oldendorf 25:279–294

Malchus N, Steuber T (2002) Stable isotope records (O, C) of Jurassic aragonitic shells from England and NW Poland: palaeoecologic and environmental implications. Geobios 35:29–39

Marsh M, Hamilton G, Sass R (1978a) The crystal sheaths from bivalve hinge ligaments. Calcified tissue research 25:45–51

Marsh M, Hamilton G, Sass R (1978b) The crystal sheaths from bivalve hinge ligaments. Calc Tis Res 25:45–51

Marshall DJ, Mariano AN (1988) Cathodoluminescence of geological materials. Taylor & Francis,

Marshall JD (1992) Climatic and oceanographic isotopic signals from the carbonate rock record and their preservation. Geological Magazine 129:143–160

Moore CH (2013) Carbonate reservoirs: porosity and diagenesis in a sequence stratigraphic framework. Elsevier Science, Amsterdam

Moss DK, Ivany LC, Judd EJ, Cummings PW, Bearden CE, Kim W-J, Artruc EG, Driscoll JR (2016) Lifespan, growth rate, and body size across latitude in marine Bivalvia, with implications for Phanerozoic evolution. Proc R Soc B 283:20161364

Munro JL, Heslinga GA (1982) Prospects for the commercial cultivation of giant clams (Bivalvia: Tridacnidae) presented at 35th Annual Meeting of the Gulf and Caribbean Fisheries Institute. ICLARM Contribution

Nauss AL, Smith PL (1988) Lithiotis (Bivalvia) bioherms in the Lower Jurassic of east-central Oregon, U.S.A. Palaeogeography, Palaeoclimatology, Palaeoecology 65:253–268

Neubrandt EV, Dumont J-F, Gutnic M, Marcoux J, Monod O, Poisson A (1976) Megalodontidae du Trias supérieurdans la chaine Taurique (Turquie méridionale). Géobios 9:199–222

Nützel A, Joachimski M, Correa ML (2010) Seasonal climatic fluctuations in the Late Triassic tropics—High-resolution oxygen isotope records from aragonitic bivalve shells (Cassian Formation, Northern Italy). Palaeogeography, Palaeoclimatology, Palaeoecology 285:194–204

Palmer AR (1992) Calcification in marine molluscs: how costly is it? Proceedings of the National Academy of Sciences 89:1379–1382

Posenato R, Masetti D (2012) Environmental control and dynamics of Lower Jurassic bivalve build-ups in the Trento Platform (Southern Alps, Italy). Palaeogeography, Palaeoclimatology, Palaeoecology 361–362:1–13

Posenato R, Parente M, Trecalli A (2014) Taphonomy and evolution of an extraordinarily exposed upper Pliensbachian-lower Toarcian succession of “Lithiotis” beds at Mercato San Severino (Salerno, southern Apennines). ANNALI ONLINE FISICA E SCIENZE DELLA TERRA 1:73–73

Rhoads DC, Lutz RA, Revelas EC, Cerrato RM (1981) Growth of Bivalves at Deep-Sea Hydrothermal Vents Along the Galápagos Rift. Science 214:911–913

Richardson CA (1990) Tidal Rhythms in the Shell Secretion of Living Bivalves. 215–226

Richardson CA, Collis SA, Ekaratne K, Dare P, Key D (1993) The age determination and growth rate of the European flat oyster, *Ostrea edulis*, in British waters determined from acetate peels of umbo growth lines. ICES Journal of Marine Science 50:493–500

Richardson CA, Kennedy H, Duarte CM, Kennedy DP, Proud SV (1999) Age and growth of the fan mussel *Pinna nobilis* from south-east Spanish Mediterranean seagrass (*Posidonia oceanica*) meadows. Marine Biology 133:205–212

Sandberg PA, Hudson JD (1983) Aragonite relic preservation in Jurassic calcite-replaced bivalves. Sedimentology 30:879–892

Savazzi E (1996) Preserved ligament in the Jurassic bivalve *Lithiotis*: adaptive and evolutionary significance. Palaeogeography, Palaeoclimatology, Palaeoecology 120:281–289

Schöne BR (2008) The curse of physiology—challenges and opportunities in the interpretation of geochemical data from mollusk shells. Geo-Marine Letters 28:269–285

Schöne BR, Giere O (2005) Growth increments and stable isotope variation in shells of the deep-sea hydrothermal vent bivalve mollusk *Bathymodiolus brevior* from the North Fiji Basin, Pacific Ocean. Deep Sea Research Part I: Oceanographic Research Papers 52:1896–1910

Schöne BR, Gillikin DP (2013) Unraveling environmental histories from skeletal diaries — Advances in sclerochronology. Palaeogeography, Palaeoclimatology, Palaeoecology 373:1–5

Schöne BR, Rodland DL, Fiebig J, Oschmann W, Goodwin D, Flessa KW, Dettman D (2006) Reliability of multitaxon, multiproxy reconstructions of environmental conditions from accretionary biogenic skeletons. The Journal of geology 114:267–285

Scott RW (1995) Global environmental controls on Cretaceous reefal ecosystems. Palaeogeography, Palaeoclimatology, Palaeoecology 119:187–199

Seed R, Brown RA (1978) Growth as a strategy for survival in two marine bivalves, *Cerastoderma edule* and *Modiolus modiolus*. The Journal of Animal Ecology 283–292

Silverman J, Lazar B, Erez J (2007) Effect of aragonite saturation, temperature, and nutrients on the community calcification rate of a coral reef. Journal of Geophysical Research: Oceans 112:

Skelton PW, Gili E, Rosen BR, Valldeperas FX (1997) Corals and rudists in the late Cretaceous: a critique of the hypothesis of competitive displacement. Boletin de la Real Sociedad Espanola de Historia Natural (Seccion Geologica) 92:225–239

Steuber T (2000) Skeletal growth rates of Upper Cretaceous rudist bivalves: implications for carbonate production and organism-environment feedbacks. Geological Society, London, Special Publications 178:21–32

Steuber T, Yilmaz C, Löser H (1998) Growth rates of early Campanian rudists in a siliciclastic-calcareous setting (Pontid MTS., North-Central Turkey). Geobios 31:385–401

Taylor JD, Layman M (1972) The mechanical properties of bivalve (Mollusca) shell structures. Palaeontology 15:73–87

Thomsen J, Haynert K, Wegner KM, Melzner F (2015) Impact of seawater carbonate chemistry on the calcification of marine bivalves. Biogeosciences (BG) 12:1543–1571

Trecalli A, Spangenberg J, Adatte T, Föllmi KB, Parente M (2012) Carbonate platform evidence of ocean acidification at the onset of the early Toarcian oceanic anoxic event. Earth and Planetary Science Letters 357–358:214–225

Vermeij GJ (2013) The evolution of molluscan photosymbioses: a critical appraisal. Biological Journal of the Linnean Society 109:497–511

Vermeij GJ (2014) The oyster enigma variations: a hypothesis of microbial calcification. Paleobiology 40:1–13

Vogel K (1975) Endosymbiotic algae in rudists? Palaeogeography, Palaeoclimatology, Palaeoecology 17:327–332

Wada K (1962) Crystal growth of molluscan shell. Bulletin of the National Pearl Research Laboratory 7:703–828

Walliser EO, Mertz-Kraus R, Schöne BR (2018) The giant inoceramid *Platyceramus platinus* as a high-resolution paleoclimate archive for the Late Cretaceous of the Western Interior Seaway. Cretaceous Research 86:73–90

Watson S-A, Morley SA, Peck LS (2017) Latitudinal trends in shell production cost from the tropics to the poles. Science Advances 3:e1701362

Weissert H, Erba E (2004) Volcanism, CO2 and palaeoclimate: a Late Jurassic–Early Cretaceous carbon and oxygen isotope record. Journal of the Geological Society 161:695–702

Wissler L, Funk H, Weissert H (2003) Response of Early Cretaceous carbonate platforms to changes in atmospheric carbon dioxide levels. Palaeogeography, Palaeoclimatology, Palaeoecology 200:187–205

Yamaguchi M (1975) Estimating growth parameters from growth rate data. Oecologia 20:321–332

Yellowlees D, Rees TAV, Leggat W (2008) Metabolic interactions between algal symbionts and invertebrate hosts. Plant, Cell & Environment 31:679–694

Yonge M (1962) On *Etheria elliptica* Lam. and the course of evolution. including assumption of monomyarianism. in the family Etheriidae (Bivalvia: Unionacea). Phil Trans R Soc Lond B 244:423–458

Figures

Table 1:

Lithiotid specimens and locality data			
Specimen number	Genus	Locality	Collection
4628z	*Cochlearites*	Cima di Malera	University of Padua Museum
4630z	*Cochlearites*	Cima di Malera	University of Padua Museum
7391	*Lithiotis*	Ponte di Veja, Sant'Anna D'alfaedo	University of Padua Museum
37	*Cochlearites*	Vaio dell'Anguilla (Erbezzo)	University of Verona Museum
52	*Lithiotis*	Corso Erbezzo	University of Verona Museum
60	*Lithiotis*	Vaio Squaranto (Pissarota)	University of Verona Museum
2496	*Lithiotis*	Pernigotti	University of Verona Museum
61	*Cochlearites*	Pernigotti	University of Verona Museum
42	*Lithioperna*	Vaio dell'Anguilla	University of Verona Museum
Fer1	*Cochlearites*	Ponte Basazenoci	University of Ferrara Collection
Fer3	*Cochlearites*	Campo d'Albero	University of Ferrara Collection
Fer4	*Lithioperna*	Vaio dell'Anguilla	University of Ferrara Collection

Figure 1: Map of study region with outline of the Trento carbonate platform in light blue (Posenato and Masetti 2012). Red sites are fossil localities.

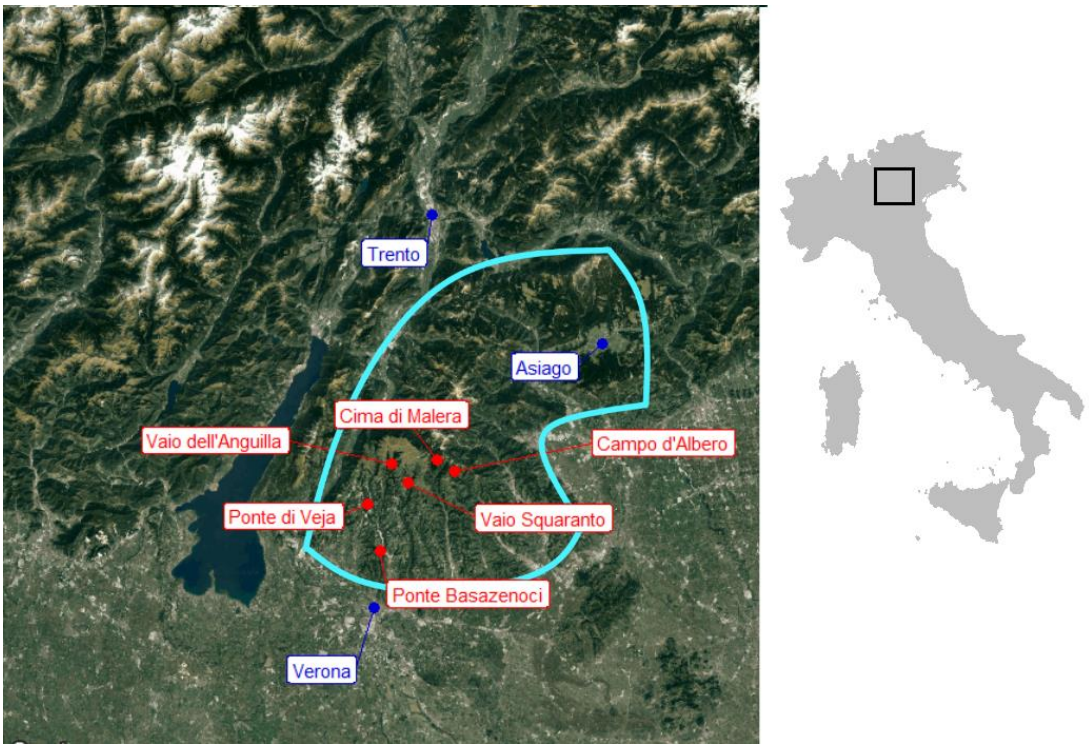

Figure 2: Example of diagenetic screening for shell 4628z, showing interior of shell consisting of fused neomorphic calcite spar under SEM (left top) with XRD showing an extreme peak diagnostic for calcite. On right we see a region at the exterior of the shell with microstructure consistent with nacre and a double spike at around 27-28° indicative of a significant fraction of aragonite.

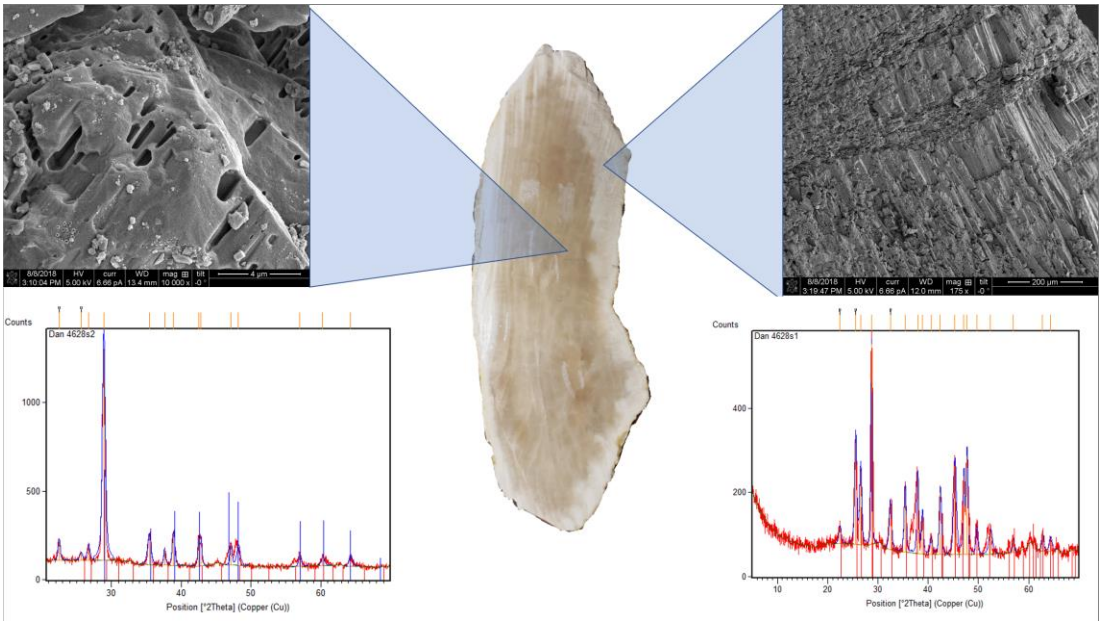

Figure 3: Profile of growth in *Cochlearites* specimen 4628. Two transects from front and rear of shell showing different growth profiles, Transect 1 is one year in length, Transect 2 is two years in length. Location of growth lines shown as vertical lines. There are 24-25 lines per annual oscillation, implying fortnightly periodicity. On the left, an idealized wireframe diagram of *Cochlearites* growth and a drawing of overall shell morphology. At the bottom right, an image of the sampled cross section showing the aragonite-rich layers and the two locations of sampling (Transect 1, blue; Transect 2, red). Location of rotary saw cut across shell shown by green line.

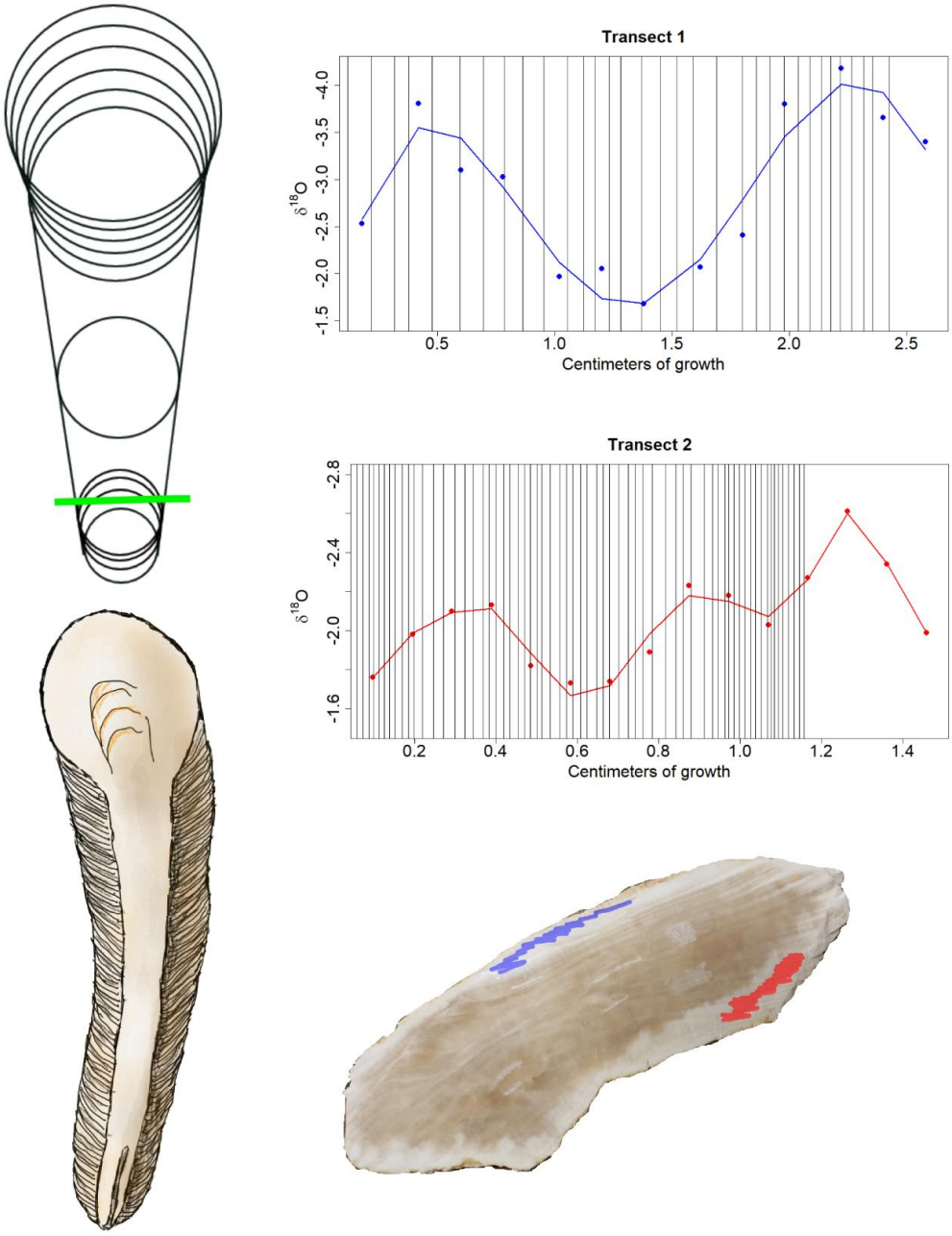

Figure 4: Distribution of annual growth rates, measured from fortnightly cross section increment widths across the studied specimens from three genera. Below is heavily recrystallized *Lithiotis* specimen 60 from University of Ferrara museum collection, showing the fortnightly bands preserved.

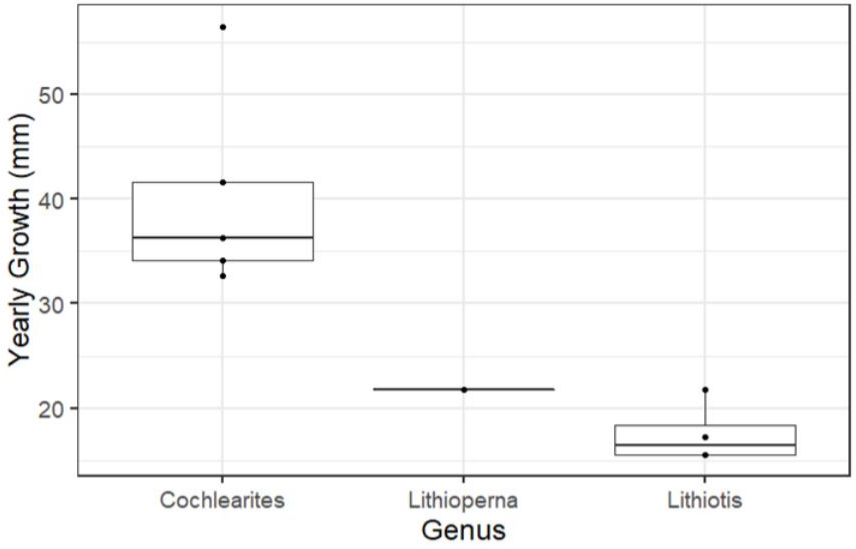

Figure 5: Relationship between $\delta^{13}C$ and $\delta^{18}O$ for the three individuals screening as presenting the best preservation of the studied specimens.

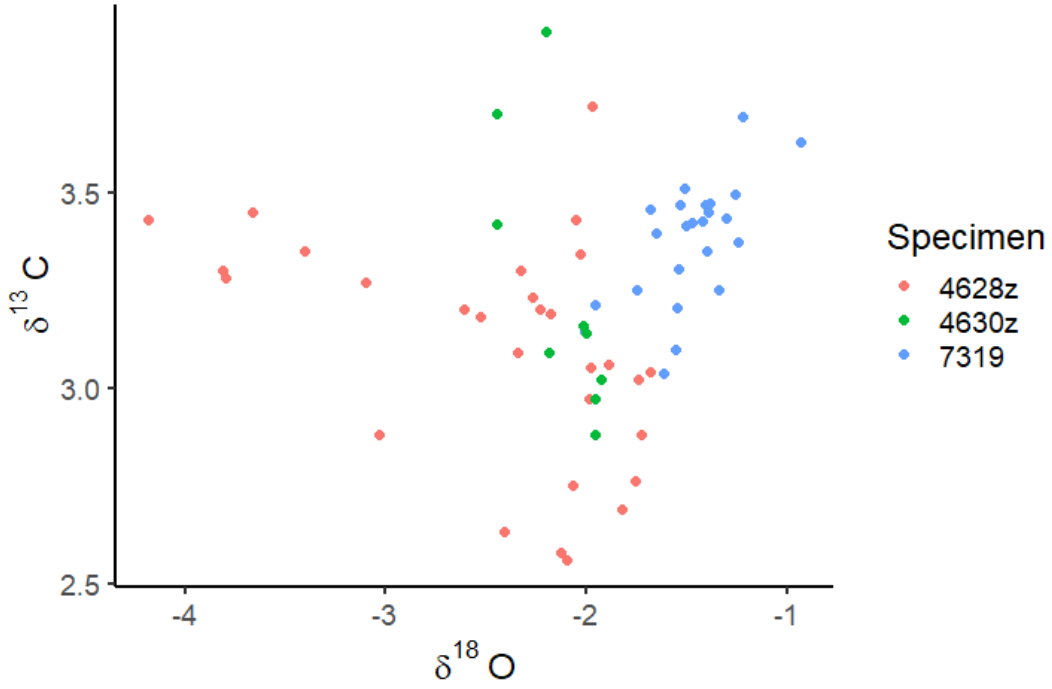

Figure 6: Comparing annual energy investment to shell height for a selection of modern and fossil bivalves. *Lithiotis* plots on a continuum with other highly elongated, thin-shelled taxa such as *Pinna nobilis*, while *Cochlearites* and

Lithioperna are hypercalcifiers similar to rudists in terms of energy investment per unit length. Raw values available in Table 2.

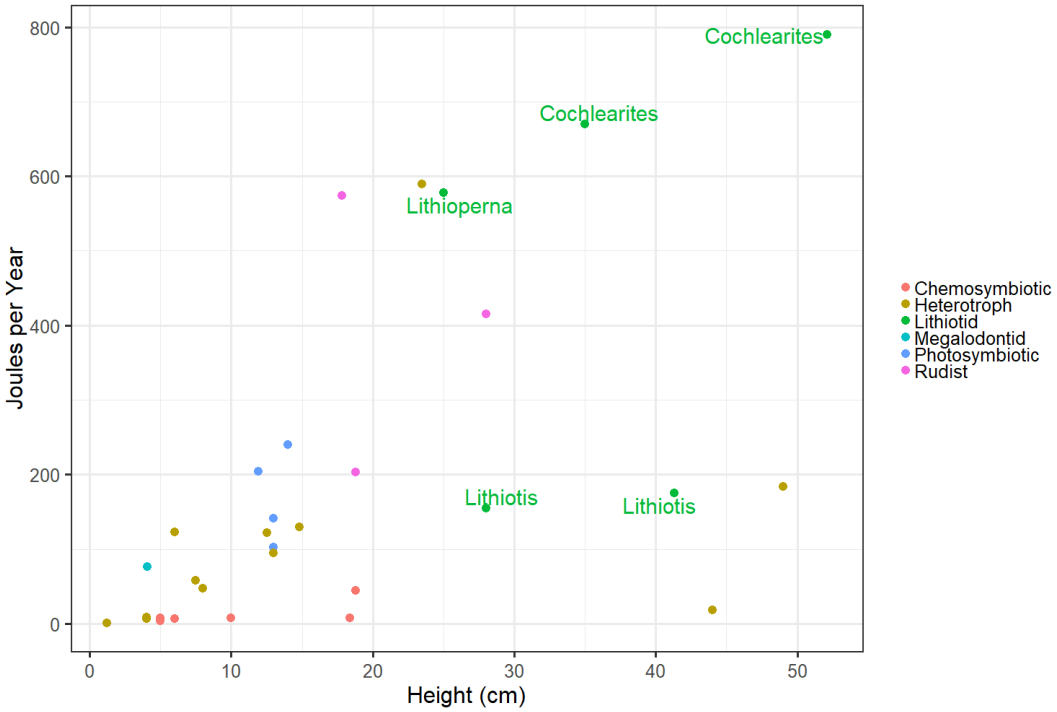

Table 2

Comparison of energy investment for several giant bivalve taxa				
Species	Height (mm)	Growth rate (mm/yr)	Energy/year (J)	k
Lithiotis	413	20	175.6027	0.084683
Cochlearites	521	30	789.705	0.078524
Lithioperna	250	20	578.151	0.035347
Cochlearites	350	40	669.438	0.079217
Lithiotis	280	20	154.6601	0.058641
Tridacna gigas	140	84	239.5602	0.064678
Tridacna derasa	130	58	141.4666	0.108949
Hippopus hippopus	119	40	204.6609	0.118692
Tridacna squamosa	130	38	103.0026	0.105232
Pinna nobilis	490	60	234.0692	0.21
Vaccinites ultimus	280	37.3	415.4612	0.112973
Vaccinites ultimus	178	30	573.6341	0.076079
Gorjanovicia costata	188	54	202.9088	0.135461
Cornucardia hornigi	40.9	27.3	76.57584	0.277853
Etheria elliptica	440	8.5	18.28031	0.07
Platyceramus platinus	1070	50	1630.855	0.035781
Crassostrea gigas	80	60	39.76	0.148762
Crassostrea gigantissima	235	21	495.5229	0.046906
Crassostrea virginica	148	74	109.2307	0.673537
Placopecten	75	40	58.46839	0.18653

magellanicus				9
Placopecten magellanicus	125	45	121.8092	0.313191
Ostrea edulis	60	25	122.6987	0.41
Cerastoderma edule	12	10	1.405521	0.653926
Mytilus edulis	40	15	6.885	0.222

See supplemental materials for full calculations and citations in table.

CHAPTER 3

Interspecific and intrashell stable isotope variation between Red Sea giant clam species

Abstract

The Gulf of Aqaba is home to three species of giant clams with differing ecological niches and varying levels of photosymbiotic activity. Giant clams grow a two-layered shell with the outer layer precipitated in close association with photosymbionts within the outer mantle, with the inner layer grown in association with the light-starved inner mantle. We investigated whether systematic offsets between these physiologically distinct body regions influence the carbonate isotope values of their associated layers and interspecific differences. We collected a sample of 38 shell specimens across the three species present in the region including the cosmopolitan *Tridacna maxima* and *T. squamosa*, as well as the rare endemic *T. squamosina*, and sampled carbonate isotopes from their inner and outer shell layers. *T. squamosina* was found to exhibit higher temperatures of shell formation relative to the other species as determined by oxygen isotope paleothermometry, confirming its status as an obligately shallow-dwelling species. However, the known negative fractionation imparted on tissue carbon isotopes by photosymbiotic algae did not carry through to produce measurable offsets in the carbonate d13C values of the more symbiotic *T. squamosina* and *T. maxima* compared to the more heterotrophic *T. squamosa*. Within the shells of the tridacnids, we found that outer shell layers were

precipitated at temperatures 1.7 °C higher on average than their respective inner layers, which we propose is a function of the high insolation, low albedo microenvironment of the outer mantle and potentially the non-photochemical quenching of the symbionts themselves. Population-wide isotopic sampling of reef-dwelling bivalve shells can help constrain the ecological niches of rare taxa and help reconstruct their internal physiology.

Introduction

The giant clams (Tridacninae) are a subfamily of very large reef-dwelling bivalves with some species growing to over 1.5 meters in size (Yonge 1975). They are also notable for their photosynthetic symbionts, belonging to the same *Symbiodinium* genus found in many photosymbiotic cnidarians, which they cultivate in an altered stomach cavity (Yellowlees et al. 2008). Giant clams are common throughout the equatorial Indo-Pacific, but three species are known to inhabit the Red Sea: *Tridacna maxima* Röding, *T. squamosa* Lamarck, and *T. squamosina* Sturany (Richter et al. 2008). *T. maxima* (small giant clam), and *T. squamosa* (fluted giant clam) are globally distributed (Neo et al. 2017) while *T. squamosina* (=*T. costata* Roa-Quioait et al.) was only recently recognized as a distinct species and is believed to be endemic to the Northern Red Sea (Richter et al. 2008, Huber & Eschner 2010). The species is extremely rare and potentially endangered today, but was the most common *Tridacna* species in Pleistocene fossil reefs (Richter et al. 2008).

Only 13 living specimens of the rare endemic *T. squamosina* were found in prior surveys along the entire Jordanian coast, however, so our understanding of its niche is still limited (Richter et al. 2008). In those underwater surveys, *T. squamosina* was noted to be obligately shallow-dwelling, living epifaunally at the topmost crests of reefs (Richter et al. 2008). In contrast, *T. maxima* inhabits a range of reef depths and may live epifaunally or semi-infaunally, and *T. squamosa* is a fore-reef specialist with a solely epifaunal life history (Roa-Quoait 2005). Despite habitat differences, *T. squamosina* and *T. maxima* have similar chlorophyll fluorescence (a measure of photosynthetic activity) , implying similarly high levels of reliance on photosymbiotic activity and therefore photosynthate nutrition (Richter et al. 2008). However, both have stronger chlorophyll fluorescence than the fore-reef *T. squamosa*, which could be more reliant on heterotrophy (Jantzen et al. 2008).

The occurrence of three cohabiting *Tridacna* species in the Northern Red Sea provides an opportunity to investigate if photosymbiosis alters the carbon isotopic composition of shell carbonates. Carbon isotopes are measured with a delta notation ($\delta^{13}C$), reflecting the ratio of the rarer and heavier ^{13}C isotope to the more common and lighter ^{12}C, relative to a standard. The equation provides a measure in units of per mille, given by the equation:

$$\delta^{13}C\ ‰ = \left[\frac{{}^{13}C/{}^{12}C_{(sample)}}{{}^{13}C/{}^{12}C_{(standard)}} - 1\right] \times 1000$$

Prior researchers have attempted to isolate a photosymbiotic "vital effect" influencing the carbonate $\delta^{13}C$ of giant clams (Jones et al. 1986; Romanek et al. 1987),

Clinocardium nuttalli (Jones et al. 1992), and other bivalves (Dreier et al. 2014). The proposed models have taken several forms, with Jones et al.'s (1986) initial proposal being that the process of photosynthesis causes isotopic fractionation that enriches the light isotope ^{12}C (a negative shift in $\delta^{13}C$) in shell carbonate compared to neighboring organisms (Jones et al. 1986). Other workers proposed that the clam's calcifying fluid is instead enriched in the heavier ^{13}C because photosymbionts preferentially use ^{12}C, leading to higher $\delta^{13}C$ values in shell carbonate during times of greater symbiotic activity (McConnaughey et al. 1997). Photosymbiotic corals indeed show such an oscillation in their shell carbonate (McConnaughey et al. 1997), but it is unclear whether these offsets are consistent across localities and broadly applicable to bivalve taxa such as giant clams (Jones et al. 1988). In the Red Sea, if such an influence was evident in giant clam carbonate, the $\delta^{13}C$ values of the more symbiotic *T. squamosina* and *T. maxima* would be higher than that of the more heterotrophic *T. squamosa*. Furthermore, *Tridacna* shells contain a prismatic aragonite internal shell layer, located far from the most photosynthetically active outer mantle of the clam, and a crossed-lamellar aragonite outer layer precipitated directly adjacent to the most photosynthetically active siphonal mantle (Gannon et al. 2017). Any photosymbiotic effect on the calcifying fluid of the animal might manifest as a systematic offset between $\delta^{13}C$ values in the inner and outer shell layers, as found in other bivalves (Trofimova et al. 2018). An isotopic signal from photosymbiosis could reveal whether ancient reef-building bivalves, such as rudists, lithiotids, and megalodontids,

were aided by symbiotic algae, as hypothesized on the basis of their shell morphology (Vermeij 2013).

There also is a demand to better understand the comparative ecology of the three *Tridacna* species in the Northern Red Sea and elsewhere. Giant clams are a broadly distributed subfamily with a high potential for additional cryptic species (Neo et al. 2017) and stable isotope techniques may assist in species recognition if systematic isotopic offsets correspond to distinct ecological niches. This method would be especially valuable for rare species such as *T. squamosina*, or for morphologically-distinctive specimens in historical museum collections. For example, we should be able to identify if *T. squamosina* is indeed an obligately shallow reef crest dweller by using shell oxygen isotope values to reconstruct preferred growth temperature. The death assemblage of Red Sea giant clams provides an opportunity to study the impacts of photosymbiosis on shell carbonate and to constrain the niche partitioning among the species of the region.

Methods

In summer 2016, 38 specimens of *Tridacna* including 5 *T. squamosina*, 15 *T. maxima*, 10 *T. squamosa*, and 8 of undetermined species were collected from beach death assemblages and from shells confiscated at the Egypt border crossing and held at the Hebrew University Museum in Jerusalem (Fig. 1). Species identifications were made according to a key previously used in local studies of *Tridacna* (Roa-Quiaoit 2005), primarily relying on margin plication morphology, presence of scutes, the size

of byssal opening and shell symmetry for identification of the three species in the assemblage. Specimens that were eroded, broken or otherwise unidentifiable are noted as "undetermined." This assemblage represents primarily a juvenile to subadult fauna, with the largest shell being less than 12 years in age as determined from internal growth band counting, and the majority much younger. As such, this study is describing *Tridacna* at an ontogenetic stage when their growth rate is largely constant and not subject to the slowing which happens at maturity in this genus (Romanek et al. 1987).

Shells were sectioned along the longest axis of growth with a diamond-bladed slow pneumatic saw. The samples were subjected to 1 hour of immersion in a weak 4 wt % sodium hypochlorite solution and then scrubbed with a metal brush to remove encrusting epibionts. The cut surfaces were then polished on rotating lathes using successively finer silicon carbide grits down to 18.3 micron size. Samples were then mounted on glass slides and micromilled with a 0.05 mm Brasseler tungsten carbide drill bit attached to a New Wave micromill to obtain approximately 100 micrograms of aragonite from the surface of the interior shell layer near the hinge and the exterior shell layer near the ventral margin for each sampled shell (Fig. 2). For shells larger than 7 cm length, a handheld Dremel tool with 3 mm tungsten carbide toothed bit was used to mill a larger amount (up to 300 micrograms) of aragonite powder, to ensure that we were measuring a similar relative area of material for small juvenile and more mature specimens.

The carbonate samples were then weighed into steel cups and roasted at 60°C under vacuum to remove water and volatile organics. After roasting, the samples were placed into glass vials with 1-2 cm of silver wire (to react with sulfur compounds) and acidified at 75°C with orthophosphoric acid in a ThermoScientific Kiel IV Carbonate Device coupled to a ThermoScientific MAT-253 dual-inlet Isotope Ratio Mass Spectrometer (IRMS). The resulting CO_2 is cryogenically separated from water and introduced to the IRMS. During an analytical run, samples are standardized relative to Vienna Pee Dee Belemnite (VPDB) versus four NBS-18 limestone standards and an in-house granular Carrera Marble standard (CM12), and two NBS-19 limestone standards are run "as-a-sample" for quality control. Long-term precision for 50-70 microgram samples is 0.08‰ for $\delta^{18}O$ and 0.05‰ $\delta^{13}C$.

$\delta^{18}O$ values were converted to equivalent temperatures of formation using a paleotemperature equation calibrated for *Tridacna maxima* based on that of Grossman and Ku (1986) (Romanek et al. 1987) We used a seawater $\delta^{18}O$ value of 1.8‰ as determined from prior measurements of seawater $\delta^{18}O$ values for the Northern Red Sea based on averaging a year of monthly direct measurements (Al-Rousan et al. 2003). This 1.8‰ value in addition is confirmed from cruise sampling near the mouth of the Gulf of Aqaba through the work of Andrie and Merlivat (1989). ANOVA and Mann-Whitney-Wilcoxon tests were conducted with R software. Due to limitations of available specimens, our sample sizes are unbalanced in regard to species and growth layer, with far more specimens of T. maxima than the other species, and more examples of outer layers overall for identified specimens due to fragmentation of

some shells with loss of the hinge area. As such we have elected for interspecies comparisons to use the outer layer as it is the closest to the exterior environment of the bivalve and the symbiont-rich outer mantle.

Results

Overall, both shell layers exhibit a significant positive correlation between $\delta^{13}C$ and $\delta^{18}O$ values, although the correlation is stronger for the inner layer (inner: rho= 0.727, $p < 0.00005$; outer: rho = 0.375, $p < 0.05$) (Fig. 3). The outer shell layer records a higher temperature of formation (23.0°C) than the inner layer (21.3°C) (Table 1; paired Wilcoxon signed rank test, V = 119.5, p-value = 0.012). In contrast, we did not detect a difference in $\delta^{13}C$ values between the inner and outer layers (V = 180, p = 0.4237).

The relationship between $\delta^{13}C$ and $\delta^{18}O$ is positive for all three species (Fig. 3). *T. squamosina* has a 3 °C higher temperature of formation for the outer shell layer, while the other species display similar mean values (Fig. 4). With a one-way Analysis of Variance, we confirmed a difference at the $\alpha = 0.005$ level among the three species ($F(2,28) = 6.46$, $p = 0.0049$). A post-hoc Tukey test shows that while *T. squamosina* is different from the other two species, we did not detect a difference between *T. squamosa* and *T. maxima*. (Table 2). A one-way ANOVA does not confirm a significant variation in $\delta^{13}C$ values between the outer layers of each species ($F(2,28) = 0.103$, $p = 0.902$; Fig. 4).

Discussion

No carbon isotope link with photosymbiosis

We did not find a consistent ^{13}C-enrichment in the outer or inner growth layers of any of the three *Tridacna* species. Prior investigations of *T. gigas* from other regions found higher $\delta^{13}C$ values in the outer layer (Gannon et al. 2017), possibly due to the influence of the photosymbionts in the outer growth layer drawing down the lighter ^{12}C available in the calcifying fluid at the outermost part of the shell, or to the greater degree of isolation from ambient water DIC in the inner mantle. The similar $\delta^{13}C$ values in inner and outer layers of *T. squamosina, T. maxima and T. squamosa* could be related to the smaller size and therefore more rapid mixing of calcifying fluid within our studied species compared to mature specimens of *T. gigas*, which may have more isolation between its inner and outer reservoirs of calcifying fluid.

The relationship between carbon and oxygen isotope values is weakly positive and consistent across layers and between species. Such positive correlations have been noted by some workers as a sign of a kinetic isotope effect in coral skeletons, originating from the incomplete equilibration with calcification site DIC, but are less likely to occur in mollusks due to their use of ambient DIC for calcification (McConnaughey et al. 2003, 2008). Positive correlations have been observed in other giant clam species (Romanek 1989) and has have proposed to represent a photosymbiosis-linked effect (Watanabe et al. 2004, McConnaughey and Gillikin 2008). In this model, the higher photosynthetic output of zooxanthellae during winter would increase $\delta^{13}C$ values (Watanabe et al. 2004). This correlation is not universally observed in giant clams (Aharon 1991), but has been proposed to occur in regions

where winter photosymbiosis is enhanced by increased nutrient availability (Romanek and Grossman 1989, McConnaughey and Gillikin 2008, Elliot et al. 2009). Alternatively, it could be due to integration of ^{12}C-rich respired carbon in summer due to higher summer photosynthetic yield. Yet in the case of our data, this correlation is noted for both internal and external shell layers across a large population and is stronger in the internal layer, which is less influenced by the activity of symbionts and generally more slowly precipitated. We suggest that the correlation may be environmentally mediated and related to seasonal factors influencing the $\delta^{13}C$ values of ambient DIC or the phytoplankton sourced carbon which is respired and subsequently integrated into giant clam carbonate. The positive correlation is unlikely to be photosymbiotically caused in the Red Sea clams, as hermatypic corals of the region show a negative correlation between $\delta^{13}C$ and $\delta^{18}O$ (Erez 1978, Klein et al. 1992), not positive as observed in corals from other regions (Swart et al. 1996, McConnaughey et al. 1997). The variety of carbon sources (environmental DIC, respired CO_2 from both endogenous and exogenous nutrition) and the conflicting seasonal variations in these sources make tridacnid shell carbonate an integration of numerous effects, which are difficult to disentangle. Long-term observation of giant clam photosynthetic activity in relation to precipitated $\delta^{13}C$ values, combined with detailed isotopic measurement and modeling of the interaction of carbon reservoirs inside and outside the organism will be needed to settle the specific cause of the positive isotope correlation often observed in giant clams.

Shell $\delta^{13}C$ values did not differ among the three species, although *T. squamosina* has a slightly higher $\delta^{13}C$ value than the other species (Fig. 3). However, *T. maxima* has the lowest mean shell $\delta^{13}C$ value, which does not align with our prior model suggesting the two more photosymbiotic groups would have higher $\delta^{13}C$ values than *T. squamosa*. With their large volume of extrapallial fluid, which is continuously exchanged with surrounding water masses (Ip et al. 2017a), giant clams may not be candidates to display photosymbiotic enrichment in carbon isotope ratios. The activity of the symbionts could be too small to overprint environmental influences on shell carbonate $\delta^{13}C$ values. The $\delta^{13}C$ values of *Tridacna* tissues have been shown to display little of the negative offset expected from a diet rich in photosynthate because their endosymbionts are carbon-limited, reducing the degree of fractionation exhibited in the sugars they produce (Johnston et al. 1995). This reduced degree of fractionation combined with a large reservoir of environmentally-sourced calcifying fluid may overwhelm any photosymbiotic offset that would be expected to appear in giant clam carbonate, even in our favorable test system of three congeners within the same environment. The large range of $\delta^{13}C$ values across these populations of closely associated tridacnids in our data suggests that microenvironmental influences may play a significant role in their shell carbon isotope composition.

Shell $\delta^{18}O$-derived temperatures as a marker of Tridacna species-specific niche

Of the three *Tridacna* species found in the region, *T. squamosina* is the rarest and believed to be endemic to the Northern Red Sea (Neo et al. 2017). In their initial description of the species, Richter et al. (2008) noted that it represents less than 5% of

the life assemblage (n=13) as observed during underwater transects, a proportion confirmed by our own informal observations of living individuals in the course of our work. Among the tested fossil and modern shells in our dataset, they are also a small proportion (n=5 of 30 species-identified individuals). While Richter et al. (2008) noted *T. squamosina* as the most common of the three congeners in fossil assemblages, the results from our collections do not corroborate this result. However, we did not sample from the breadth of sites (including several fossil reefs in Sinai) which Richter et al. (2008) was able to survey. Our fossil sites in Israel and Jordan could be anomalous in their higher concentration of *T. maxima* compared to the localities visited by the prior workers.

Oxygen isotope values of *T. squamosina* imply temperatures 1-3 °C warmer than the other two species, corroborating arguments from underwater transects proposing *T. squamosina* to be an obligate shallow-dwelling epifaunal recliner present only on the reef crest and reef flat (Roa-Quiaoit 2005, Richter et al. 2008). *T. maxima* in the region has been proposed to exhibit greater plasticity of life habits in terms of depth preference and reliance on coral substrate, while *T. squamosa* has been assigned as a fore-reef specialist due to its greater reliance on heterotrophy than its congeners (Roa-Quioit 2005, Jantzen et al. 2008). Oxygen isotope values and resulting calculated temperatures of formation of the three species in the depth assemblage corroborate some of these prior observations. These differences in outer shell layer calculated temperatures were found to be statistically significant for *T. squamosina* in comparison to the other two species (3°C warmer for outer and 1-2°C

higher for the inner shell layer), though a Tukey post-hoc test demonstrated that *T. maxima* and *T. squamosa* were not statistically significant in their difference compared to each other (Fig. 3).

Past studies of *T. maxima*, *T. gigas*, *T. squamosa* and other giant clams have used paleotemperature equations which are close variations of the original equation developed by Grossman and Ku (1986) (e.g., Romanek et al. 1987, Aharon 1991, Watanabe et al. 2004, Batenburg et al. 2011). As *T. squamosina* is closely related to *T. maxima* (Richter et al. 2008), a species which has been previously been demonstrated to precipitate aragonite in oxygen isotope equilibrium with seawater like all other tested *Tridacna* species (Romanek et al. 1987), species-specific differences likely cannot explain the warmer temperatures recorded in *T. squamosina* shells.

The reef flats of the Northern Red Sea are typical for fringing reefs of the region in displaying higher temperature than the reef slope due to trapped thermally stratified water, with about a 1.2°C difference in mean temperature experienced between corals at 7 versus 42 m water depth in Jordanian coastal waters (Al-Rousan et al. 2003). Spatiotemporal variability is quite high on diurnal scales (Monismith et al. 2005), but in general, average temperature should decrease with depth, particularly at microenvironmental scale on the reef. In addition, researchers have determined that corals increase the temperature of their local microenvironment by up to 1.5°C on top of existing temperature variability due to the combined influences of their own albedo and disturbance of laminar flow (and therefore less heat exchange with cooler water)

(Fabricius 2006; Jimenez et al. 2011). The shallowest portion of the reef may reach even warmer temperatures than ambient sea surface temperature if they experience tidal emersion and exposure to warmer air temperatures (Head 1987, Schoepf et al. 2015), and on the shallow reef, the heating impact of insolation can be dramatic, with up to 2.2°C differences in temperature between shaded and unshaded areas (Bahr et al. 2016).

We also observed that the oxygen isotope composition of differing shell layers in giant clams has relevance to understanding physiological partitioning within the bivalve itself. Oxygen isotope values for the three species are lower in the outer growth layer, consistent with a calcifying fluid temperature elevated by ~ 1.7 °C. This aligns with of the few prior studies to measure oxygen isotope composition from the inner and outer shell layers of a giant clam, in this case of one individual of *T. gigas* (Pätzold et al. 1991). In that specimen, calculated mean paleotemperatures are 0.6 °C higher on average for the outer layer than those of the inner layer, though the sampling frequency differed between the two transects and comparing the results of the two layers was not the aim of their experiment.

The disparity between inner and outer growth layers could also be due to kinetic effects within the calcifying fluid. This phenomenon has been observed in shells of other bivalves with differing crystal fabric between layers, which are governed by differing calcification systems which may introduce non-equilibrium fractionation to one or both layers (Trofimova et al. 2018). However, the more structurally homogenous layer of *Arctica islandica* has lower $\delta^{18}O$ values than the

cross-lamellar shell layer compared by Trofimova et al. (2018), opposing the relation we observe between prismatic and cross-lamellar shell layers in *Tridacna*. Other researchers have found that outer growth layer $\delta^{18}O$ paleotemperatures in tridacnids correspond well to environmental temperature variability (Komagoe et al. 2018), implying that $\square^{18}O$ differences could be a function of a true temperature difference between the outer and inner mantle of the giant clam.

We have no direct observations of mantle temperature differences throughout the tissue of a giant clam to corroborate this, but the outer mantle would be expected to be warmer. The outer mantle is a lower albedo tissue exposed to greater solar radiation and also endogenous heat from non-photochemical quenching within the symbiont-rich tissue (Yau and Fan 2011). The inner mantle is symbiont poor, largely isolated from sunlight and of higher albedo (Ip et al. 2017a, 2017b), and this difference in mantle microenvironments could explain the difference in calculated temperature between the inner and outer mantles of the giant clams. This effect runs parallel to the differences in $\delta^{18}O$ values between corallites on the sun-drenched "bumps" of coral heads as compared to the shaded "valleys" (Cohen & Hart 1997).

Significance of comparative ecology via oxygen isotope analysis for closely related species

Fossil reefs are important archives of baseline reef community structure, which in some cases can be more accurate in assessing the true diversity of the reef biome than both life and death assemblages alone (Edinger et al. 2001). Endangered

endemics such as *T. squamosina* are at risk of disappearing before they are fully described (Lees & Pim 2015), the comparative isotopic analysis of reef fossils will become more important in characterizing the full preindustrial niches of vulnerable species too rare to observe in large sample sizes in the wild, particularly in regions such as the Red Sea which were not described by SCUBA transect observations until relatively recently. Stable isotope approaches have already proven useful for description of cryptic marine vertebrates (Owen et al. 2011). As new cryptic species of *Tridacna* and other vulnerable reef organisms continue to be genetically described (Huelsken et al. 2013, Su et al. 2014, Monsecour 2016), stable isotope techniques may prove increasingly necessary to characterize their comparative ecology.

References

Aharon P (1991) Recorders of reef environment histories: stable isotopes in corals, giant clams, and calcareous algae. Coral Reefs 10:71–90

Al-Rousan S, Al-Moghrabi S, Pätzold J, Wefer G (2003) Stable oxygen isotopes in *Porites* corals monitor weekly temperature variations in the northern Gulf of Aqaba, Red Sea. Coral Reefs 22:346–356

Andrié C, Merlivat L (1989) Contribution des données isotopiques de deutérium, oxygène-18, hélium-3 et tritium, à l'étude de la circulation de la Mer Rouge. Oceanologica Acta 12:165–174

Bahr KD, Jokiel PL, Rodgers KS (2018) Influence of solar irradiance on underwater temperature recorded by temperature loggers on coral reefs. Limnology and Oceanography: Methods 14:338–342

Batenburg SJ, Reichart G-J, Jilbert T, Janse M, Wesselingh FP, Renema W (2011) Interannual climate variability in the Miocene: High resolution trace element and stable isotope ratios in giant clams. Palaeogeography, Palaeoclimatology, Palaeoecology 306:75–81

Cohen AL, Hart SR (1997) The effect of colony topography on climate signals in coral skeleton. Geochimica et Cosmochimica Acta 61:3905–3912

Dreier A, Loh W, Blumenberg M, Thiel V, Hause-Reitner D, Hoppert M (2014) The isotopic biosignatures of photo-vs. thiotrophic bivalves: are they preserved in fossil shells? Geobiology 12:406–423

Edinger EN, Pandolfi JM, Kelley RA (2001) Community structure of Quaternary coral reefs compared with Recent life and death assemblages. Paleobiology 27:669–694

Elliot M, Welsh K, Chilcott C, McCulloch M, Chappell J, Ayling B (2009) Profiles of trace elements and stable isotopes derived from giant long-lived *Tridacna gigas* bivalves: Potential applications in paleoclimate studies. Palaeogeography, Palaeoclimatology, Palaeoecology 280:132–142

Erez J (1978) Vital effect on stable-isotope composition seen in foraminifera and coral skeletons. Nature 273:199–202

Fabricius KE (2006) Effects of irradiance, flow, and colony pigmentation on the temperature microenvironment around corals: implications for coral bleaching? Limnology and Oceanography 51:30–37

Gannon ME, Pérez-Huerta A, Aharon P, Street SC (2017) A biomineralization study of the Indo-Pacific giant clam *Tridacna gigas*. Coral Reefs 36:503–517

Goreau TF, Goreau NI, Yonge CM (1973) On the utilization of photosynthetic products from zooxanthellae and of a dissolved amino acid in *Tridacna maxima f. elongata* (Mollusca: Bivalvia). Journal of Zoology 169:417–454

Grossman EL, Ku T-L (1986) Oxygen and carbon isotope fractionation in biogenic aragonite: temperature effects. Chemical Geology: Isotope Geoscience Section 59:59–74

Head SM (1987) Corals and coral reefs of the Red Sea. Red Sea 128–151

Huber M, Eschner A (2010) *Tridacna (Chametrachea) costata* Roa-Quiaoit, Kochzius, Jantzen, Al-Zibdah & Richter from the Red Sea, a junior synonym of *Tridacna squamosina* Sturany, 1899 (Bivalvia, Tridacnidae). Annalen des Naturhistorischen Museums in Wien Serie B für Botanik und Zoologie 112:153–162

Huelsken T, Keyse J, Liggins L, Penny S, Treml EA, Riginos C (2013) A novel widespread cryptic species and phylogeographic patterns within several giant clam species (Cardiidae: *Tridacna*) from the Indo-Pacific ocean. PLOS ONE 8:e80858

Ip YK, Hiong KC, Goh EJK, Boo MV, Choo CYL, Ching B, Wong WP, Chew SF (2017) The whitish inner mantle of the giant clam, *Tridacna squamosa*, expresses an apical Plasma Membrane Ca2+-ATPase (PMCA) which displays light-dependent gene and protein expressions. Front Physiol 8:

Ip YK, Koh CZY, Hiong KC, Choo CYL, Boo MV, Wong WP, Neo ML, Chew SF (2018) Carbonic anhydrase 2-like in the giant clam, *Tridacna squamosa*: characterization, localization, response to light, and possible role in the transport of inorganic carbon from the host to its symbionts. Physiological Reports 5:e13494

Jantzen C, Wild C, El-Zibdah M, Roa-Quiaoit HA, Haacke C, Richter C (2008) Photosynthetic performance of giant clams, *Tridacna maxima* and *T. squamosa*, Red Sea. Marine Biology 155:211–221

Jimenez IM, Kühl M, Larkum AWD, Ralph PJ (2011) Effects of flow and colony morphology on the thermal boundary layer of corals. J R Soc Interface 8:1785–1795

Johnston M, Yellowlees D, Gilmour I (1995) Carbon isotopic analysis of the free fatty acids in a tridacnid—algal symbiosis: interpretation and implications for the symbiotic association. Proc R Soc Lond B 260:293–297

Jones DS, Jacobs DK (1992) Photosymbiosis in *Clinocardium nuttalli*: Implications for tests of photosymbiosis in fossil molluscs. PALAIOS 7:86–95

Jones DS, Williams DF, Romanek CS (1986) Life history of symbiont-bearing giant clams from stable isotope profiles. Science 231:46–48

Jones DS, Williams DF, Spero HJ (1988) More light on photosymbiosis in fossil mollusks: The case of *Mercenaria* "tridacnoides." Palaeogeography, Palaeoclimatology, Palaeoecology 64:141–152

Klein R, Pätzold J, Wefer G, Loya Y (1992) Seasonal variations in the stable isotopic composition and the skeletal density pattern of the coral *Porites lobata* (Gulf of Eilat, Red Sea). Mar Biol 112:259–263

Komagoe T, Watanabe T, Shirai K, Yamazaki A, Uematu M (2018) Geochemical and microstructural signals in giant clam *Tridacna maxima* recorded typhoon events at Okinotori Island, Japan. Journal of Geophysical Research: Biogeosciences 123:1460–1474

Lees AC, Pimm SL (2015) Species, extinct before we know them? Current Biology 25:R177–R180

McConnaughey TA (2003) Sub-equilibrium oxygen-18 and carbon-13 levels in biological carbonates: carbonate and kinetic models. Coral Reefs 22:316–327

McConnaughey TA, Burdett J, Whelan JF, Paull CK (1997) Carbon isotopes in biological carbonates: respiration and photosynthesis. Geochimica et Cosmochimica Acta 61:611–622

McConnaughey TA, Gillikin DP (2008) Carbon isotopes in mollusk shell carbonates. Geo-Mar Lett 28:287–299

Monismith SG, Genin A, Reidenbach MA, Yahel G, Koseff JR (2006) Thermally driven exchanges between a coral reef and the adjoining ocean. J Phys Oceanogr 36:1332–1347

Monsecour K. (2016) A new species of giant clam (Bivalvia: Cardiidae) from the Western Indian Ocean. Conchylia 46:66–77

Neo ML, Wabnitz CC, Braley RD, Heslinga GA, Fauvelot C, Van Wynsberge S, Andréfouët S, Waters C, Tan AS-H (2017) Giant clams (Bivalvia: Cardiidae: Tridacninae): a comprehensive update of species and their distribution, current threats and conservation status. Oceanography and Marine Biology: An Annual Review 55:87–387

Norton JH, Jones GW (1992) The giant clam: an anatomical and histological atlas. The giant clam: an anatomical and histological atlas

Owen K, Charlton-Robb K, Thompson R (2011) Resolving the trophic relations of cryptic species: An example using stable isotope analysis of dolphin teeth. PLOS ONE 6:e16457

Pätzold J, Heinrichs JP, Wolschendorf K, Wefer G (1991) Correlation of stable oxygen isotope temperature record with light attenuation profiles in reef-dwelling *Tridacna* shells. Coral Reefs 10:65–69

Richter C, Roa-Quiaoit H, Jantzen C, Al-Zibdah M, Kochzius M (2008) Collapse of a new living species of giant clam in the Red Sea. Current Biology 18:1349–1354

Roa-Quiaoit HAF (2005) The ecology and culture of giant clams (Tridacnidae) in the Jordanian sector of the Gulf of Aqaba, Red Sea. PhD, Universitat Bremen

Romanek CS, Jones DS, Williams DF, Krantz DE, Radtke R (1987) Stable isotopic investigation of physiological and environmental changes recorded in shell carbonate from the giant clam Tridacna maxima. Marine Biology 94:385–393

Schoepf V, Stat M, Falter JL, McCulloch MT (2015) Limits to the thermal tolerance of corals adapted to a highly fluctuating, naturally extreme temperature environment. Scientific Reports 5:17639

Su Y, Hung J-H, Kubo H, Liu L-L (2014) *Tridacna noae* (Röding, 1798)–a valid giant clam species separated from *T. maxima* (Röding, 1798) by morphological and genetic data. Raffles Bulletin of Zoology 62:124–135

Swart PK, Leder JJ, Szmant AM, Dodge RE (1996) The origin of variations in the isotopic record of scleractinian corals: II. Carbon. Geochimica et Cosmochimica Acta 60:2871–2885

Trofimova T, Milano S, Andersson C, Bonitz FGW, Schöne BR (2018) Oxygen isotope composition of *Arctica islandica* aragonite in the context of shell

architectural organization: Implications for paleoclimate reconstructions. Geochemistry, Geophysics, Geosystems 19:453–470

Vermeij GJ (2013) The evolution of molluscan photosymbioses: a critical appraisal. Biological Journal of the Linnean Society 109:497–511

Watanabe T, Suzuki A, Kawahata H, Kan H, Ogawa S (2004) A 60-year isotopic record from a mid-Holocene fossil giant clam (*Tridacna gigas*) in the Ryukyu Islands: physiological and paleoclimatic implications. Palaeogeography, Palaeoclimatology, Palaeoecology 212:343–354

Wynsberge SV, Andréfouët S, Gaertner-Mazouni N, Wabnitz CCC, Menoud M, Moullac GL, Levy P, Gilbert A, Remoissenet G (2017) Growth, survival and reproduction of the giant clam *Tridacna maxima* (Röding 1798, Bivalvia) in two contrasting lagoons in French Polynesia. PLOS ONE 12:e0170565

Yau AJ-Y, Fan T-Y (2012) Size-dependent photosynthetic performance in the giant clam *Tridacna maxima*, a mixotrophic marine bivalve. Mar Biol 159:65–75

Yellowlees D, Rees TAV, Leggat W (2008) Metabolic interactions between algal symbionts and invertebrate hosts. Plant, Cell & Environment 31:679–694

Yonge CM (1975) Giant clams. Scientific American 232:96–105

Figures

Figure 1: Map of sampling sites used for shells featured in this study (with a box indicating the potential location of the Sinai shells

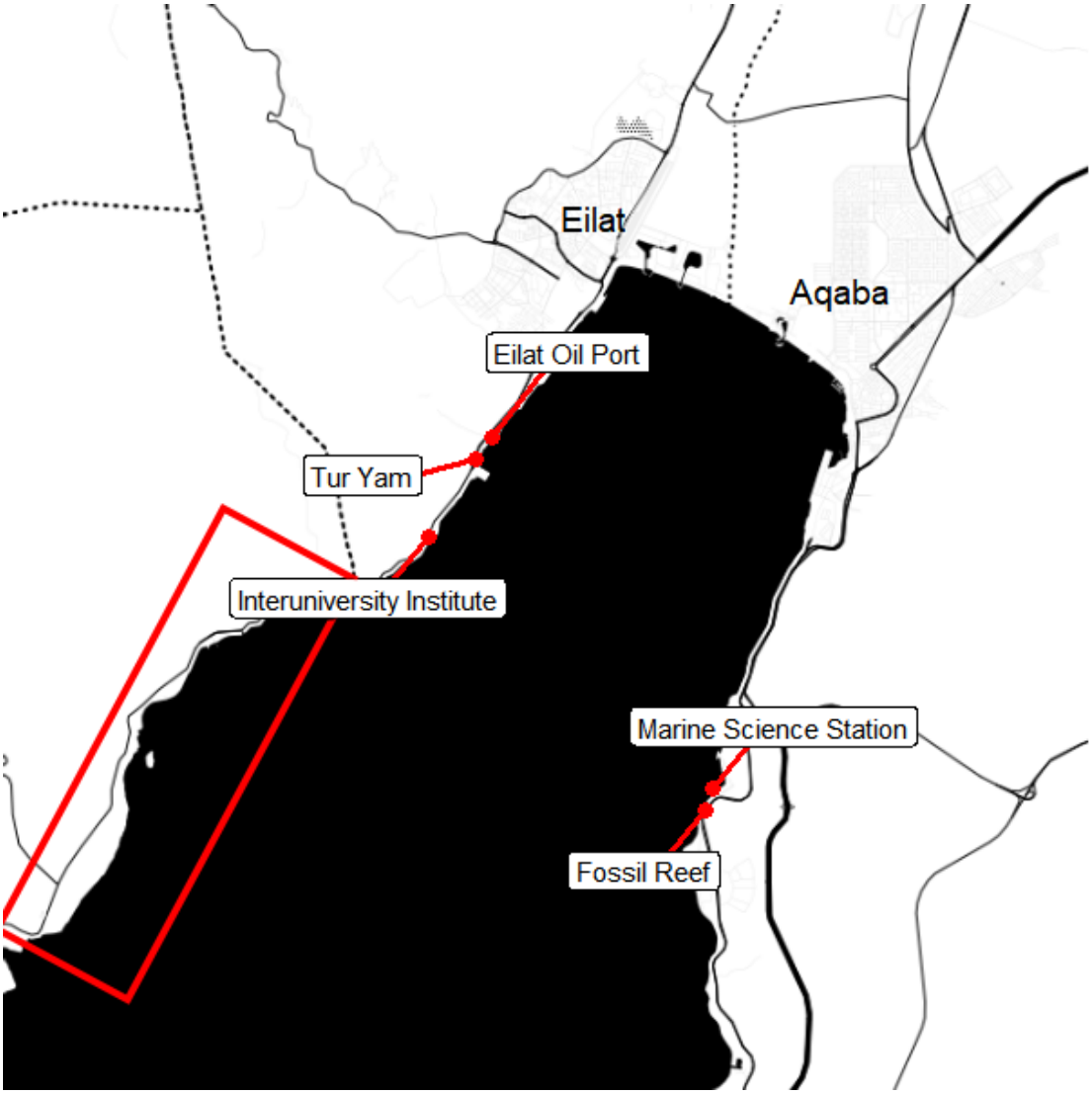

Figure 2: Cross section of a typical specimen of *Tridacna maxima* highlighting inner and outer growth layers

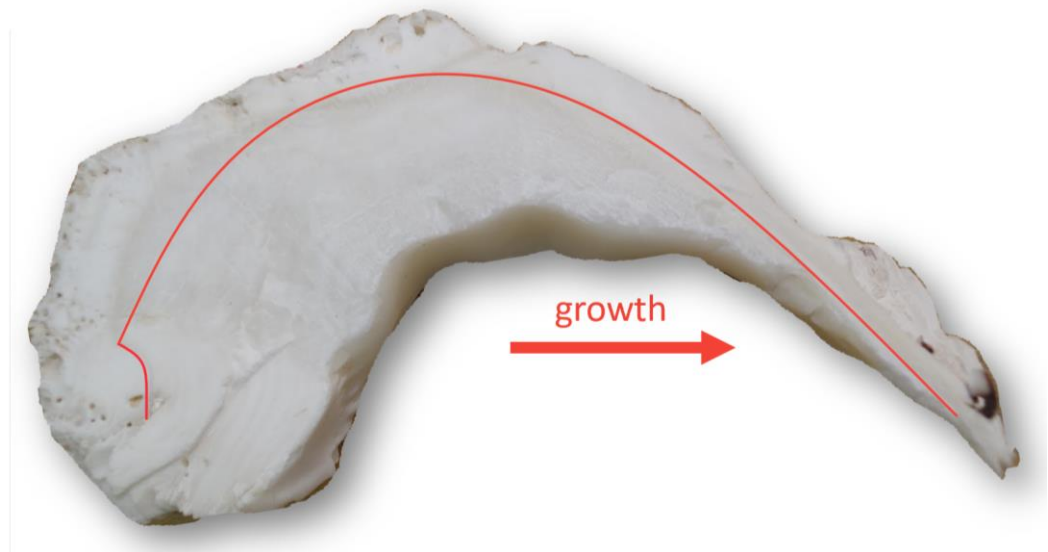

Figure 3: Relationship between $\delta^{18}O$ and $\delta^{13}C$ values of different species by shell layer.

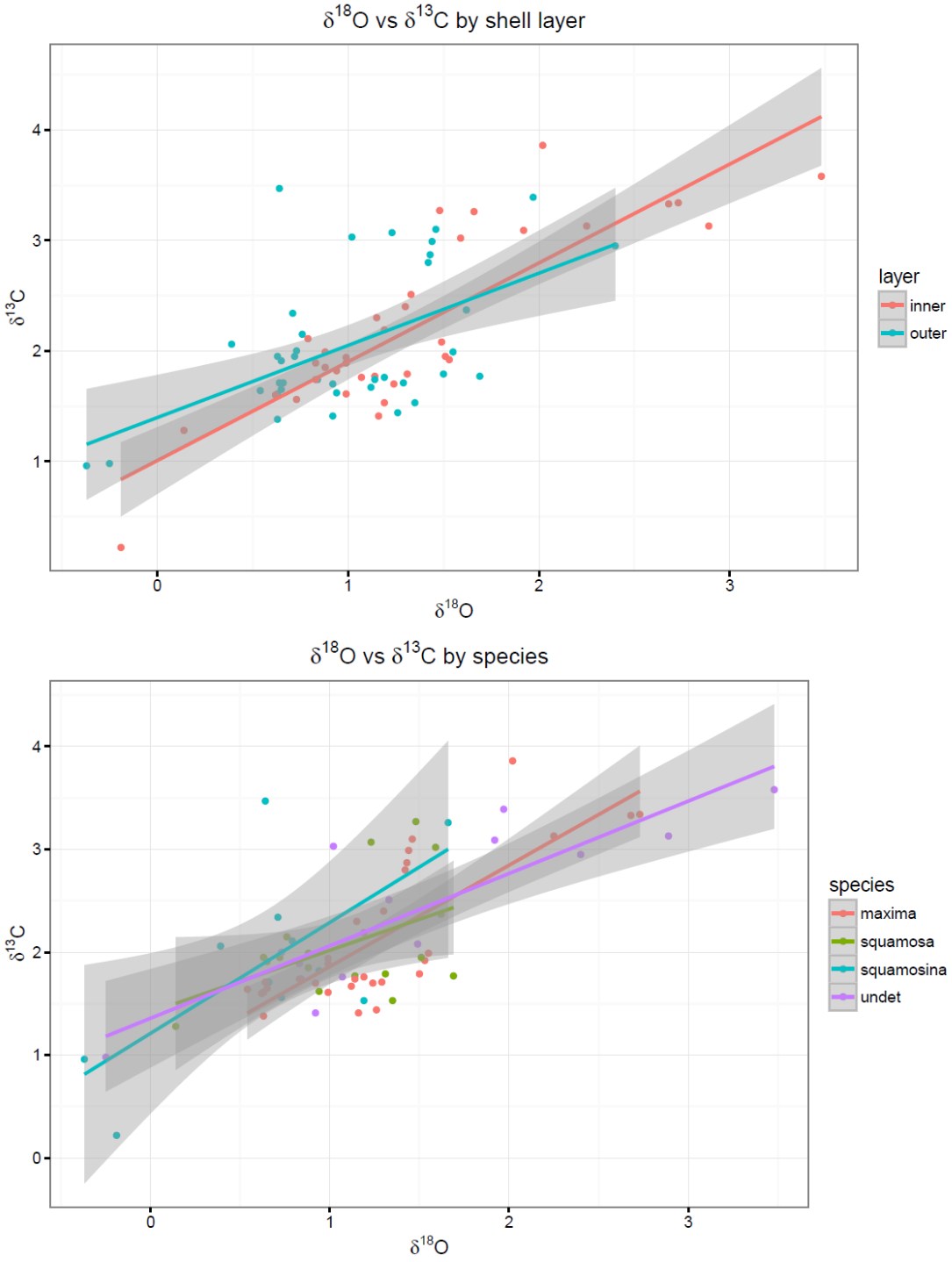

Figure 4: Distributions of $\delta^{13}C$ and $\delta^{18}O$-derived temperatures for the three species, inner and outer shell layers. Middle quartiles contained in boxes, whiskers are 1.5xIQR, horizontal lines are the medians, black points are outliers.

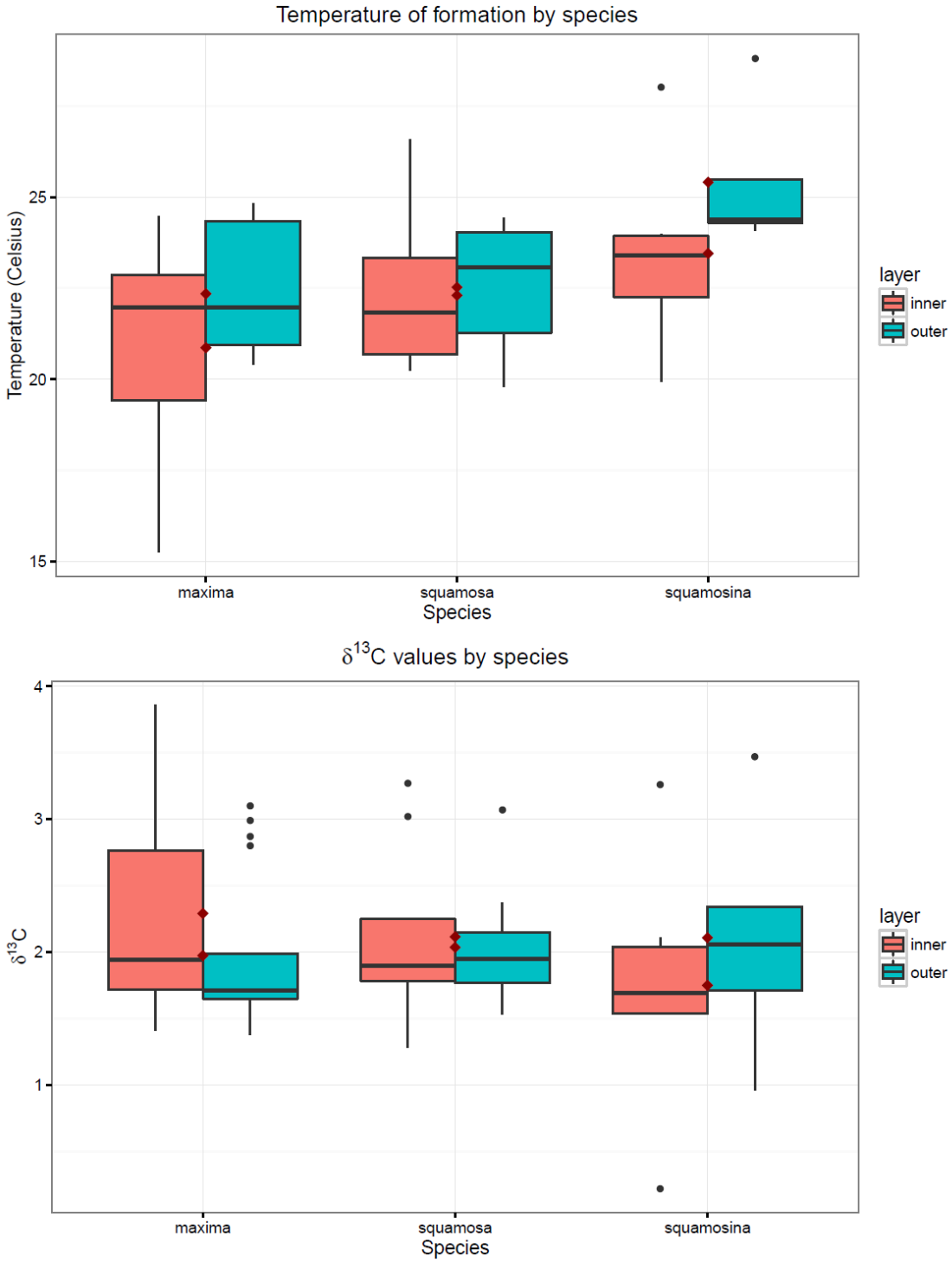

Tables

Table 1: Means of isotope values and calculated temperatures of shell layers

Shell layer	$\delta^{13}C$	$\delta^{18}O$	Temperature °C (Romanek et al. 1987)
Inner	2.2	1.4	21.3
Outer	1.9	1.0	23.0

Table 2: Tukey HSD results for the Analysis of Variance for temperature differences between the species

Species comparison	Difference	Lower	Upper	p-value (adjusted)
squamosa-maxima	0.178799	-1.56846	1.926054	0.965319
squamosina-maxima	3.061057	0.904716	5.217397	0.004221
squamosina-squamosa	2.882258	0.518118	5.246398	0.01445

CHAPTER 4

Giant clam growth in the Gulf of Aqaba is accelerated compared to fossil populations

Abstract

The giant clams are globally distributed reef-dwelling bivalves which use the same photosymbiotic partnership characteristic of reef-building corals. But while the declining health of corals in the face of climate change and human pollution are the topic of intensive research, comparatively little work has been dedicated to understanding trends in the health of giant clams in relation to environmental change. We have collected fossil and modern specimens of three species of *Tridacna* from reefs fringing the Gulf of Aqaba in the Northern Red Sea. After calibrating the daily/twice-daily growth bands from the outer layer of their shells, we have determined that all three species are growing more quickly in the modern day compared to fossil specimens from Holocene and Pleistocene reefs. We found that giant clam shell organic $\delta^{15}N$ of modern specimens show a 4.5‰ lower average value compared to fossil specimens, an offset which we propose is most likely attributable to increased deposition of isotopically light nitrate aerosols in the modern era. As nitrate is a known accelerant of giant clam growth, it may play a role in the faster growth seen in modern populations. We found that that growth is positively correlated to temperature as measured by oxygen isotope paleothermometry of their shell carbonate, and discuss how lower winter cold temperatures in the past may have

depressed giant clam growth compared to the relatively small seasonal availability seen today. Giant clams can serve as isotopic and physiological sentinels of reef environmental change, both to determine their own comparative health and that of the coral reefs they inhabit.

Introduction

The giant clams of genus *Tridacna* have a cosmopolitan distribution throughout reef environments of the tropical Indo-Pacific (Neo et al. 2017). The coral reefs they inhabit are currently in crisis due to the combined stress of rising ocean temperatures, acidification, and pollution, particularly in the form of nitrate-mediated eutrophication. Reef-building corals and giant clams share a partnership with photosymbiotic dinoflagellates of the same genus, *Symbiodinium*. These symbiotic algae provide their hosts with photosynthate sugars in exchange for nitrogenous waste and a stable internal environment (Goreau et al. 1973, Fitt et al. 1995). The impacts of environmental change on the coral-*Symbiodinium* partnership are the subject of intensive research. Much less is known about the nature of photosymbiosis in giant clams, how it varied during their natural history, and how it will be influenced as their reef environments continue to be altered by human activity.

In the Gulf of Aqaba in the Northern Red Sea (Figure 1), three giant clam species are known: *Tridacna squamosa, T. maxima* and the rare endemic *T. squamosina*. All three rely on photosymbiosis, and similar to reef-building corals, these species are reliant on clear oligotrophic water within a constrained range of

temperatures (Neo et al. 2015). Corals from the Central Red Sea have been recorded to be growing more slowly in the modern day, largely attributed to the impact of heat stress (Cantin et al. 2010), even though Red Sea corals and their symbionts are thought to be strongly selected for heat tolerance (Baker et al. 2004, Fine et al. 2013, Hume et al. 2016). Giant clams, similar to corals, are sensitive to temperature-linked bleaching (Leggat et al. 2003, Andréfouët et al. 2013), but their comparative physiological response is not as well studied. In addition, giant clam calcification has been found to be very light-sensitive (Sano et al. 2012; Warter et al. 2018), and shaded giant clams are typically growth-stunted compared to those with full access to light (Lucas et al. 1989). The calcification of giant clams is believed to be aided by the activity of their symbionts, with their increased activity during daylight hours drawing down CO_2, which increases mantle pH and accelerates shell growth (Fitt et al. 1995). This photosystem may be vulnerable to the same climatological and pollution-linked stresses experienced by corals.

The Northern Red Sea experienced rapid industrial development in the 20th century. Local pollution sources such as phosphate mining (Walker and Ormond 1982), sewage effluent (Lazar et al. 1995), oil spills (Fishelson 1973; Rinkevich and Loya 1977), fish farming (Bongiorni et al. 2003) and urbanization have increased environmental nitrate, phosphate and trace metal concentrations in Red Sea water, harming the local reefs (Abelson et al. 1999). Anthropogenic nitrate and phosphate influx can increase algal productivity, which reduces seawater clarity and can "smother" light-dependent reef taxa (Bell 1992). Trace metals, such as copper from

oil importation, land use change, and mining, have servedact as phytotoxins that lower giant clam production (Elfwing et al. 2002). Fortunately, while the ecological impacts of eutrophication were severe in the late 20th century (Walker et al. 1982; Loya 2004), recent improvements in environmental management have reduced the frequency of oil and sewage spills (Lazar et al. 2005) and closed the effluent-producing fish farms (Oron et al. 2014). However, nearly 30 tonnes of nitrogen and phosphorus were input into the Gulf of Eilat by anthropogenic point sources in 2014 alone, despite the closure of fish farms, which had discharged nearly 300 tons of N per year (Berman-Frank et al. 2016).

While anthropogenic climate change has thus had only subtle influences on annual mean sea surface temperature (SST) in the industrial era, the Northern Red Sea of the last interglacial is thought subject greater SST seasonality based on coral records (Felis et al. 2004). During multi-year periods of above average SST in the Northern Red Sea, corals were observed to display depressed skeletal growth (Cantin et al. 2010), despite their apparent locally bred resistance to hyperthermal events (Fine et al. 2013, Hume et al. 2016). Giant clams are thought to display high resilience to large swings in temperature (Schwartzmann et al. 2011), which contrasts with the relative ease of bleaching of corals in the face of extreme temperatures (Baker et al. 2008). It would be valuable to determine whether giant clams from the more variable past of the Red Sea show different growth patterns compared to their modern counterparts in the presently stable tropical-type temperature regime. Their daily growth can be benchmarked in fossil and modern specimens using

sclerochronology techniques (Pätzold et al. 1991), while oxygen isotope paleothermometry can be used to reconstruct their past and present temperature environments (Aharon 1991).

The Northern Red Sea represents an opportune environment to study the comparative growth of fossil and modern giant clams, because there are well-preserved, exposed late Holocene reefs directly onshore from modern fringing reefs, which still contain extensive populations of *Tridacna*. By comparing the growth of giant clam species in pre-industrial and modern specimens through the measurements of sequential growth bands in their shells (sclerochronology), we can better understand how their calcification has changed through time.

In addition, as with all mollusks, giant clam shells contain a small fraction of proteinaceous organic matrix. Prior investigations have determined that the nitrogen isotopes contained within this shell matrix can serve as a record of the nutritional environment and trophic level of bivalves in the fossil record (O'Donnell et al. 2003). Differing nitrogen sources have characteristic $\delta^{15}N$ signatures, with nitrate aerosols having lower $\delta^{15}N$ values (Wankel et al. 2010), and sewage pollution having very high values (Heaton 1986; Carmichael et al. 2008). Some studies have dissolved shell samples in acid or reagents such as EDTA to extract organic material (Carmichael et al. 2008, Watanabe et al. 2009, Dreier et al. 2014), but other investigations have determined that mollusk shell organic material can be directly combusted to determine shell organic matrix nitrogen isotope composition (Versteegh et al. 2011). Combustion-based investigations of Chesapeake Bay oysters have shown a ^{15}N-

enrichment of the the modern day oyster organic matrix, which was attributed to the increased supply of ^{15}N- enriched sewage into the watershed (Black et al. 2017, Darrow et al. 2017). Other research has applied this technique to Panamanian bivalves (Graniero et al. 2016). We will determine the nitrogen isotope composition of pre-industrial and modern giant clam shell matrix, with the intention of tracing the fingerprint of their comparative environment in relation to their growth. We wish to know whether Red Sea giant clam growth is depressed in the modern day compared to historical specimens, as is the case for corals, and if their growth can be related back to pollution-linked changes in nutrient availability or climate change.

Methods

From June-August 2016, we collected shells from recently deceased individuals of the three known Red Sea *Tridacna* species (Figure 1). All collection was conducted in the surf zone with approval from Israeli and Jordanian authorities of the local Marine Protected Areas. In addition, several shells were obtained from the Hebrew University of Jerusalem, which had been confiscatedfrom smugglers at the Taba border crossing. These modern shells are believed to have been collected illegally in Northern Sinai.

We collected subfossil remains of late Holocene *Tridacna* from several field sites along the Israeli coast (Fig. 1), including shells surfaced during construction of the Interuniversity Insititute in Eilat, Israel. These shells are of unknown age, but are from the same horizon underground as a buried reef previously radiocarbon dated as

4500 +/- 100 yr in age (Shaked et al. 2011). We pried *Tridacna* shells from cemented "reef rock" at the Tur Yam site (with permission of local MPA managers), coeval with corals U/Th dated between 6800 and 5400 yr age (Weil 2008). On the Jordanian side, we collected shells from an emerged reef of uncertain age on the landward side of the road south of the Aqaba Marine Science Station. This lower platform (terrace "R2" in the description of Yehudai et al. 2017) above the coastal road was previously suggested to be less than 6500 years old (Al-Rifaiy and Cherif 1988) but was later found to contain corals of up to 117,000 +/- 3,000 kyr in age according to U-series dating (Scholz et al. 2004, Yehudai et al. 2017), so we will refer to shells from this platform as "last interglacial" in age.

We then identified shells to species using the taxonomic key for *Tridacna* previously used for studies of giant clams in the Gulf of Aqaba (Roa-Quiaoit 2005). The most useful diagnostic traits were shell symmetry, geometry of plications at the ventral margin, shape and spacing of shell scutes and the size of the byssal opening. We then sectioned shells longitudinally to ease transport to UC Santa Cruz. We collected small chips from a selection of shells for microstructural observation with scanning electron microscopy at the UCSC W.M. Keck Center for Nanoscale Optofluidics. Shells which did not display microstructural characteristics of crossed-lamellar aragonite were not used for subsequent carbon, oxygen or nitrogen stable isotope analyses (Figure 2). This ruled out the shells from the Tur Yam site, though growth increments were still measurable even in their recrystallized calcite. We milled several shells using a Merchantek New Wave micromill with a 0.05 mm

Brasseler dental burr. We milled sequentially at around 3-4 mm resolution with the aim of replicating a seasonal oscillation of temperatures as determined by $\delta^{18}O$ paleothermometry. We also used a Dremel tool with 2 mm tungsten carbide bit to collect bulk oxygen isotope samples from the outer growth layer of a selection of bivalves for determination of mean paleotemperature.

50 microgram subsamples were weighed out and baked at 60°C under vacuum overnight to remove volatile organics, halogen ions and water. At the UCSC Stable Isotope Laboratory, freshly baked powder samples were then acidified in vials with 1-2 cm of silver wire (to react with sulfur compounds) and acidified at 75°C with orthophosphoric acid in a ThermoScientific Kiel IV Carbonate Device. The released CO2 is cryogenically separated from water and then introduced to the coupled ThermoScientific MAT-253 dual-inlet Isotope Ratio Mass Spectrometer (IRMS). All $\delta^{13}C$ and $\delta^{18}O$ values are reported relative to the Vienna Pee Dee Belemnite (VPDB) standard using four NBS-18 limestone standards and an inhouse Carrera Marble standard (CM12). Two NBS-19 standards are run as a sample for quality control. Long-term lab precision for 50-70 microgram samples is 0.08‰ for $\delta^{18}O$ and 0.05‰ $\delta^{13}C$.

$\delta^{18}O$ values were converted to equivalent temperatures of formation using a paleotemperature equation calibrated for *Tridacna maxima* based on that of Grossman and Ku (1982) (Romanek et al. 1987) and a seawater $\delta^{18}O$ value of 1.8‰ as determined from prior measurements of seawater $\delta^{18}O$ values for the northern Red Sea, obtained from over a year of continuous monthly direct measurements of

seawater $\delta^{18}O$ values (Al-Rousan et al. 2003). This value was independently confirmed by the work of Andrie and Merlivat (1989), who obtained a seawater $\delta^{18}O$ value between 1.8-1.9‰ from a cruise near the mouth of the Gulf of Aqaba.

We then collected chips from each shell specimen and ground them with a porcelain mortar and pestle. We weighed 60 mg of powder into tin capsules and loaded them into a CE Instruments NC2500 elemental analyzer interfaced to a ThermoFinnegan Delta Plus XP Isotope Ratio Mass Spectrometer (IRMS) at the UCSC Stable Isotope Laboratory. These capsules were then flash combusted at 1020 °C in a quartz column. The resulting gas was run through a Carbosieve GC column at 45°C to scrub out CO_2 gas before introduction of N_2 gas to the IRMS. Pugel and Acetanilide standards were used to monitor quality before the samples were run and during as a drift control. Results are reported relative to Air for $\delta^{15}N$. For analyses, we only will use $\delta^{15}N$ values where more than 5 micrograms of nitrogen were measured, as the confidence intervals for measurements below that threshold grow much larger.

Once isotopic sampling was complete, we collected a subsample of shells for detailed growth band profiling. These shells were stained with Mutvei's solution mixed according to the formula described by Schöne et al. (2005) and immersed in the solution at 60°C for 45 minutes. Mutvei's solution etches the shell surface and binds to organic molecules in the intercrystalline matrix, making growth bands more readily visible under light microscopy. The outer layers of each shell were then photographed under a stereomicroscope and growth band widths were landmarked

using the cell counter tool available in ImageJ. These coordinates were then used to calculate widths of neighboring growth bands according to the distance equation. Because these bands were measured at an angle facing downward from the longest direction of growth, we transformed them using the trigonometric equation:

$$Growth = \frac{w_{increment}}{angle * \pi/180}$$

with the angle measured as the angle of declination from that of maximum growth (Figure 2). Growth bands consistently follow this angle throughout the shell because they track to the geometry of the ventral margin during deposition. The clam extends its siphonal mantle over this curved margin to precipitate additional growth layers, which manifest as high-frequency growth bands of daily or twice daily periodicity (Gannon et al. 2017).

Once growth was calculated for each shell, we determined whether these microincrements were daily or twice daily by comparing to annual growth estimates obtained from oxygen isotope paleothermometry seasonal curves. As an additional control we also counted annual bands from the interior growth layers of the giant clams to determine their approximate age, and then divided their total shell length by this age to get an approximate growth per year value. While these interior annual bands are known to overestimate age due to non-seasonal interruptions of growth, they can serve as a rough confirmation of whether the high-resolution outer layer bands are deposited daily or twice daily. When age estimations from both isotope and annual band growth approximation are plotted in comparison to lines representing

365 and 730 bands per year, all specimens plot closely against one of those two continua (Figure 3b).

Giant clam daily growth layer deposition is strongly controlled by light (Sano et al. 2012, Warter and Müller 2016). While it is outside the scope of our investigation, we suspect that the subpopulation of clams with twice-daily increments may have the typical nighttime interruption and additionally an average of one tidal interruption during daylight hours. We were unable to find these outer shell bands in two cultured clam shells obtained from the Israel National Center for Mariculture in Eilat. These shells were grown in a sun-shaded outdoor growing tank, and it may be that the sun shade or access to nutrition from the culturing environment disrupted the diel cycle mediating outer layer growth layer periodicity.

Annual growth for bivalves varies through ontogeny. The majority of our collection are subadult or juveniles still in the linear growth phase prior to deceleration which occurs in tridacnids that have reached mature size. To control for comparison of growth among our tridacnid shells, which range from 2.5 to 23 cm in length, we have used two common growth indices as metrics for tridacnid growth: the Von Bertalanffy growth constant k and the related standardized growth performance index ϕ'. The coefficient k is calculated with the equation from Munro (1982):

$$k = [\ln(L_\infty - L_1) - \ln(L_\infty - L_2)]/(t_2 - t_1)$$

Where L_∞ values are the theoretical maximum height found for each species from a previous aquaculture survey conducted in the thesis of Roa-Quiaoit (2005) but scaled

using previously calibrated allometric relationships (Chan et al. 2008, Richter et al. 2005) to measure height opposed to length (along the hinge) used in her study, as our sections occurred along the height of the shell instead of along the total length. L_1 and L_2 values are two shell lengths and t_2-t_1 represents the time elapsed between those lengths, as recorded in the growth increments of the animal.

ϕ' can be calculated with the equation described in Pauly and Munro (1984):

$$\phi' = log_{10}k + 2log_{10}L_{\infty}$$

With k and L_{∞} values obtained from the previous Von Bertalanffy equation. ϕ' was used in the global bivalve growth database developed by Vakily (1992) and will allow us in combination with the work of Roa-Quiaoit (2005) to assess the comparative fossil and modern growth of Red Sea tridacnids.

Growth rate indices were compared to oxygen and carbon isotope values using two-way Analyses of Variance (ANOVA). When data was normally distributed as indicated by Shapiro-Wilks test results and visual inspection of Q-Q plots, we utilized parametric tests such as Fisher's t-test to determine the statistical significance of the difference of means. Data subsets that were not normally distributed were analyzed with nonparametric tests such as Kendall correlation in the comparison of growth rate and temperature/nitrogen isotope content. All statistical analyses and visualization were conducted with R software.

Results

The growth metrics, including mean shell extension rate and k, and ϕ' values, are shown in Table 1. Among the three species, *Tridacna squamosina* shows the fastest growth by all three measures, with *T. squamosa* next and *T. maxima* growing less quickly. Based on the aggregated growth metrics of Roa-Quiaoit (2005) and Vakily (1992), our k values are in the range known from other giant clams (though modern *T. squamosina* shows high growth), while our calculated measures of ϕ' are lower than those of other past studies. Because we lacked direct estimates of L_∞ for our populations, we utilized the values from Roa-Quiaoit (2005), which are based on caliper measurements.

For all three species of Red Sea giant clams, growth is faster among modern day specimens as measured by both k and ϕ' (Figure 4). These changes for both k and ϕ' between the two cohorts of shells are statistically significant as indicated by a two-way Analysis of Variance, as is the difference between species (Table 2).

The mean $\delta^{15}N$ values for fossil and modern populations are significantly different as well ($t = 3.4363$, $df = 15.9$, p-value < 0.005; Figure 5). Fossil populations have a mean $\delta^{15}N$ value ~4.3‰ lower than the mean of modern shells. Shell mean temperatures calculated based on $\delta^{18}O$ values indicate that modern shells have a higher mean temperature of formation (23.4 °C) than fossil shells (22.5 °C), but these means were not significantly different ($t = -1.3109$, $df = 16.957$, p-value = 0.2074; Figure 5).

There is a positive relationship between temperature and φ' across all species (Kendall rank correlation: tau = 0.27, p-value = 0.032; Figure 5) Faster growing species *T. squamosa* and *T. squamosina* appear to also record higher temperatures. For one shell that experienced heat stress over 27.5 °C, which likely depressed its growth, there is a weak negative relationship between ϕ' and $\delta^{15}N$ (tau = -0.15, p = 0.31; Figure 5).

Discussion

Temperature

The growth of *Tridacna* in the Northern Red Sea is faster compared to fossil populations as measured by linear growth rates and when scaled to ontogeny using two growth metrics. The first potential explanation for this change is temperature. Among our specimens, we find a positive correlation between overall growth rate and temperature, in agreement with tridacnids from other regions (Schwartzmann et al. 2011). The depression in growth of the individual measuring shell temperatures above 27 °C also agrees with past observations of tridacnid thermal tolerance thresholds (Schwartzmann et al. 2011). The Red Sea has experienced relatively little change in mean annual sea surface temperature in the last 130 years (Felis et al. 2000), and experienced similar mean temperatures at the last interglacial (Reiss et al. 1980, Felis et al. 2004), which may explain the lack of a statistically significant difference between the mean temperatures recorded for our fossil and modern shells. However, prior investigations of mid-Holocene (4.6-5.75 kyr) and interglacial coral $\delta^{18}O$

records from the region suggested seasonality was greater than it is today (Moustafa et al. 2000; Felis et al. 2004). These two intervals represent the windows of time encompassed by our fossil specimens. Modern Red Sea giant clams experience a relatively constricted annual range of in temperature of around 7 °C from winter to summer (Al-Rousan et al. 2003), with diurnal variations exceeding the annual temperature variability experienced in the region. Greater historical seasonality may have depressed the historical growth of Red Sea giant clams by causing lower winter temperatures compared to those experienced by giant clams today.

Nitrate Fertilization

Nitrate is a well-recognized accelerant of giant clam growth. Giant clams ingest ammonia and nitrate directly, with this activity varying directly in proportion to the rate of photosynthesis of their endosymbionts (Fitt et al. 1995). Studies of cultured giant clams have confirmed that exposure to excess nitrate and ammonia accelerates shell growth (Belda et al. 1993) to the extent that it is standard practice to "fertilize" giant clam stocks with nitrate in aquaculture to increase yield (Lucas 1994). Phosphate has also benefits for growth, but only when introduced in addition to nitrate (Belda et al 1993).

In the 1990s and early 2000s, the development of fish farms in the Gulf of Aqaba led to a reef crisis, as coral growth and reproduction was harmed by the influx of fish waste effluent (Biongiorni et al. 2003; Loya et al. 2004, Lazar et al. 2005). In 2008, the fish cages were removed (Berman-Frank et al. 2016), and subsequent

studies suggested recovery of some benthic taxa as water quality improved (Oron et al. 2014). However, the modern Red Sea is still thought to experience higher nitrate supply compared to historical levels, particularly in summer, due to an increase in anthropogenic nitrate aerosol deposition (Wankel et al. 2010). Such aerosols are thought to account for up to 35% of the dissolved inorganic N delivered to the Red Sea during summer months, and could support most of the limited new summer production which occurs in the region (Chen et al. 2007). These aerosols, sourced primarily from the photochemical oxidation of human NOx pollutants by ozone and other radical ions (Wankel et al. 2010), are a nitrate source that would not have been accessible to historical giant clams in the quantities that they are today.

The organic material within the modern giant clam shells displays much lower $\delta^{15}N$ values than those found in historical specimens. This negative offset in modern shells may be partially explained by the increased deposition of nitrate aerosols generated by atmospheric oxidation of human NOx pollution, which has very low $\delta^{15}N$ values (Wankel et al. 2010). Aerosols in the Gulf of Aqaba have a mean $\delta^{15}N$ value of -2.6‰ but can be as low as -6.9‰ in the summer months (Wankel et al. 2010). By extension, they may explain some of the increase in growth experienced by the giant clams of the region, which could ingest the additional available nitrogen in the highly oligotrophic region for use by their symbiotic algae. In addition, phosphates sourced from mining operations up to 8 km away reach the Red Sea and influence reef health (Abelson et al. 1999). While mining activity has waned on the Israeli side, there are still active mining operations in Jordan and Egypt which release

phosphate into the Gulf of Aqaba as dust. The additional phosphate could have an interactive effect on growth (Belda et al. 1993), though we lack a historical proxy for phosphorus intake in giant clams to demonstrate this.

We must also account for the influence that diagenesis and microbial denitrification can have on the $\delta^{15}N$ value of shells. Prior investigations of $\delta^{15}N$ values in skeletal parts have been conducted with historical and subfossil specimens including subfossil oysters (Darrow et al. 2016, Black et al. 2017), historical fish otoliths (Lueders-Dumont et al. 2018), Triassic corals (Frankowiak et al. 2016, Tornabene et al. 2017) and even Devonian corals (Hickey et al. 2017). Shell organic matrix is thought to be more resistant to diagenetic fractionation than the surrounding carbonate. For example, completely recrystallized Triassic coral skeletal regions have similar $\delta^{15}N$ values to well-preserved samples of original mineralogy (Tornabene et al. 2017), and another investigation found no change in $\delta^{15}N$ values of oysters with severely reduced %N values compared to those with better preserved organic matrix nitrogen (Darrow et al. 2017). One study determined that $\delta^{15}N$ values can be enriched by 2‰ in heated sediments (Qian et al. 1992), while other attempts to influence oyster shell and ostrich eggshell isotopic values via direct cooking did not produce systematic changes in $\delta^{15}N$ (Johnson et al. 1998, Black 2014). In general, the impact of diagenesis on $\delta^{15}N$ values has been small enough in prior investigations to likely not explain the entire 4.5‰ negative offset between in modern shells compared to fossils that we observe.

While the shells in our collection show a negative correlation between growth and $\delta^{15}N$ which would be expected if fertilization by light aerosol nitrates were at work, the relationship is not statistically significant. This is perhaps unsurprising, as giant clam growth is an integration of numerous competing factors related to differing nitrogen sources (Hawkins and Klumpp 1995). The fact that growth increased in the modern specimens for all three species, including the more heterotrophic *T. squamosa*, suggests that factors besides fertilization of symbionts could also be at play. The eastern oyster *Crassostrea virginica* experienced accelerated growth following the rise of anthropogenic eutrophication in the Chesapeake Bay (Kirby and Miller 2005). If phytoplankton availability in the modern Gulf of Aqaba is greater than in the past, particularly in the summer months when productivity is lower due to stratification (Laiolo et al. 2014), the clams could be growing more quickly due to the greater availability of ambient phytoplankton food, which makes up 30% of the incoming nitrogen even in the most photosymbiotic giant clam *T. gigas* (Hawkins and Klumpp 1995). Nitrogen isotope values are also a record of the degree of nitrogen utilization in an environment, with water from plankton cultures with a nitrogen excess showing lower $\delta^{15}N$ values compared to cultures where nitrate drawdown occurs (Waser et al. 1998). In the Red Sea, lower $\delta^{15}N$ values could be due to increased nitrogen fractionation of phytoplankton in the face of greater modern nitrate supply, rather than a signal of the source nitrogen itself.

In giant clams, the symbiotic relationship is present from the larval stage (Mies et al. 2016), and specialized stomach tubules are already well established by

the time giant clams are less than 0.5 mm in size (Hirose et al. 2006). Our specimens range from 2.5 to 23 cm in length, which is still under the theoretical maximum known for all three giant clams in the region (Roa-Quiaoit 2005). While the symbiotic relationship is a significant proportion of the giant clam's nutrition at this point, an investigation of truly mature specimens might find a different relationship between nutrient availability and continued growth late in ontogeny. Mature adults continue to increase their rate of ammonia uptake (Fitt et al. 1993), and prior investigations found approximately a 1‰ decrease in $\delta^{15}N$ value compared to nonsymbiotic bivalves (Dreier et al. 2014), a less extreme version the 7-8‰ offset observed in symbiotic corals (Muscatine et al. 2005; Tornabene et al. 2017). This offset is due partially to the ^{15}N-depleted nitrogen sources available to giant clams (such as nitrate aerosols and ammonia) as compared to heterotrophic organisms (Muscatine et al. 2005). If the degree of this offset corresponds to the amount of photosymbiotic activity, our data could be a record of increased photosymbiotic nutrition within the giant clams in the modern day compared to fossil specimens, which could have used more heterotrophically-sourced nitrogen.

Conclusion

The relative resilience of giant clams in the face of growing environmental stresses like climate change and pollution is poorly known relative to other photosymbiotic groups such as corals. In the Northern Red Sea, giant clams are growing more quickly in the modern day than in the past, which may be related to decreased seasonality and increased nitrate availability. Giant clams may be

responding to these environmental signals with accelerated growth, whether due to increased photosynthesis, heterotrophic filter feeding, or both.

It is important to caution that accelerated growth does not mean that the giant clams have greater fitness or overall health. In fertilization studies of giant clams, shell density and the orderliness of crystal fabrics both declined even as shell extension rates became higher (Belda et al. 1993). In corals, individual extension rates may be unchanged by eutrophication even as net carbonate erosion increases across the reef (Eidinger et al. 2000). In addition, atmospheric aerosols can be phytotoxic in some contexts and often also contain copper which is toxic to the photosystems of giant clams and other photosymbiotic organisms (Paytan et al. 2009, Elfwing et al. 2002). Moreover, the acceleration of giant clam growth will not be a boon for their survival if the broader fringing reef ecosystem they depend on is harmed. Their status as filtering reef sentinels and shell records could shed light on the comparative health of other reef ecosystems impacted by environmental change, and the trends observed in their comparative growth are evidence of the variable responses that different photosymbiotic reef taxa may exhibit to anthropogenic environmental stress.

References

Abelson A, Shteinman B, Fine M, Kaganovsky S (1999) Mass transport from pollution sources to remote coral reefs in Eilat (Gulf of Aqaba, Red Sea). Marine Pollution Bulletin 38:25–29

Adams AL, Needham EW, Knauer J (2013) The effect of shade on water quality parameters and survival and growth of juvenile fluted giant clams, *Tridacna squamosa*, cultured in a land-based growth trial. Aquacult Int 21:1311–1324

Aharon P (1991) Recorders of reef environment histories: stable isotopes in corals, giant clams, and calcareous algae. Coral Reefs 10:71–90

Al-Rifaiy IA, Cherif OH (1988) The fossil coral reefs of Al-Aqaba, Jordan. Facies 18:219–229

Al-Rousan S, Al-Moghrabi S, Pätzold J, Wefer G (2003) Stable oxygen isotopes in *Porites* corals monitor weekly temperature variations in the northern Gulf of Aqaba, Red Sea. Coral Reefs 22:346–356

Andréfouët S, Van Wynsberge S, Gaertner-Mazouni N, Menkes C, Gilbert A, Remoissenet G (2013) Climate variability and massive mortalities challenge giant clam conservation and management efforts in French Polynesia atolls. Biological conservation 160:190–199

Andrié C, Merlivat L (1989) Contribution des données isotopiques de deutérium, oxygène-18, hélium-3 et tritium, à l'étude de la circulation de la Mer Rouge. Oceanologica Acta 12:165–174

Baker AC, Glynn PW, Riegl B (2008) Climate change and coral reef bleaching: An ecological assessment of long-term impacts, recovery trends and future outlook. Estuarine, Coastal and Shelf Science 80:435–471

Baker AC, Starger CJ, McClanahan TR, Glynn PW (2004) Coral reefs: Corals' adaptive response to climate change. Nature 430:741

Belda CA, Cuff C, Yellowlees D (1993) Modification of shell formation in the giant clam *Tridacna gigas* at elevated nutrient levels in sea water. Marine Biology 117:251–257

Bell PRF (1992) Eutrophication and coral reefs—some examples in the Great Barrier Reef lagoon. Water Research 26:553–568

Berman-Frank I, Chernov D, Diamant A, Fine M, Genin A, Gildor H, Gothilf Y, Lazar B, Levy O, Shaked Y, van Rijn J (2016) Scientific committee

concerned with effluent dischange from aquaculture activities into the Gulf of Eilat.

Black HD (2014) $\delta^{15}N$ in mollusk shells as a potential paleoenvironmental proxy for nitrogen loading in Chesapeake Bay. The University of Alabama

Black HD, Andrus CFT, Lambert WJ, Rick TC, Gillikin DP (2017) $\delta^{15}N$ Values in *Crassostrea virginica* Shells Provides Early Direct Evidence for Nitrogen Loading to Chesapeake Bay. Scientific Reports 7:44241

Bongiorni L, Shafir S, Rinkevich B (2003) Effects of particulate matter released by a fish farm (Eilat, Red Sea) on survival and growth of *Stylophora* pistillata coral nubbins. Marine Pollution Bulletin 46:1120–1124

Cantin NE, Cohen AL, Karnauskas KB, Tarrant AM, McCorkle DC (2010) Ocean Warming Slows Coral Growth in the Central Red Sea. Science 329:322–325

Carmichael RH, Hattenrath T, Valiela I, Michener RH (2008) Nitrogen stable isotopes in the shell of *Mercenaria mercenaria* trace wastewater inputs from watersheds to estuarine ecosystems. Aquatic Biology 4:99–111

Chan KR, Todd PA, Chou LM (2008) An allometric analysis of juvenile fluted giant clam shells (*Tridacna squamosa* L.). Journal of Conchology 39:621

Chen Y, Mills S, Street J, Golan D, Post A, Jacobson M, Paytan A (2007) Estimates of atmospheric dry deposition and associated input of nutrients to Gulf of Aqaba seawater. Journal of Geophysical Research: Atmospheres 112:

Darrow ES, Carmichael RH, Andrus CFT, Jackson HE (2017) From middens to modern estuaries, oyster shells sequester source-specific nitrogen. Geochimica et Cosmochimica Acta 202:39–56

Doney SC, Mahowald N, Lima I, Feely RA, Mackenzie FT, Lamarque J-F, Rasch PJ (2007) Impact of anthropogenic atmospheric nitrogen and sulfur deposition on ocean acidification and the inorganic carbon system. PNAS 104:14580–14585

Dreier A, Loh W, Blumenberg M, Thiel V, Hause-Reitner D, Hoppert M (2014) The isotopic biosignatures of photo-vs. thiotrophic bivalves: are they preserved in fossil shells? Geobiology 12:406–423

Edinger EN, Limmon GV, Jompa J, Widjatmoko W, Heikoop JM, Risk MJ (2000) Normal Coral Growth Rates on Dying Reefs: Are Coral Growth Rates Good Indicators of Reef Health? Marine Pollution Bulletin 40:404–425

Elfwing T, Blidberg E, Tedengren M (2002) Physiological responses to copper in giant clams: a comparison of two methods in revealing effects on photosynthesis in zooxanthellae. Marine Environmental Research 54:147–155

Felis T, Lohmann G, Kuhnert H, Lorenz SJ, Scholz D, Pätzold J, Al-Rousan SA, Al-Moghrabi SM (2004) Increased seasonality in Middle East temperatures during the last interglacial period. Nature 429:164–168

Felis T, Pätzold J, Loya Y, Fine M, Nawar AH, Wefer G (2000) A coral oxygen isotope record from the northern Red Sea documenting NAO, ENSO, and North Pacific teleconnections on Middle East climate variability since the year 1750. Paleoceanography 15:679–694

Fine M, Gildor H, Genin A (2013) A coral reef refuge in the Red Sea. Global Change Biology 19:3640–3647

Fishelson L (1973) Ecology of coral reefs in the Gulf of Aqaba (Red Sea) influenced by pollution. Oecologia 12:55–67

Fitt WK, Heslinga GA, Watson TC (1993a) Utilization of dissolved inorganic nutrients in growth and mariculture of the tridacnid clam *Tridacna derasa*. Aquaculture 109:27–38

Fitt WK, Rees T a. V, Yellowlees D (1995) Relationship between pH and the availability of dissolved inorganic nitrogen in the zooxanthella-giant clam symbiosis. Limnology and Oceanography 40:976–982

Fitt WK, Rees TAV, Braley RD, Lucas JS, Yellowlees D (1993b) Nitrogen flux in giant clams: size-dependency and relationship to zooxanthellae density and clam biomass in the uptake of dissolved inorganic nitrogen. Marine Biology 117:381–386

Frankowiak K, Wang XT, Sigman DM, Gothmann AM, Kitahara MV, Mazur M, Meibom A, Stolarski J (2016) Photosymbiosis and the expansion of shallow-water corals. Science Advances 2:e1601122

Gannon ME, Pérez-Huerta A, Aharon P, Street SC (2017) A biomineralization study of the Indo-Pacific giant clam *Tridacna gigas*. Coral Reefs 36:503–517

Goreau TF, Goreau NI, Yonge CM (1973) On the utilization of photosynthetic products from zooxanthellae and of a dissolved amino acid in *Tridacna maxima f. elongata* (Mollusca: Bivalvia). Journal of Zoology 169:417–454

Graniero LE, Grossman EL, O'Dea A (2016) Stable isotopes in bivalves as indicators of nutrient source in coastal waters in the Bocas del Toro Archipelago, Panama. PeerJ 4:e2278

Heaton TH (1986) Isotopic studies of nitrogen pollution in the hydrosphere and atmosphere: a review. Chemical Geology 59:87–102

Heslinga GA, Fitt WK (1987) The Domestication of Reef-Dwelling Clams. BioScience 37:332–339

Hickey AN, Junium CK, Uveges BT, Ivany LC, Martindale RC (2017) Carbon and nitrogen isotopic analysis of coral-associated nitrogen in rugose corals of the Middle Devonian, implications for paleoecology and paleoceanography.

Hirose E, Iwai K, Maruyama T (2006) Establishment of the photosymbiosis in the early ontogeny of three giant clams. Marine Biology 148:551–558

Huber M, Eschner A (2010) *Tridacna (Chametrachea) costata* ROA-QUIAOIT, KOCHZIUS, JANTZEN, AL-ZIBDAH & RICHTER from the Red Sea, a junior synonym of *Tridacna squamosina* STURANY, 1899 (Bivalvia, Tridacnidae). Annalen des Naturhistorischen Museums in Wien Serie B für Botanik und Zoologie 153–162

Hume BCC, Voolstra CR, Arif C, D'Angelo C, Burt JA, Eyal G, Loya Y, Wiedenmann J (2016) Ancestral genetic diversity associated with the rapid spread of stress-tolerant coral symbionts in response to Holocene climate change. PNAS 113:4416–4421

Jantzen C, Wild C, El-Zibdah M, Roa-Quiaoit HA, Haacke C, Richter C (2008) Photosynthetic performance of giant clams, *Tridacna maxima* and *T. squamosa*, Red Sea. Marine Biology 155:211–221

Johnson BJ, Fogel ML, Miller GH (1998) Stable isotopes in modern ostrich eggshell: a calibration for paleoenvironmental applications in semi-arid regions of southern Africa. Geochimica et Cosmochimica Acta 62:2451–2461

Kirby MX, Miller HM (2005) Response of a benthic suspension feeder (*Crassostrea virginica* Gmelin) to three centuries of anthropogenic eutrophication in Chesapeake Bay. Estuarine, Coastal and Shelf Science 62:679–689

Klumpp DW, Griffiths CL (1994) Contributions of phototrophic and heterotrophic nutrition to the metabolic and growth requirements of four species of giant clam (Tridacnidae). Marine Ecology Progress Series 115:103–115

Laiolo L, Barausse A, Dubinsky Z, Palmeri L, Goffredo S, Kamenir Y, Al-Najjar T, Iluz D (2014) Phytoplankton dynamics in the Gulf of Aqaba (Eilat, Red Sea): A simulation study of mariculture effects. Marine Pollution Bulletin 86:481–493

Lazar B, Erez J, Silverman J, Rivlin T, Rivlin A, Dray M, Meeder E, Iluz D (2008) Recent environmental changes in the chemical-biological oceanography of the Gulf of Aqaba (Eilat). Aqaba-Eilat, the improbable gulf Environment, biodiversity and preservation Magnes Press, Jerusalem 49–61

Leggat W, Buck BH, Grice A, Yellowlees D (2003) The impact of bleaching on the metabolic contribution of dinoflagellate symbionts to their giant clam host. Plant, Cell & Environment 26:1951–1961

Levin Z, Gershon H, Ganor E (2005) Vertical distribution of physical and chemical properties of haze particles in the Dead Sea valley. Atmospheric Environment 39:4937–4945

Loya Y (2004) The Coral Reefs of Eilat — Past, Present and Future: Three Decades of Coral Community Structure Studies. In: Rosenberg E., Loya Y. (eds) Coral Health and Disease. Springer Berlin Heidelberg, Berlin, Heidelberg, pp 1–34

Loya Y, Lubinevsky H, Rosenfeld M, Kramarsky-Winter E (2004) Nutrient enrichment caused by in situ fish farms at Eilat, Red Sea is detrimental to coral reproduction. Marine Pollution Bulletin 49:344–353

Lucas JS (1994) The biology, exploitation, and mariculture of giant clams (Tridacnidae). Reviews in Fisheries Science 2:181–223

Lucas JS, Nash WJ, Crawford CM, Braley RD (1989) Environmental influences on growth and survival during the ocean-nursery rearing of giant clams, Tridacna gigas (L.). Aquaculture 80:45–61

Lueders-Dumont JA, Wang XT, Jensen OP, Sigman DM, Ward BB (2018) Nitrogen isotopic analysis of carbonate-bound organic matter in modern and fossil fish otoliths. Geochimica et Cosmochimica Acta 224:200–222

Mies M, Van Sluys MA, Metcalfe CJ, Sumida PYG (2017) Molecular evidence of symbiotic activity between *Symbiodinium* and *Tridacna* maxima larvae. Symbiosis 72:13–22

Moss DK, Ivany LC, Judd EJ, Cummings PW, Bearden CE, Kim W-J, Artruc EG, Driscoll JR (2016) Lifespan, growth rate, and body size across latitude in marine Bivalvia, with implications for Phanerozoic evolution. Proc R Soc B 283:20161364

Moustafa YA, Pätzold J, Loya Y, Wefer G (2000) Mid-Holocene stable isotope record of corals from the northern Red Sea. Int Journ Earth Sciences 88:742–751

Munro JL (1982) Estimation of the parameters of the von Bertalanffy growth equation from recapture data at variable time intervals. ICES J Mar Sci 40:199–200

Muscatine L, Goiran C, Land L, Jaubert J, Cuif J-P, Allemand D (2005) Stable isotopes ($\delta^{13}C$ and $\delta^{15}N$) of organic matrix from coral skeleton. Proceedings of the National Academy of Sciences 102:1525–1530

Nelson BK, Deniro MJ, Schoeninger MJ, De Paolo DJ, Hare PE (1986) Effects of diagenesis on strontium, carbon, nitrogen and oxygen concentration and isotopic composition of bone. Geochimica et Cosmochimica Acta 50:1941–1949

Neo ML, Eckman W, Vicentuan K, Teo SL-M, Todd PA (2015) The ecological significance of giant clams in coral reef ecosystems. Biological Conservation 181:111–123

Neo ML, Wabnitz CC, Braley RD, Heslinga GA, Fauvelot C, Van Wynsberge S, Andréfouët S, Waters C, Tan AS-H, Gomez ED (2017) Giant clams (Bivalvia: Cardiidae: Tridacninae): a comprehensive update of species and their distribution, current threats and conservation status. Oceanogr Mar Biol 55:87–387

O'Donnell TH, Macko SA, Chou J, Davis-Hartten KL, Wehmiller JF (2003) Analysis of $\delta^{13}C$, $\delta^{15}N$, and $\delta^{34}S$ in organic matter from the biominerals of modern and fossil Mercenaria spp. Organic Geochemistry 34:165–183

Oron S, Angel D, Goodman-Tchernov B, Merkado G, Kiflawi M, Abramovich S (2014) Benthic foraminiferal response to the removal of aquaculture fish cages in the Gulf of Aqaba-Eilat, Red Sea. Marine Micropaleontology 107:8–17

Pätzold J, Heinrichs JP, Wolschendorf K, Wefer G (1991) Correlation of stable oxygen isotope temperature record with light attenuation profiles in reef-dwellingTridacna shells. Coral Reefs 10:65–69

Pauly D, Munro JL (1984) Once more on the comparison of growth in fish and invertebrates. Fishbyte (Philippines)

Paytan A, Mackey KRM, Chen Y, Lima ID, Doney SC, Mahowald N, Labiosa R, Post AF (2009) Toxicity of atmospheric aerosols on marine phytoplankton. Proc Natl Acad Sci USA 106:4601

Peierls BL, Paerl HW (1997) Bioavailability of atmospheric organic nitrogen deposition to coastal phytoplankton. Limnology and Oceanography 42:1819–1823

Qian Y, Engel MH, Macko SA (1992) Stable isotope fractionation of biomonomers during protokerogen formation. Chemical Geology: Isotope Geoscience section 101:201–210

Reiss Z, Luz B, Almogi-Labin A, Halicz E, Winter A, Wolf M, Ross DA (1980) Late Quaternary Paleoceanography of the Gulf of Aqaba (Elat), Red Sea 1. Quaternary Research 14:294–308

Richter C, Roa-Quiaoit H, Jantzen C, Al-Zibdah M, Kochzius M (2008) Collapse of a new living species of giant clam in the Red Sea. Current Biology 18:1349–1354

Rinkevich B, Loya Y (1977) Harmful effects of chronic oil pollution on a Red Sea scleractinian coral.

Roa-Quiaoit HAF (2005) The ecology and culture of giant clams (Tridacnidae) in the Jordanian sector of the Gulf of Aqaba, Red Sea. PhD, Universitat Bremen

Romanek CS, Jones DS, Williams DF, Krantz DE, Radtke R (1987) Stable isotopic investigation of physiological and environmental changes recorded in shell carbonate from the giant clam *Tridacna maxima*. Marine Biology 94:385–393

Sano Y, Kobayashi S, Shirai K, Takahata N, Matsumoto K, Watanabe T, Sowa K, Iwai K (2012) Past daily light cycle recorded in the strontium/calcium ratios of giant clam shells. Nature Communications 3:761

Scholz D, Mangini A, Felis T (2004) U-series dating of diagenetically altered fossil reef corals. Earth and Planetary Science Letters 218:163–178

Schöne BR, Dunca E, Fiebig J, Pfeiffer M (2005) Mutvei's solution: An ideal agent for resolving microgrowth structures of biogenic carbonates. Palaeogeography, Palaeoclimatology, Palaeoecology 228:149–166

Schwartzmann C, Durrieu G, Sow M, Ciret P, Lazareth CE, Massabuau J-C (2011) In situ giant clam growth rate behavior in relation to temperature: A one-year coupled study of high-frequency noninvasive valvometry and sclerochronology. Limnology and Oceanography 56:1940–1951

Shaked Y, Lazar B, Marco S, Stein M, Agnon A (2011) Late Holocene events that shaped the shoreline at the northern Gulf of Aqaba recorded by a buried fossil reef. Isr J Earth Sci 58:355–368

Singer A, Ganor E, Dultz S, Fischer W (2003) Dust deposition over the Dead Sea. Journal of Arid Environments 53:41–59

Tomascik T, Sander F (1985) Effects of eutrophication on reef-building corals. Mar Biol 87:143–155

Tornabene C, Martindale RC, Wang XT, Schaller MF (2017) Detecting photosymbiosis in fossil scleractinian corals. Scientific reports 7:9465

Vakily JM (1992) Determination and comparison of bivalve growth, with emphasis on Thailand and other tropical areas. WorldFish,

Versteegh EAA, Gillikin DP, Dehairs F (2011) Analysis of $\delta^{15}N$ values in mollusk shell organic matrix by elemental analysis/isotope ratio mass spectrometry without acidification: an evaluation and effects of long-term preservation. Rapid Communications in Mass Spectrometry 25:675–680

Walker DI, Ormond RFG (1982) Coral death from sewage and phosphate pollution at Aqaba, Red Sea. Marine Pollution Bulletin 13:21–25

Wankel SD, Chen Y, Kendall C, Post AF, Paytan A (2010) Sources of aerosol nitrate to the Gulf of Aqaba: Evidence from δ15N and δ18O of nitrate and trace metal chemistry. Marine Chemistry 120:90–99

Warter V, Müller W (2016) Daily growth and tidal rhythms in Miocene and modern giant clams revealed via ultra-high resolution LA-ICPMS analysis—A novel methodological approach towards improved sclerochemistry. Palaeogeography, Palaeoclimatology, Palaeoecology

Waser N a. D, Harrison PJ, Nielsen B, Calvert SE, Turpin DH (1998) Nitrogen isotope fractionation during the uptake and assimilation of nitrate, nitrite, ammonium, and urea by a marine diatom. Limnology and Oceanography 43:215–224

Watanabe S, Kodama M, Fukuda M (2009) Nitrogen stable isotope ratio in the manila clam, *Ruditapes philippinarum*, reflects eutrophication levels in tidal flats. Marine Pollution Bulletin 58:1447–1453

Weil N (2008) Holocene coral reefs evolution in the Gulf of Eilat: Terraces, sea-levels and growth patterns. Masters, Hebrew University of Jerusalem

Yonge CM (1975) Giant clams. Scientific American 232:96–105

Figures

Figure 1: Map showing study sites around the edges of the Red Sea, with purple sites representing sources of modern shells, red sites as sources of fossil shells and green sites as sources of both fossil and modern shells. Shells at the Taba Crossing site originated along the Egyptian coast south of there, but were confiscated at the checkpoint. Map created with GGMap, imagery from Stamen Group.

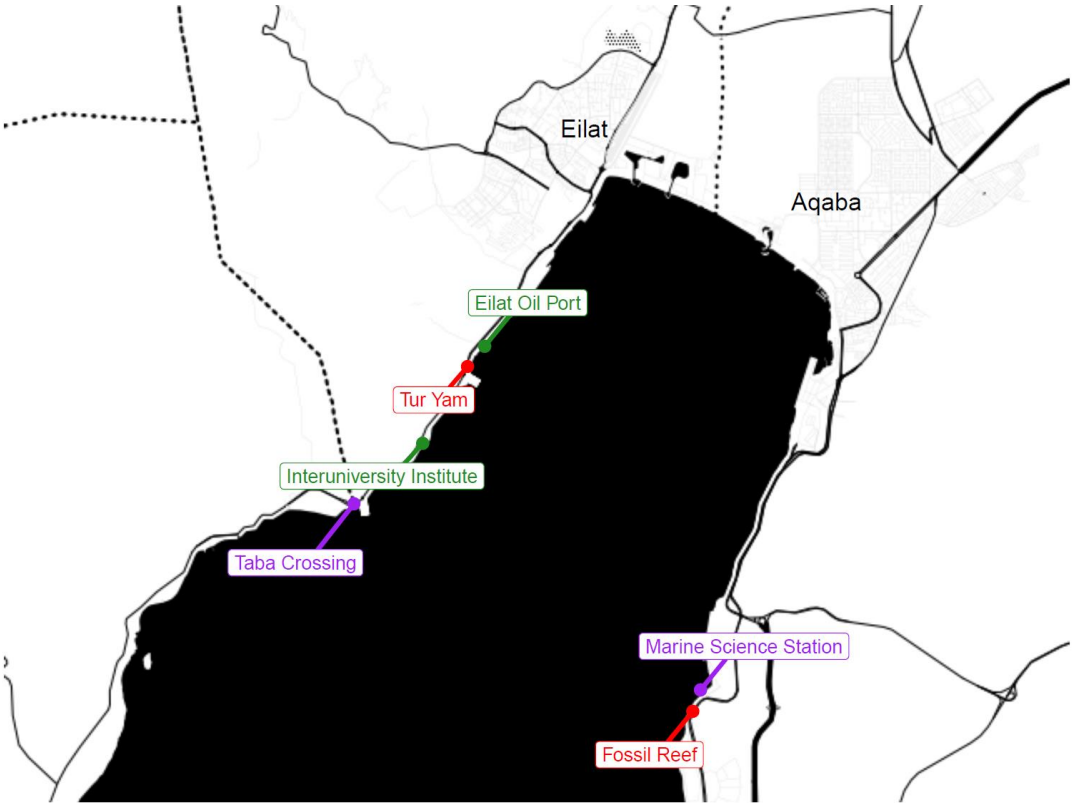

Figure 2: Left: Shell J38, *Tridacna squamosina* found at the top of the Jordan fossil terrace. Original crossed-lamellar aragonite structures are preserved. Middle: TY1: a badly recrystallized shell of T. maxima from the reef rock at Tur Yam showing extensive fusion of crossed-lamellar structures. Lamellae were still visible in this shell but no isotopic analyses were conducted. Right: J40, modern Tridacna squamosina collected on the beach onshore of the reef MPA at Marine Science Station, Aqaba.

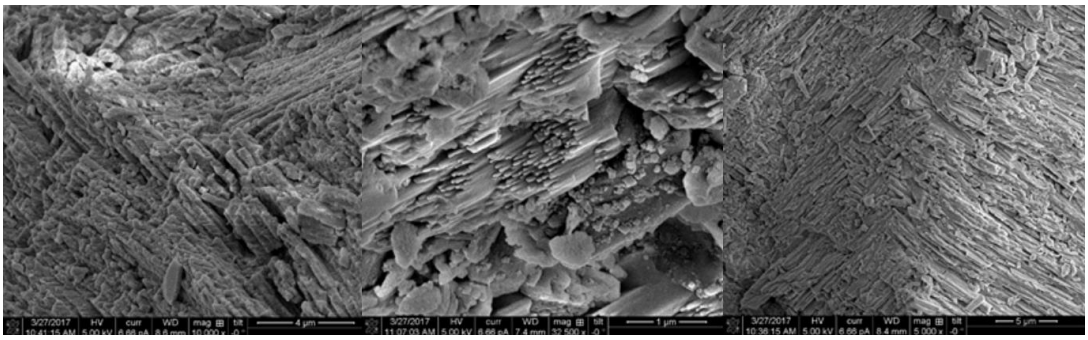

Figure 3a: Picture of *T. squamosina* from Hebrew University Museum, shell H5, with transects of growth band landmarks in blue on lower image relative to overall direction of growth. Top includes close-up view of these increments. Scale bar refers to 1 cm in bottom picture.

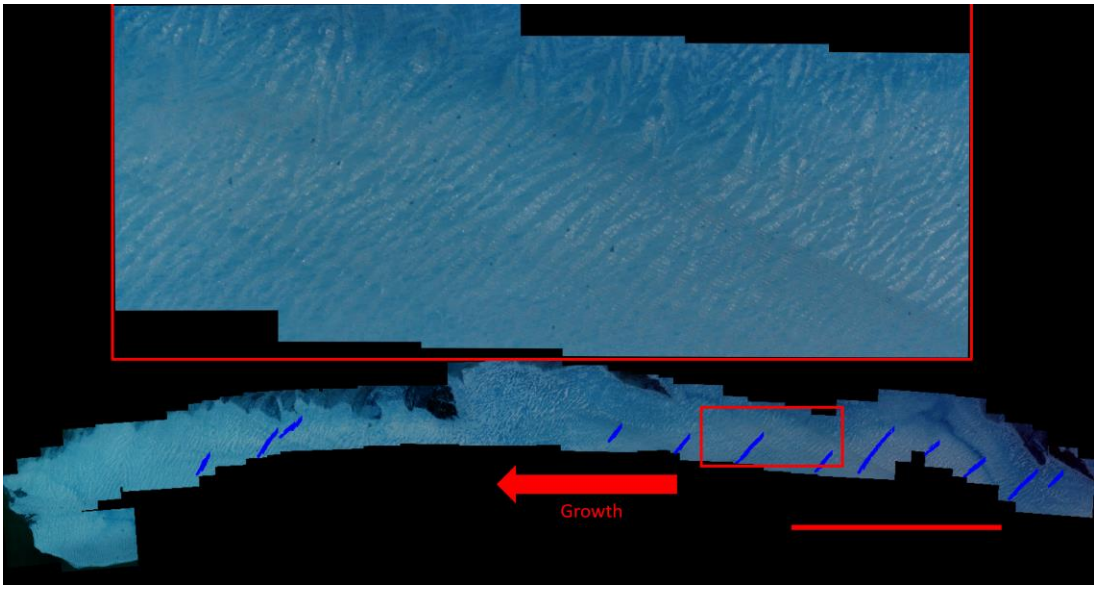

Figure 3b: Validation of periodicity of daily/subdaily growth bands. Blue points are confirmed by peak-to-peak measurements of isotopic transects. Red points represent total length divided by the number of daily/subdaily bands.

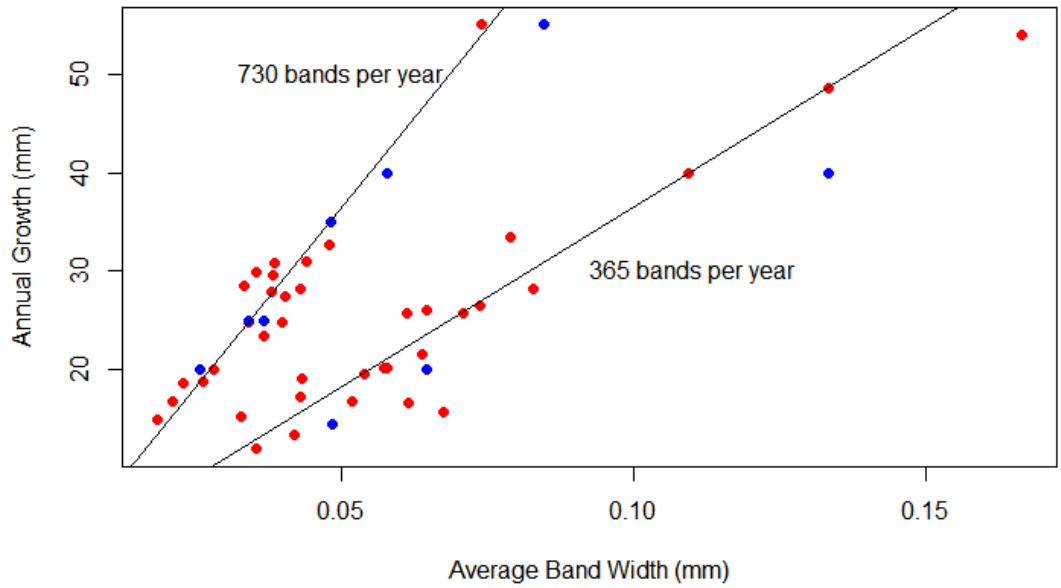

Figure 4: Fossil and modern box plot split by species for k and ϕ' indices. Boxes encompass the middle quartiles while the whiskers represent 1.5xIQR. Points are outliers, and horizontal lines are the medians.

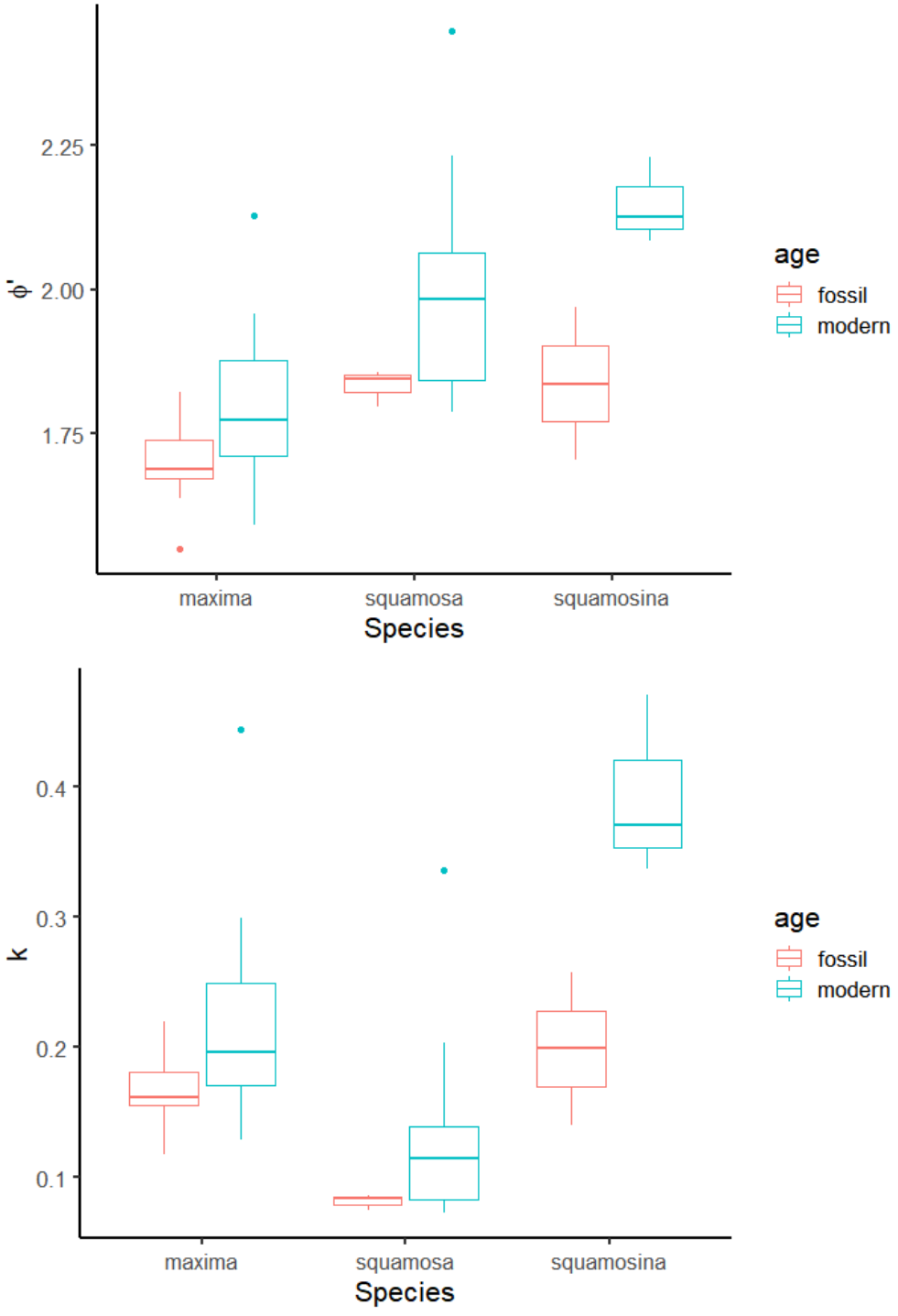

Figure 5: Top left: comparison of fossil and modern nitrogen isotope values. Top right: comparison of fossil and modern oxygen isotope paleotemperature output. Bottom left: comparison of ϕ' and nitrogen isotope values. Bottom right: comparison of ϕ' and shell formation temperature. Legend for both scatter plots at bottom.

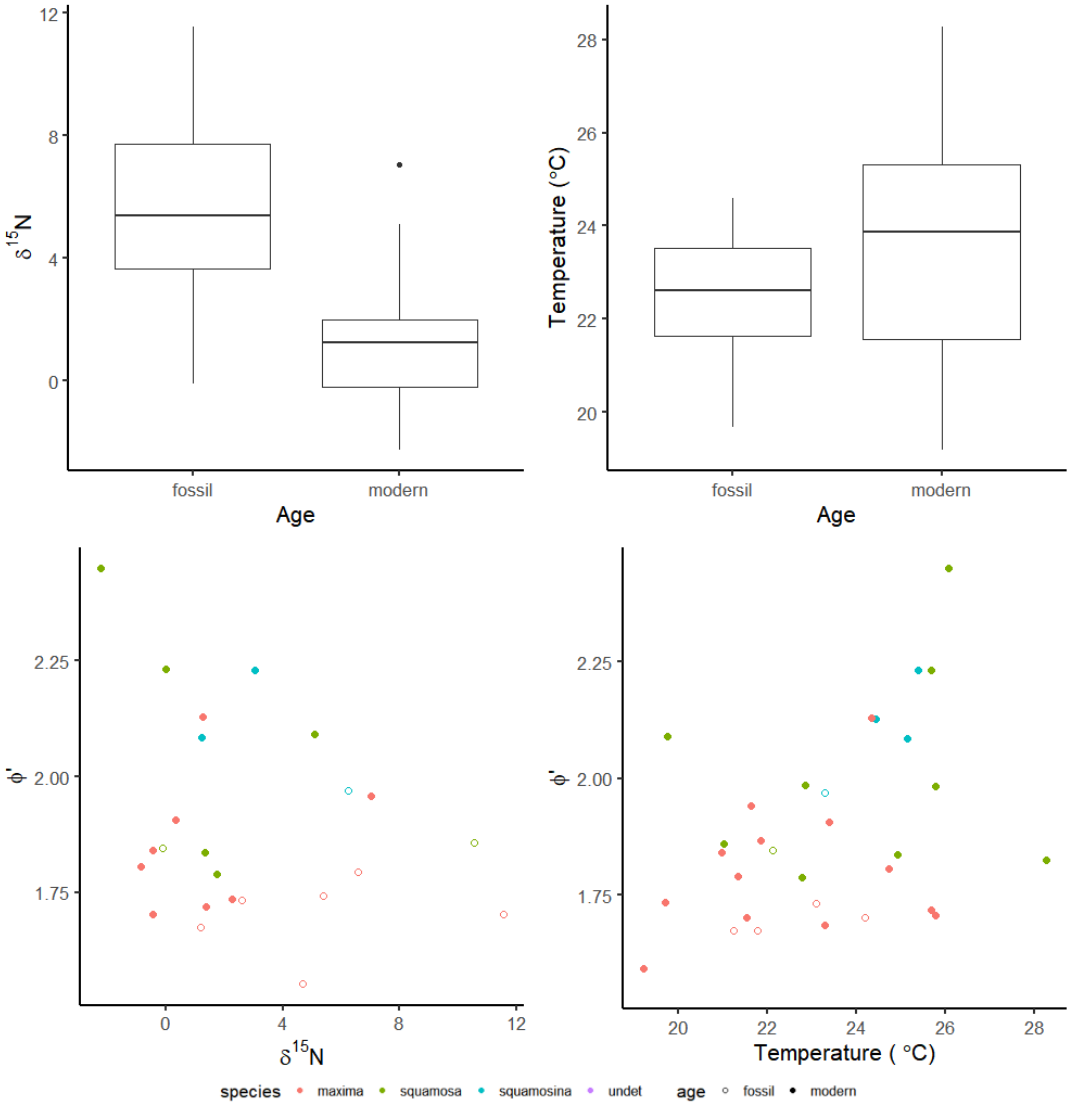

Tables

Table 1

Growth indices for different *Tridacna* species

Species	*Tridacna maxima*		*T. squamosa*		*T. squamosina*	
Age	Fossil	Modern	Fossil	Modern	Fossil	Modern
Growth rate (mm/year)	23.8	26.7	20.0	29.0	31.0	52.3
k	0.17	0.21	0.08	0.14	0.20	0.39
ϕ’	1.69	1.79	1.83	2.00	1.97	2.14

Table 2

ANOVA: ϕ’ vs species and age

Source	df	Sum squares	Mean Squares	p
Species	2	0.5210	0.2560	4.98e-05
Age	1	0.2022	0.2022	0.00283
Residuals	40	0.7986	0.0200	

Tukey post-hoc test for ϕ’ ANOVA

Species interaction				
	Difference	Lower	Upper	p
squamosa-maxima	0.2003	0.0835	0.3172	0.00045
squamosina-maxima	0.2592	0.0912	0.4271	0.0016
squamosina-squamosa	0.0588	-0.1222	0.2398	0.7109
Age interaction				
	Difference	Lower	Upper	p
Modern-fossil	0.1414	0.0505	0.2321	0.0031

ANOVA: k in relation to species and age

Source	df	Sum squares	Mean Squares	p
Species	2	0.13975	0.06987	1.85e-05
Age	1	0.04747	0.04747	0.00382
Residuals	40	0.19291	0.00482	

Tukey post-hoc test for k ANOVA

Species interaction				
	Difference	Lower	Upper	p
squamosa-maxima	-0.0773	-0.1347	-0.0199	0.0060
squamosina-maxima	0.1151	0.0325	0.1976	0.0044
squamosina-squamosa	0.1924	0.1035	0.2814	<0.0005
Age interaction				
	Difference	Lower	Upper	p
Modern-fossil	0.685	0.0238	0.1131	0.0035

SUPPLEMENTAL FILES

Chapter 1:

All supplementary data available at PALAIOS Data Archive http://www.sepm.org/pages.aspx?pageid=332.

Chapter 2:

AllIncrementSizes.csv is the raw fortnightly increment data from all shells

AllIsotopeResults.csv includes all isotope $\delta^{13}C$ and $\delta^{18}O$ values grouped by specimen

Hypercalcifierdatabase.xlsx includes data of different large bivalves and their growth

Chapter 3

All data included in one csv file: Chapter3.csv

Chapter 4

All growth, nitrogen isotope and oxygen isotope data included in file: Chapter4.csv